NAGOYA INSTITUTE OF TECHNOLOGY

Fabrication and characterization of ultraviolet photoresponsive devices

紫外光応答デバイスの作製とその特性評価

by

Ajinkya Kishor Ranade

A thesis submitted to the Department of Physical Science and Engineering of Nagoya Institute of Technology in partial fulfillment of the requirement for the degree of Doctor of Philosophy (Ph.D.)

March 2021

Declaration of Authorship

I, Ajinkya Kishor Ranade, declare that this thesis titled, “Fabrication and characterization of ultraviolet photoresponsive devices” and the work presented in it is my own.

I confirm that:

- This work was done wholly or mainly while in candidature for a research degree at this University.
- Where any part of this thesis has previously been submitted for a degree or any other qualifications at this University or any other institution, this has been clearly stated.
- Where I have consulted the published work of others, this is always clearly attributed.
- Where I have quoted from the work of others, the source is always given. With the exception of such quotations, this thesis is entirely my own work.
- I have acknowledged all main sources of help.
- Where the thesis is based on work done by myself jointly with others, I have made clear exactly what was done by others and what I have contributed myself.

Signed:

Date:

Dedication

This thesis work is in loving memory of my father Late. Mr. Kishor Parshuram Ranade, who left us for heavenly abode.

Baba, thank you so very much for being a constant support system and teaching by example the valuable lesson of

"Help others without thinking about the returns"

My Doctoral journey would not have been possible without you. You will forever be in my heart and I miss you immensely.

Acknowledgment

My deepest gratitude goes to my supervisor **Associate Professor Golap Kalita** for providing an opportunity to carry out research under his kind guidance. He offered me so much advice, patiently supervising me, and always guiding me in the right direction. I've learned a lot from him, without his guidance, I could not have completed my dissertation. It was an honor to be his student. I will always be indebted to him.

I sincerely extend my heartfelt thank you to Professor **Masaki Tanemura** for his insightful comments and encouragement. Thank you so much for guiding me in my research endeavors and writing this thesis.

I wish to sincerely give my heartfelt thanks to committee members and Associate Professor **Shingo Ono** for his critical comments and suggestion to improve on the weaknesses in my thesis.

I sincerely thank **Professor. Toshio Kawahara** for his valuable comments to improve quality of my thesis.

I acknowledge my indebtedness to **NGK Insulators Pvt. Ltd.** for providing me with scholarship during my Ph. D. research. Thank you very much for your help and I will be forever indebted.

I am so thankful to my lab colleagues **Dr. Rakesh Mahyavanshi** and **Mr. Pradeep Desai** who helped me right from the beginning. Mr. Pradeep Desai has helped me at every turn of my research journey for which I will be always indebted. Also, I would like to thank my other lab mates **Miss. Bhagyashri Todankar**, **Mr. Mandar Shinde, Mr. Venkata Krishna Rama Rao, Mr. Shuhei Nakanishi, Mr. Kai Okazaki** for their support during my research and writing of my thesis.

I wish to extend my heartfelt thanks to my extended family and friends. My uncle **Mr. Vijay Kulkarni** has been a role model for me. His understanding of subject and teaching qualities are an inspiration and it will be my attempt throughout my life to achieve the same magnitude of those

qualities as him. I also want to thank my aunt **Late. Mrs. Anjali Sharad Kulkarni** for being an inspiration, I will miss you very much. My heartfelt thanks to **Mrs. Madhavi Kulkarni, Dr. Sanjay Kulkarni, Dr. Veena Kulkarni, and Mr. Sharad Kulkarni** for their constant support in my most difficult times. I say from the bottom of my heart that you all are a family I can fall back to and am I am so grateful to have you. My grandparents **Late Prof. Bhalchandra A. Kulkarni and Mrs. Sharda Kulkarni** has been the constant source of inspiration to me and I hope to have made them proud. My cousin brothers and sisters, **Mrs. Rama Kulkarni, Mrs. Aditi Kulkarni, Mr. Shantanu Kulkarni, Mr. Abhijeet Kulkarni, Mr. Abhishek Kulkarni, Isha Amrute, Mr. Aashay Ranade, Mr. Vishal Ranade** have helped me throughout my life, and I am so very grateful to have you all as family. The times we all were together will always be cherished. My other family **Late Mrs. Renuka Gawande**, **Mr. Dinesh Gawande, Mrs. Vijaya Sahasane and Mrs Sarika Kulkarni**, **Mrs. Dipika Gawande,** thank you for your support and being there for me through thick and thin. My niece **Miss. Devyani Gawande**, even at a young age of 9 years has taught me a valuable lesson to stay strong and fight in the face of adversity. The support of my friends during my stay in Japan has been immense. I wish to thank my good friend **Mr. Sunil Kumar Singh** who helped me in my time of need and believing in me when I didn't. You gave me an opportunity to sustain myself in Japan for which I am grateful. Your zest for life and greater things is unparalleled. **Mr. Rahul Deshmukh,** with whom I started this journey of Ph.D., thank you so very much for being a ray of hope. The positivity you radiate is infectious and I cannot imagine my life in Japan without you. As we always say "till the end of line". You both are a support system on whom I could rely on and thank you for being there for me. My heartfelt thanks to **Dr. Rupesh Kumar Singh** for helping me in my initial stay in Japan. I will always be indebted to you for the support you provided me and being my first friend in Japan. My heartfelt thanks to

my other friends **Miss. Nishtha Tiwari, Mr. Gaurav Thapa, Mr. Arijit Bose and Mr. Rohith Kiran** for their constant support. Trust me when I say that you all are family to me and you made an otherwise boring life in Japan a lot easier, funnier and bearable. Thank you for being there with me in my most difficult times and I will forever cherish our friendship. My heartfelt thanks to my oldest friend **Mr. Shreyas Apte** for always supporting and believing in me. We literally started our journey of life together and I am very grateful to have you in my life. I cherish our friendship. My childhood friends **Mr. Varad Pawar** and **Mr. Ajinkya Thorat**, thank you for being in my life. You mean a lot to me. I am blessed to have friends like you. I also want to thank **Miss. Akanksha Kanade** for being such a good friend and supporting me in difficult times.

I also want to thank **Late Prof. Maheshwar Sharon and Dr. Madhuri Sharon** for introducing me to the world of nanotechnology. You both provided me an opportunity when I least expected it. The humbleness and constant love you showered on all your students is legendary. You both are like grandparents to me. A turning point in my life was when I attended the lecture series of Prof Sharon and Dr. Sharon, on "Basics of Carbon Nanotechnology". The whole topic was crystal clear to me after just 5 days and I had decided then itself to follow footsteps of Prof. Sharon and Dr. Sharon in the field of research. More importantly you both have given me life lessons. I will forever be indebted. **Professor Maheshwar Sharon**, who is my guru, will always be an inspiration to me. Values inculcated by him will always be with me and it will be my lifelong effort to make him proud. I am very fortunate and proud to be student of the great **Prof Maheshwar Sharon** and **Dr. Madhuri Sharon.**

Finally, I want to thank my family **Baba, Aai and Aditya** for providing support throughout my life and making me who I am today. My heartfelt thanks to my mother **Dr. Anuradha Ranade** who has been a source of inspiration throughout my life. You have sacrificed a lot to give me and

Aditya everything and I cannot be begin to fathom the hardships you went through. You are a role model, support system and everything to me. I hope to achieve the success you have achieved in life. You have taught me by example to be strong and fight the hardships that come in our way. Most importantly you taught me by your actions to be humble, grateful and helpful of other even in our bad times. My journey to achieve a Doctorate started when at a young age I saw you getting awarded your Doctorate degree after much hardship, resilience and effectively managing both family and job. I had decided then to follow your footsteps and to be a doctorate myself. Your thirst for knowledge and self-confidence are unparalleled. You have set the bar very high for us to achieve the greatness of your level. **Aai**, I want to thank you from the bottom of my heart, and you will always be my source of inspiration. This work has been a humble attempt of mine to follow the footsteps and achieve the same success as my mother.

My brother **Mr. Aditya Kishor Ranade** is second source of inspiration to me. You have always supported me in every aspect of life, and I am lucky to have an elder brother like you. The unconventional paths you have chosen to travel, inspired me to believe in myself and not fearing the unknown. Your keen nature of research and resilience are some of the many qualities that have inspired me, and I hope to achieve the same level keen focus, self-belief and lot other qualities as you. Aditya, you are the constant support system which I fall back to every time. Thank you very much for your support and being there for me in my worst and good times. I respect you immensely and look up to you.

Finally, I want to thank my late father Mr. Kishor Parshuram Ranade from the bottom of my heart. Baba, thank you very much for your constant support and belief in me. You have been the silent support system to me. You have taught me a valuable lesson of helping others in the time of need. You have given me the confidence to take unconventional decisions and

you have always supported them unconditionally. Baba, you are the lighthouse under whose light I have found my path. You will forever be in my heart. Without your strength I could not have taken this journey of Ph.D. and your encouragement proved to be a guiding light for me. You not being with us during this phase of life has diminished the essence of this achievement, nevertheless I hope you are watching me from above and I hope to make you proud. Baba, thank you so very much.

This thesis is dedicated to my father. Baba, thank you so very much and I miss you immensely.

Abstract

Ultraviolet (UV) photoresponsive devices are important component for various application in modern day technologies. Among various wide bandgap semiconductors for UV photoresponsive devices, gallium nitride (GaN) and gallium oxide (Ga_2O_3) are significantly attractive considering their excellent electrical, chemical and mechanical properties. In this thesis work, fabrication of GaN and Ga_2O_3 based heterojunctions with graphene and p-type γ-copper iodide (γ-CuI) are investigated. The interface quality of respective fabricated devices is analyzed with and without UV illumination, which clarifies the UV photoresponse properties.

Chapter 1 describes background of UV photoresponsive devices and gives a detailed account of various device structures of photodiode. Then, discussion is made about the electrical, chemical and mechanical properties of the three-dimensional (3D) GaN and Ga_2O_3 wide bandgap semiconductors, which is used to fabricate the UV photoresponsive devices. The motivation and objective behind this thesis work are also established.

Chapter 2 introduces the two-dimensional (2D) graphene material, which is integrated with GaN and Ga_2O_3 for device fabrication. Graphene with its zero-bandgap and one atom thickness is an attractive material to integrate with GaN and Ga_2O_3 to fabricate unconventional heterojunctions. The challenges in fabricating and effect of such 2D/3D heterojunction devices are addressed in the motivation and objective part.

Chapter 3 discusses about the UV light induced electrical hysteresis effect in graphene/GaN vertical heterojunction Schottky device. In this chapter, the interface quality of graphene/GaN heterojunction is evaluated for presence of interfacial impurities by UV illumination. The interfacial impurities act as trap for charge carriers, thus inducing electrical hysteresis in the heterojunction. Our findings can be significant in understanding the graphene/GaN and other

2D/3D heterojunction interfaces by UV illumination process for developing high performance devices.

Chapter 4 compares the electrical hysteresis effect obtained in graphene/GaN Schottky device with the fabricated **γ**-CuI/GaN p-n heterojunction device. The fabricated device showed excellent rectifying diode characteristics with high bias voltage (-20V to +20V). The device also showed excellent photovoltage of 0.93V under UV illumination with consistent photoresponsivity. The electrical hysteresis for the **γ**-CuI/GaN heterojunction device was not prominent, indicating interface of graphene/GaN heterojunction device are more sensitive for UV photoresponse.

Chapter 5 discusses the fabrication of a graphene/β-Ga_2O_3 heterojunction Schottky diode to evaluate the DUV photoresponse properties. The device shows rectifying diode characteristic along with a photovoltaic action under DUV illumination. The open circuit photovoltage of 10 mV was observed along with an excellent photoresponsivity of 6.1 A/W at a bias voltage of -1.5 V. Further, the interface quality of a similar heterostructure is studied with and without DUV illumination. It is observed that the interface is free of residual impurities, however the current density-voltage characteristics shows hysteresis at a higher bias voltage under the DUV illumination. The transient photoresponse study shows faster photoresponse in photovoltaic mode, while significantly slower response is observed at a bias voltage considering the charge trapping/de-trapping phenomena. Thus, the graphene/β-Ga_2O_3 heterojunction device also shows electrical hysteresis at a bias voltage, which can be corelated with significantly sensitive graphene/GaN Schottky heterojunction.

Chapter 6 Overall conclusion and future scope of research.

Table of content

1. Introduction to UV photoresponsive devices 16
1.1 Background 16
1.2 Working principle and device structures 19
1.2.1 Schottky junction 22
1.2.2 p-n junction 23
1.3 Importance of heterojunction interface quality 26
1.4 Recent trends in UV photodetectors 27
1.5 Wide bandgap semiconductors for present work 29
1.6 Gallium nitride (GaN) 29
1.6.1 Introduction 29
1.6.2 Properties of gallium nitride 30
1.6.3 Electronic structure 31
1.7 Gallium oxide (Ga_2O_3) 32
1.7.1 Introduction 32
1.7.2 Properties of β-Ga_2O_3 33
1.7.3 Electronic structure of β-Ga_2O_3 34
1.8 Motivation and objective of present work 35
1.8.1 Major challenges 36
1.8.2 Objective of present work: 37
1.9 Organization of dissertation 40
1.10 References 42
2. Potential of graphene for integration with GaN and Ga_2O_3 semiconductors 45
2.1 Introduction and background of graphene 45
2.2 Structure of graphene 46
2.3 Properties of graphene 48
2.4 Characterization of graphene 49
2.4.1 Raman spectroscopy 50
2.5 Graphene based optoelectronic devices 52
2.6 Motivation of integrating graphene with semiconductors: 54
2.7 References 55
3. Ultraviolet light induced electrical hysteresis effect in graphene/GaN heterojunction 57
3.1 Introduction 57
3.2 Experimental section 59
3.3 Results and discussion 61
3.3.1 Raman spectroscopy 62
3.3.2 FESEM and EDX analysis 63
3.3.3 X-ray photoelectron spectroscopy 65
3.3.4 Current density– voltage characteristics (J-V) 68
3.3.5 Capacitance – voltage characteristics (C-V) 72

3.3.6 Band diagram:..... 73
3.3.7 Possible origin of impurities at the interface..... 74
3.3.8 UV spectroscopy..... 77
3.4 Conclusion..... 78
3.5 References..... 79
4. Formation of effective CuI-GaN heterojunction with excellent ultraviolet photoresponsive photovoltage..... 81
4.1 Introduction..... 81
4.2 Experimental section..... 83
4.3 Results and discussion:..... 84
4.3.1 Ball and stick crystal diagram:..... 85
4.3.2 Raman spectroscopy..... 85
4.3.3 X-ray diffraction analysis..... 86
4.3.4 Field emission scanning electron microscopy:..... 88
4.3.5 X- ray photoelectron spectroscopy..... 88
4.3.6 Current density – voltage characteristics (J-V)..... 90
4.4. Conclusion..... 99
4.5 References..... 100
5. Photovoltaic action in graphene-Ga_2O_3 heterojunction with deep-ultraviolet irradiation..... 103
5.1 Introduction..... 103
5.2 Experimental..... 104
5.3 Results and discussion..... 105
5.3.1 Raman spectroscopy..... 106
5.3.2 UV-visible absorption spectroscopy..... 107
5.3.3 Field emission scanning electron microscopy (FE-SEM):..... 108
5.3.4 X-ray photoelectron spectroscopy..... 109
..... 109
5.3.5 Current density -voltage (J-V) characteristics..... 111
5.4 Conclusions..... 116
5.5 References..... 118
6. Conclusion and future scope of research..... 120
6.1 Overall conclusion..... 120
6.2 Future scope of work..... 121
6.2.1. Modification of transfer process or direct growth of graphene..... 122
6.2.2 Investigation of suitable p-type semiconductor for GaN and Ga_2O_3 for photoresponse device applications..... 122
6.3 List of research achievements..... 123

List of Figures:

Figure 1.1 shows the electromagnetic radiation with focus on UV region [1-3] 17
Figure 1.2 shows photoconductive effect in a semiconductor. [3] 20
Figure 1.3 shows the types of device structures used for fabricating UV photodetectors devices.[3] 21
Figure 1.4 (a) shows the formation a typical Schottky junction (b) show the band diagram of a typical Schottky junction with band bending and Schottky barrier height. 23
Figure 1.5 shows the formation of a depletion layer the interface of typical p-n junction. 24
Figure 1.6 shows the wurtzite and zinc blend crystal structures of GaN as reported by Hangbo Qin *et at.* [63] 31
Figure 1.7 shows band structure of wurtzite GaN structure as reported by Michele Goano *et al.*[64] 31
Figure 1.8 shows crystal diagram of monoclinic beta-Ga_2O_3 (β-Ga_2O_3) 33
Figure 1.9 shows electronic structure (DOS) of gallium oxide as reported by Dong *et al.*[59] 34
Figure 1.10 (a) shows the UV absorption spectra of β-Ga_2O_3 used in the present study. (b) shows the corresponding Tauc's plot to calculate bandgap of the 4.53eV. 35
Figure 2.1 (a) shows the separation of single layer from graphite structure gives us a new material called graphene. 46
Figure 2.2 shows the honeycomb structure of graphene. 47
Figure 2.3 shows the band diagram of graphene, showcasing the zero-bandgap due to touching of valence and conduction band at Dirac point. 48
Figure 2.4 (a) shows the Raman spectra of the graphene/Si heterostructure shows the peaks for silicon as well as graphene. (b) shows the Raman spectra of graphene/Si heterostructure focusing on only graphene peaks. 51
Figure 2.5 ball and stick diagram of n-type GaN and graphene to form a unconventional Van der waal's heterojunction. 53
Figure 2.6 ball and stick diagram of β-Ga_2O_3 and graphene to form a unconventional Van der waal's heterojunction. 53
Figure 3.1 schematic diagram of low pressure chemical vapor deposition of graphene using polystyrene as carbon source. 60
Figure 3.2 shows the Raman spectra of the free standing GaN at various points. (b) shows the Raman spectra of graphene/GaN heterostructure (device 1) at various points. (c) shows the G and 2D peaks of graphene transferred on GaN. 62
Figure 3.3 (a) shows the FESEM image of the graphene/GaN heterostructure (Device 1) (b) shows the EDAX spectra of the graphene/GaN heterostructure signifying the presence of Ga, N, C and O elements in the sample. 64
Figure 3.4 (a) shows the XPS survey spectra of bare GaN and graphene/GaN heterostructure (Device 1) (b) C1s (c) O1s (d) Ga3d shows the core level peaks for the GaN and graphene/GaN heterostructure samples. 66
Figure 3.5 shows XPS spectra of device 2 (a) Ga3d peak of pristine GaN and graphene/GaN heterostructure with carefully transferred graphene film (b) C1s peak of the graphene for graphene/GaN heterojunction. 67

Figure 3.6 shows J-*V* characteristics of the device 1 for (a) voltage range of -2V to 2V in dark condition, (b) J-V curve in dark and UV light illumination (-2V to 2V). (c) J-V curve (-1V to 1V) in dark and UV illumination, presenting the hysteresis behavior. (d) J-V characteristics for -5V to 5V in dark. (e) J-V curve in dark and UV illumination (-5V to 5V). (f) J-V curve (-1V to 1V) in dark and UV illumination, presenting the hysteresis behavior (forward and reverse sweeps)..... 69
Figure 3.7 shows the J-V characteristics of device 2 i.e. graphene/GaN Schottky junction with a cleaner transferred graphene. (a) J-V characteristics in dark condition in applied voltage range of -1V to +1V, (b) log plot of J-V characteristics in dark, (c) J-V characteristics in dark and UV light in voltage range of -1 V to +1V, (d) log plot of J-V curve for dark and UV illumination conditions (forward and reverse sweeps)..... 70
Figure 3.8 C-V curve of graphene/GaN heterojunction devices with (a) interfacial impurities (device 1) (b) Device 2 with cleaner transferred graphene..... 72
Figure 3.9 shows (a) band diagram for graphene/GaN heterojunction Schottky junction with interfacial states under applied bias voltage (b) band diagram under UV illumination, where photogenerated carriers (electrons and holes) trapping/de-trapping occurs at the interface of graphene/GaN. 73
Figure 3.10 shows schematic diagram for transfer process employed for device 1 which showed high electrical hysteresis and low photoresponsivity..... 75
Figure 3.11 shows schematic diagram for transfer process employed for device 2 which showed high photoresponsivity and low electrical hysteresis..... 76
Figure 3.12 shows (a) UV absorption spectra of freestanding GaN and newly fabricated graphene/GaN heterojunction (b) Tauc plot to calculate optical bandgap of the pristine GaN.... 77
Figure 4.1 shows the experimental setup of the thermal evaporation chamber for deposition of CuI on GaN film. 83
Figure 4.2 shows ball and stick model of CuI and GaN crystal structure. 85
Figure 4.3 shows Raman spectra of the γ-CuI/GaN heterostructure at various points. 86
Figure 4.4 shows the XRD spectra of the thermally evaporated γ-CuI film on glass and γ-CuI/GaN heterostructure comparing with the JCPDS values, dominant (111) orientation of γ-CuI cubic crystal was obtained on GaN..... 87
Figure 4.5 shows the FESEM cross sectional view of γ-CuI/GaN heterostructure..... 88
Figure 4.6 shows XPS (a) survey spectra indicating the Ga3d peak of GaN, Cu2p and I3d peaks for CuI, (b) Ga3d peaks for the GaN and CuI/GaN heterostructure. (c) Cu ($2p^{3/2}$~932.2 eV and $2p^{1/2}$~952 eV) (d) I ($3d^{5/2}$~619.5 eV and 631 eV for $3d^{3/2}$) peaks of the CuI film on GaN. 89
Figure 4.7 (a) schematic diagram of the γ-CuI/GaN heterojunction device on Al_2O_3 substrate. (b) J-V characteristics under dark condition (inset shows the log plot). (c) J-V characteristics for higher applied bias voltage (-20V to +20V), presenting low reverse saturation current (inset shows the log plot), (d) probable energy band diagram for the γ-CuI/GaN heterojunction device. 91
Figure 4.8 J-V characteristics under dark conditions in the temperature range of 298 K to 373 K (a) for applied bias voltage of -2V to +2V and (b) -2V to 0V (c) Log plot in voltage range of -2V to +2V. 93
Figure 4.9 (a) J-V characteristic under dark and UV light illumination (100 mW/cm^2) conditions for the γ-CuI/GaN heterojunction device. (b) corresponding quantum efficiency (QE) curve. ... 94

Figure 4.10 J-V characteristics under UV illumination in the temperature range of (298 K -373 K) (a) -2V to +2V and (b) +1V to -2V (c) variation in open circuit voltage (V_{oc}) and short circuit current density (J_{sc}) with change in temperature (298~373 K) for the fabricated heterojunction. 96
Figure 4.11 J-V characteristics of the fabricated γ-CuI/GaN heterojunction under dark and UV illumination (a) forward and reverse sweep in voltage range of -2V to +2V in dark (b) forward and reverse sweep for bias voltage of -2V to 2V in dark and under UV light illumination (c) *J-V* curve showing no change in J_{sc} and V_{oc} in forward and reverse sweep measurements under UV illumination. 98
Figure 5.1 shows the schematic representation of fabrication of graphene/ β-Ga_2O_3 heterojunction. 105
Figure 5.2 Raman spectra of (a) single crystal β-Ga_2O_3 (b) monolayer graphene/β-Ga_2O_3 heterojunction. 106
Figure 5.3 (a) shows the UV-visible absorption spectra of single crystal β-Ga_2O_3 and graphene/β-Ga_2O_3 heterostructure. (b) Tauc plot of β-Ga_2O_3 and graphene/β-Ga_2O_3 to calculate optical bandgap of the heterostructure. 107
Figure 5.4 shows the FESEM image of the graphene/ β-Ga_2O_3 heterostructure. 108
Figure 5.5 shows the (a) XPS survey spectra (b) Ga 3d peak and (c) valence band maximum (VBM) for pristine β-Ga_2O_3. (d) Ga3d peak and (e) C1s peak for graphene/β-Ga_2O_3 heterostructure 109
Figure 5.6 (a) shows the J-V characteristics of the graphene/β-Ga_2O_3 heterojunction under dark condition in applied voltage range of -2V to +2V. (b) shows the corresponding log plot. 111
Figure 5.7 shows the J-V characterization (a) under UV light illumination in comparison under dark condition. (b) focusing in the applied voltage range of -0.03V to +0.03V displaying the photovoltaic action. 113
Figure 5.8 (a) shows the transient response of the device under 0V, -0.5V, -1V and -1.5V bias voltage. (b) probable energy band diagram of the graphene/β-Ga_2O_3 heterojunction device. ... 113
Figure 5.9 (a) shows the forward and reverse sweep under no DUV irradiation condition for applied bias voltage of -2V to +2V (b) forward and reverse sweep under DUV irradiation (254 nm) for applied bias voltage of -2V to + 2V 115

List of Table

Table 1: Comparative properties of Schottky and p-n junctions. 25

Table 2: Comparative Photoresponsivity (A/W) of various graphene-GaN heterostructures … 72

CHAPTER 1

1. Introduction to UV photoresponsive devices

1.1 Background

In the electromagnetic spectrum, the ultraviolet region (UV) is one of the strongest and most important of all radiations to be incident on the earth's surface. The UV region in general constitutes electromagnetic radiation in the wavelength range 100 nm to 400 nm and thus corresponds to high energy region i.e. from photon energies of 3.0 eV to 12.4 eV. The source of UV radiation on earth can be classified into two groups, one is natural and most abundant source i.e the sun and other one is the artificial source that can be generated using UV light emitting diodes, mercury lamps etc. The International commission on illumination has divided the UV region into three spectral bands namely UV-A (400-320 nm), UV- B (319-280 nm) and UV-C (279-100 nm).[1-3] In the UV region, the radiation in the wavelength range of 200-280 nm is called solar blind radiation as they are strongly absorbed by the ozone layer and hence are nonexistent or rather supposed to be nonexistent on the earth's surface. While UV rays in the range of 300 to 400 nm i.e UV-A region possess high penetration rate and can pass through ozone layer unabsorbed hence UV-A region is called as the UV window to the atmosphere. UV rays are of utmost importance for the survival and development of humans as well as flora and fauna. UV rays are extremely essential for the generation of Vitamin D in human body (about 90%) which is produced by the interaction of human's stratum corneum and UV radiation. However, excessive exposure of the UV rays of higher energies i.e. UV-A, UV-B and UV-C radiation is reported to be harmful for humans. Overexposure to UV radiation leads can lead to skin cancer and cataracts. [1,7]

In a nutshell, the ozone layer which is the protective cover over the earth's atmosphere attenuates UV radiation of higher energies i.e part of UV-B and UV-C regions, while UV-A radiations penetrate the ozone layer, which helps to warm the planet and balance the temperatures on earth to sustain life.

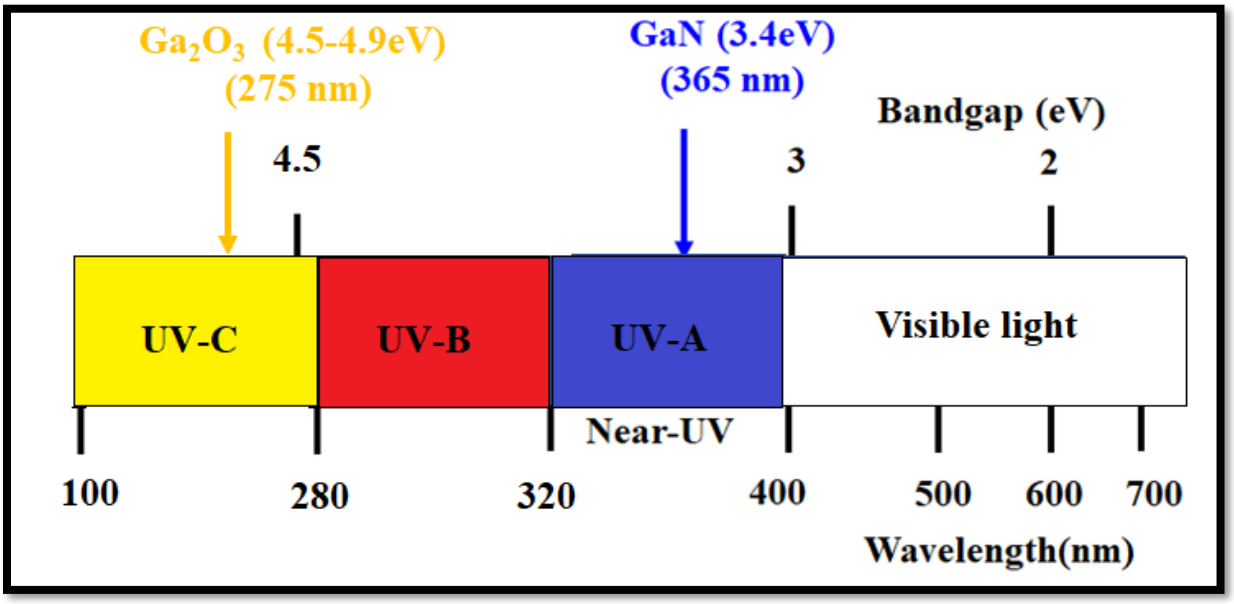

Figure 1.1 shows the electromagnetic radiation with focus on UV region [1-3]

The industrial revolution and unchartered air pollution have led to global warming and hence depletion of the ozone layer is observed. This results in unattenuated passage of UV-B and UV-C radiation into the earth's atmosphere. It is estimated that 1 % reduction of the ozone layer results in 2% increase in UV radiation on ground level which could lead to 3% increase in occurrence of skin cancer. [1] Thus, ozone layer and by extension UV rays helps in balancing the temperature of the earth to help sustain life and are extremely important for survival of mankind on this earth. Hence, there needs to be a balance in UV rays and corresponding ozone layer over earth's atmosphere as excess presence of harmful UV rays can prove to be disastrous for mankind. In this

regard, monitoring, detection and leak at ground level of UV rays is of critical importance. The monitoring of UV rays is achieved using UV photoresponsive devices.

The UV photoresponsive devices are defined as devices which can convert incident UV photon energy to electric current due to their bandgap corresponding to energies of UV radiations. Typically, UV photoresponsive devices use semiconductors which possess wide bandgap i.e above 3.1eV which corresponds to UV radiation. The high energies of UV radiations provide enough energy to an electron present in the valence band to overcome the high energy difference to jump to conduction band which leads flow of current in the external circuit. This phenomenon is possible in wide bandgap semiconductors only when the incident radiation possesses high energies to overcome the large bandgap between valence and conduction band of the semiconducting material. Wide bandgap semiconductors which are insensitive to visible and infrared radiations respond to only UV radiations corresponding to wide band gap. Thus, as this UV photoresponsive devices can detect UV radiations corresponding to their wide bandgaps they are also called as UV photodetectors. In the following sections, the UV photoresponsive devices will be addressed as UV photodetectors. Now as mentioned earlier, the high energies of UV radiation have rendered UV detection possible by only wide bandgap semiconductors. Typically, materials like III nitride, ZnO, SiC have been explored for their application as UV photodetectors due to their wide bandgaps.[2-3]Apart from the classification of wide bandgap semiconductors are a class of semiconductors called as ultra-wide bandgap semiconductors (UWBG) which possess ultra-wide bandgap and correspond to higher UV radiation and being insensitive to lower UV radiation. Some semiconductors which belong to UWBG materials are diamond and Ga_2O_3 with band gaps of 5.5 eV and 4.5-4.9 eV respectively. These UWBG semiconductors possess advantage of being

insensitive to UV-A, visible and infrared region of the electromagnetic spectrum and hence leads to forming of solar blind UV photodetectors.

In the recent times, other than the environmental monitoring, UV photodetectors have attracted various application in fields like chemical and biological analysis, internet of things (IOT), flame detection, astronomical studies (in radiation atmosphere) and communication technologies, military applications.[9-19] Considering the importance of UV monitoring along with the versatile applications in various fields the development of versatile and unconventional UV and solar blind UV photodetectors is of utmost importance in present times.[1,17] Now after discussing the background of the UV photodetectors, I will move on to explain the basic working principle of the UV photodetectors.

1.2 Working principle and device structures

The photoconductive effect is the prevalent mechanism in a photodetector wherein absorption of the incident UV light by wide bandgap semiconductor results in generation of electron-hole pairs when the incident photon energy (hv) is equal or greater than the bandgap (E_g) of the semiconductor. [2,3] This gives rise to photocurrent which is nothing but collection of generated electron-holes in external circuit. This mechanism happens mainly in three steps:

(i) Absorption of incident UV light to generate electron - hole pairs.

(ii) Separation of photogenerated (e^--h^+) through a transportation process.

(iii) Collection of photogenerated electrons and holes in the form of photogenerated current.

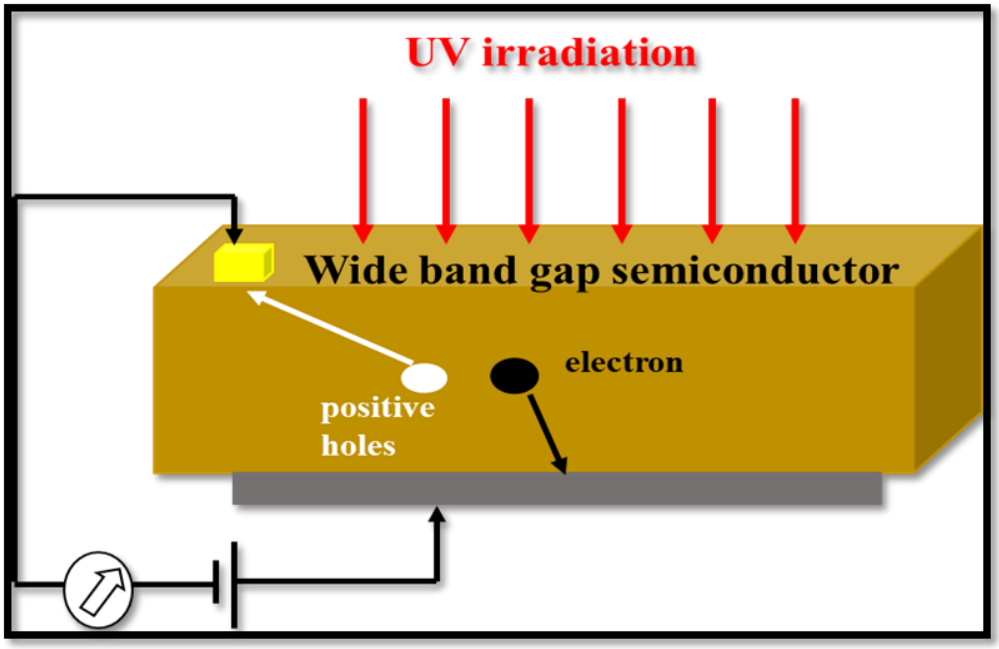

Figure 1.2 shows photoconductive effect in a semiconductor. [3]

The photocurrent can be generated by separation of the electron-holes pair by applying external bias voltage or generating an external built-in electric field. Thus, UV radiation detection is dependent on the bandgap of the material. If the radiation energy is equal or greater than the bandgap of material, photoconductive principle kicks in and a photocurrent is generated which is detected in the external circuit.

Further, the UV photodetectors are classified into two categories

a) Photoconductive detectors

b) Photovoltaic detectors

While both the types of photodetectors work on photoconductive effect, they are separated by their device structures. Figure 1.3 shows the classification and their subsequent types of device structures.

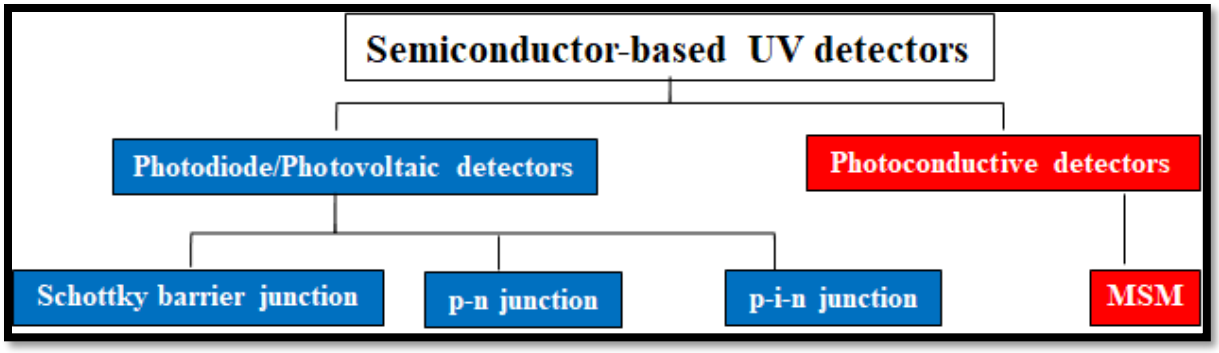

Figure 1.3 shows the types of device structures used for fabricating UV photodetectors devices.[3]

a) Photoconductive detectors:

Photoconductive detectors are made by a simple semiconductor with ohmic contacts. This working principle is the same as explained earlier and shown in figure 1.2. The photoconductive detectors are characterized by easy operation, simple structures along with low efficiency and slow response. [3]

b) Photovoltaic detectors:

The photovoltaic UV detectors also work on photoconductive effect principle wherein the incident UV radiation will generate electron hole which when separated leads to generation of photocurrent in external circuit. The photovoltaic UV detectors differ from photoconductive UV detectors in the structure of device i.e in photovoltaic UV detectors the semiconductors forms a junction with same materials (homojunction) or with a different material (heterojunction) which forms built-in field and leads to separation of electron hole pairs to generate photocurrent. While in photoconductive UV detectors only single semiconductor material is used with metal contacts.

The photovoltaic UV detectors can form various device structures as follows:

1) Schottky barrier
2) p-n junction
3) p-i-n junction

Since the Schottky and p-n junction are the most investigated UV photodetectors, I will discuss in detail the basics of Schottky and p-n junction comparing their properties as following.

1.2.1 Schottky junction

Schottky barrier junctions are one of the most used diodes in photodetectors application. A Schottky barrier is formed between a semiconductor and a semi-transparent metal contact. By Mott-Schottky theory, there is a presence of electrostatic barrier between the semiconductor and metal which is due to difference in work functions ($q\emptyset_B$) of semiconductor and metal. This gives rise to the rectifying property in Schottky junctions. The formation of Schottky junction is characterized by band bending at the interface due to potential barrier and is given by the difference between work function of metal and semiconductor [3]. Further, the band bending and electrostatic barrier leads to formation of Schottky barrier height which is of utmost importance in Schottky junctions. The Schottky barrier height is a function of the metal and semiconductor and hence with different metal contacts will form different Schottky barrier height with same semiconductor. In n-type semiconductor/Schottky junction, the barrier height is against the flow of electrons between Schottky junction while in p-type semiconductor/Schottky junction, the barrier height is against the flow of holes. Figure 1.4 shows the band diagram between the n-type semiconductor based Schottky junction. The Schottky junctions are characterized by majority charge carrier transport as there in no diffusion of charge carriers, whereas diffusion of charge carriers across the junction is observed in a p-n junctions. Hence, the charge transport properties in a Schotkky junction is dependent on the heterojunction interface and surface states of semiconductors. For smooth transition of charge carriers, the interface of the Schottky jucntion should be free of surface

defects and impurties. Further, Schottky jucntions possess various advantages such as high quantum efficiency, high responsitvity and low turn on voltage.[3]

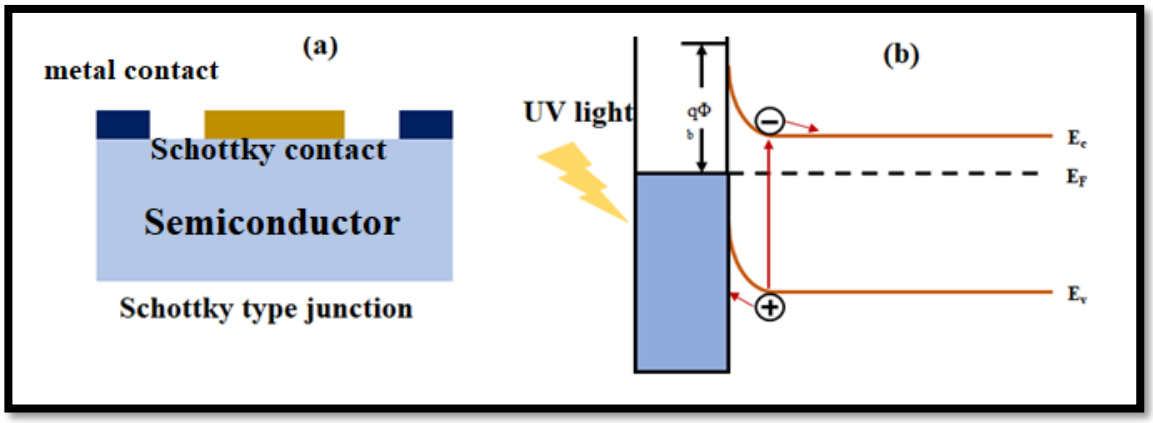

Figure 1.4 (a) shows the formation a typical Schottky junction (b) show the band diagram of a typical Schottky junction with band bending and Schottky barrier height.

However, it does have some disadvantages of metal contact thickness, loss of UV radiation to thick metal contacts, surface state affecting the charge carrier transport.[3] Nevertheless, Schotkky contact is one of the widely used device structure for UV photodetectors with conventional metal electrodes. In this study, I have studied the GaN and Ga_2O_3 based Schottky junctions with graphene and their UV photoresponsivity.

1.2.2 p-n junction

A p-n junction is formed by integration of a p-type semiconductor and a n-type semiconductor to form either a p-n homojunction or a p-n heterojunction. In p-n junction, the depletion region is instantaneously formed with charge diffusion. In the p-n heterojunction, the n-type semiconductor has excess of electrons with respect to p-type semiconductor and p-type of semiconductors have excess of holes with respect to n-type semiconductor and thus when a p-n junction is formed

electrons from n-type diffuse into p-type and vice versa.[3] This leads to the formation of a depletion region which is defined as the region at the interface of the junction where generated majority charge carriers are diffused away. Further, when UV irradiation with energy equal or greater than the band gap of the material is incident, it creates additional electron-hole pairs on both sides of the junction. After the equilibrium is attained at the depletion region the electron hole pair stop to diffuse into depletion region and start to get separated and generate a photocurrent which is detected at the external circuit. The band diagram and device structure of a typical p-n junction given in figure 1.5.

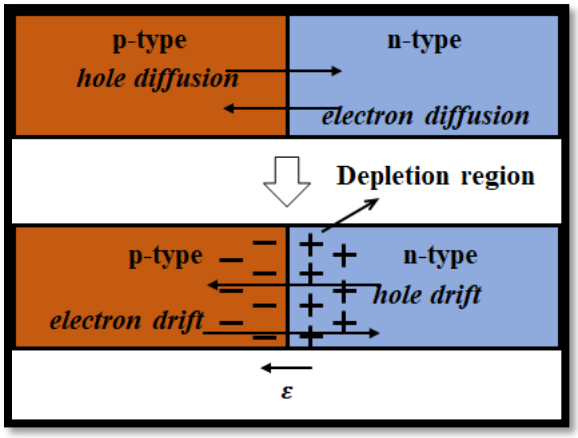

Figure 1.5 shows the formation of a depletion layer the interface of typical p-n junction.

The charge transport phenomenon in a p-n junction is due to minority charge carriers as the majority charge carriers are diffused in the depletion region. This results in less effect of interface quality on the charge transport across the interface junction. [2-3] This separates the p-n junction from the Schottky junction. Further, p-n junctions are observed to have higher turn on voltage than of Schottky junctions. Schottky barrier photodiodes have been studied quite extensively and found application as UV detectors. The following table presents some advantages of Schottky junction

devices over p-n junction photodiodes: fabrication simplicity, absence of high-temperature diffusion processes, and high speed of response

Table 1 shows the comparison of properties between Schottky and p-n junction. [2,3]

Property	Schottky junction	p-n junction
1) Charge carrier	**Majority charge transport due to absence of diffusion**	**Minority charge transport due to diffusion.**
2) Effect of surface states	**Surface state effect on charge carrier transport**	**Not applicable**
3) Turn on voltage	**Low turn on voltage**	**High turn on voltage**
4) Switching speed	**High switching speed**	**Low switching speed**
5) Loss of radiation	**Loss of incident radiation due to metal contact thickness**	**No such issue in p-n junction**

Thus, as discussed above, both Schottky and p-n junctions have their own advantages and disadvantages. However, they are the most studied device structures for UV photodetector application and possess collective advantages over other type of junctions such as MSM (metal - semiconductor-metal) based p-i-n junction in respect to ease of fabrication, easy operation, high responsivity, less loss of UV irradiation to metal contacts etc. Hence, for the present research thesis, I have worked on both Schottky junction and p-n junctions based on GaN and Ga_2O_3 semiconductors. The next section sheds light on the importance of interface quality on device performance of the Schottky and p-n junctions.

1.3 Importance of heterojunction interface quality

We have discussed about the Schottky and p-n junction devices. The major difference between the two device structures is that in Schottky junction charge carrier transport is due to majority carriers. While on the other hand, in the p-n junction there is formation of a depletion region which leads to charge carrier transport due to minority carriers. Hence, the Schottky junctions are highly sensitive to the surface states of semiconductor and the charge transport phenomenon is affected due to presence of surface states. Thus, interface quality i.e. the presence or absence of organic or inorganic impurities at the interface of the junction will directly affect the device performance. As the majority charge carriers are responsible for current generation, if the interface has any impurities which subsequently implies poor formation of Schottky contact will result in poor transport of charge carriers and hence the device performance will be directly affected. In p-n junction the charge transport phenomenon is due to minority carrier and hence the surface state effect does not affect the quality of p-n device performance. However, for both types of junction structure, the device performance is quite affected by the presence of impurities at the interface. The interfacial impurities act as trap sites for the charge carriers and subsequently lead to trapping and de-trapping of charge carriers at the interface and could lead to loss of photocurrent or may induce hysteresis in the device. The latter phenomenon can be exploited for memory device application. [61] However, for the UV photodetector application, the presence of impurities and trapping and de-trapping phenomenon is not good for device performance. Hence, in recent times where graphene based unconventional Schottky UV photodetectors are being researched, interface quality is of utmost importance for ensuring the better device performance. Further, if the residual interfacial impurities are present at the heterojunction the device performance will be negatively affected. In this regard, the present work explores the role of interface quality of various fabricated

Schottky and p-n junction using simple UV illumination irradiation and monitoring the *J-V* characteristics to check the device performance. The next section will talk about the recent trends in UV photodetectors and the wide bandgap semiconductors chosen for the present study.

1.4 Recent trends in UV photodetectors

Due to attractive properties of silicon (Si) like optimum bandgap, low cost, abundance in occurrence, silicon-based UV photodetectors are being extensively used for UV photodetector application. However, Si based photodetectors possess limitation in detection due to their narrow bandgaps, which correspond to near UV and infrared region. The narrow band gaps result in part of energy being used in heating which results in low quantum efficiency. [3,19] Further, Si based photodetectors has shown to have low efficiency as well as limit in working at higher temperature. [3] This negative aspect of Si based UV photodetectors has led exploration for other novel UV photodetectors which overcome this limitation. In this prospect, wide bandgap semiconductors like GaN, SiC, ZnO, Ga_2O_3 and diamond have been extensively explored for the solar blind UV photodetector application.[1-3] Their wide bandgap (GaN, ZnO , SiC) and ultrawide bandgap (Ga_2O_3) correspond to the UV and deep UV region respectively which opens the possibilities of solar blind UV photodetectors and reduces the chance of losing the incident energy to heating thus resulting in high quantum efficiency and hence overcomes some of the limitations of the Si based photodetectors. Moreover, these semiconductors possess high chemical and thermal stability thus making it possible for application in harsh environments such as outer space. Among the wide bandgap and ultrawide bandgap semiconductors due to their attractive properties GaN and Ga_2O_3 have emerged as the ideal candidate to fabricate UV and deep UV photodetectors respectively. The advancement of nanotechnology has made it possible for fabrication of various high performing UV photodetectors. [3] Nanomaterials bring a lot of versatile properties such as

tunability of band gap, high surface to volume ratio, extraordinary electrical, mechanical and optical properties. [3-10] Hence, integration of nanomaterials specifically 2D materials like graphene, TMDC's with wide bandgap semiconductors is considered a new horizon for UV photodetector application. Specifically, integration of graphene with various compound semiconductors has led to fabrication of unconventional transparent Schottky devices. [29,59,62] Graphene due to its high transparency and zero bandgap forms transparent Schottky junction with the semiconductors and cuts out the disadvantages of UV irradiation blockage in conventional metal Schottky contacts. Kalita et al have reported on temperature dependent photovoltaic action in graphene/GaN Schottky junction [58], while Kong *et al* have reported on the fabrication of graphene with Ga_2O_3[13]. Furthermore, conventional UV photodetectors have been using external power source, typically a battery for its operation. [62] The use of battery is highly inefficient, expensive, is not environmentally friendly, hazardous to humans, difficult to use and hence, to overcome this disadvantage vast amount of research is done to achieve self-powered UV photodetector operations. [62] It is expected that future application like IOT sensors, flexible and wearable devices will require high performing, low maintenance and self-powered UV photodetectors. In this regard, various reports are available on photovoltaic based i.e Schottky and p-n junction UV photodetectors to achieve high performance. Thus, in the present times where world is moving to smart device's and reducing dependence on non-renewable energy sources with environment conservation in mind, self-powered high performing UV photodetectors is the answer to sustain the needs of tomorrow. In this regard, the present thesis explores the possibility of fabricating the self-powered Schottky and p-n junctions and further exploring individual device performance by analyzing the heterojunction interface by simple electrical hysteresis technique. The further section discusses about the chosen wide bandgap and ultrawide bandgap semiconductors.

1.5 Wide bandgap semiconductors for present work

As mentioned in section 1.1 the bandgap of the semiconductors corresponds to specific UV region of the electromagnetic radiation. While wide bandgap semiconductors comprise of materials possessing bandgap of 3.1eV and above. The present thesis has explored two different wide bandgap semiconductor materials whose bandgap correspond to UV-A region and deep UV i.e UV-C region of the electromagnetic spectrum. In this regard, Gallium Nitride and Gallium oxide with a bandgap of 3.4 eV and 4.5-4.9 eV correspond to UV-A and UV-C region respectively. Gallium oxide due to its ultrawide bandgap is insensitive to UV-A, UV-B and the visible region radiation which makes it a unique semiconductor which can be used in fabrication of UV-A and UV-B transparent deep UV photodetectors. The next section discusses about the structure and properties of the chosen wide bandgap semiconductor i.e GaN and ultra-wide bandgap semiconductor Ga_2O_3.

1.6 Gallium nitride (GaN)

1.6.1 Introduction

Gallium nitride belongs to wide band semiconductor family as it possesses a wide bandgap of 3.4 eV. The wide bandgap GaN corresponds to UV-A region of the electromagnetic radiation. Among various wideband gap semiconductors GaN has emerged as a preferred candidate due to its attractive electronic properties such as direct bandgap, tunability of band gap, high breakdown voltage, high carrier mobility.[20-29] Further, GaN stands out among other wide bandgap semiconductors as it shows high stability towards high temperature, ionizing radiation and chemicals and hence can be used in applications involving harsh conditions.[60] This has led to extensive research of GaN for various applications like UV photodetectors, light emitting diodes (LED), solar cells, high mobility transistors, high frequency power devices.[31-34] Gallium Nitride in its native form is a n-type semiconductor due to nitrogen vacancies and hence opens possibility

of fabricating p-n heterojunction by integration with various suitable p-type semiconductors. The n-type GaN has also been explored to form Schottky junction with conventional metal contacts. The GaN based Schottky devices have been greatly explored for application in high response diodes. [35-39] While recently significant attention has been given to fabricate unconventional GaN Schottky junction by integration of graphene. Graphene with its zero bandgap behaves as a metal due to free movement of electrons along its sheet and thus when integrated with GaN forms a Schottky junction. Recently, gallium nitride has also been integrated with transition metal chalcogenides (TMDC's) which are direct bandgap in visible range materials to form p-n and n-n heterojunctions. Thus, GaN has been successfully explored with Schottky junctions, van der Waal's heterostructures as well as p-n heterojunction.[39-42] In this regard, the present thesis explores the interface properties of the GaN based Schottky devices as well as the fabrication of novel GaN based p-n heterojunction. The below section talks about the properties of GaN.

1.6.2 Properties of gallium nitride

In general, group III- nitrides exist in both wurtzite and zinc blend structure. Figure 1.6 shows the wurtzite and zinc blend crystal structures. However, under normal conditions wurtzite structure is thermodynamically more stable than zinc blend structures. The lattice constants for wurtzite structure of GaN are (a = 3.189 Å and c = 5.186 Å), however some deviations have been reported in lattice constants due to growth process.[43] Due to lack to native substrates GaN is usually grown on foreign substrates like SiC, sapphire despite 17% mismatch in crystal lattice. Further, n-type and p-type conductivity is obtained by controlled inducing Si and Mg impurities and in the present work we have used Si doped n-type GaN. Figure 1.7 shows the band structure for wurtzite GaN.

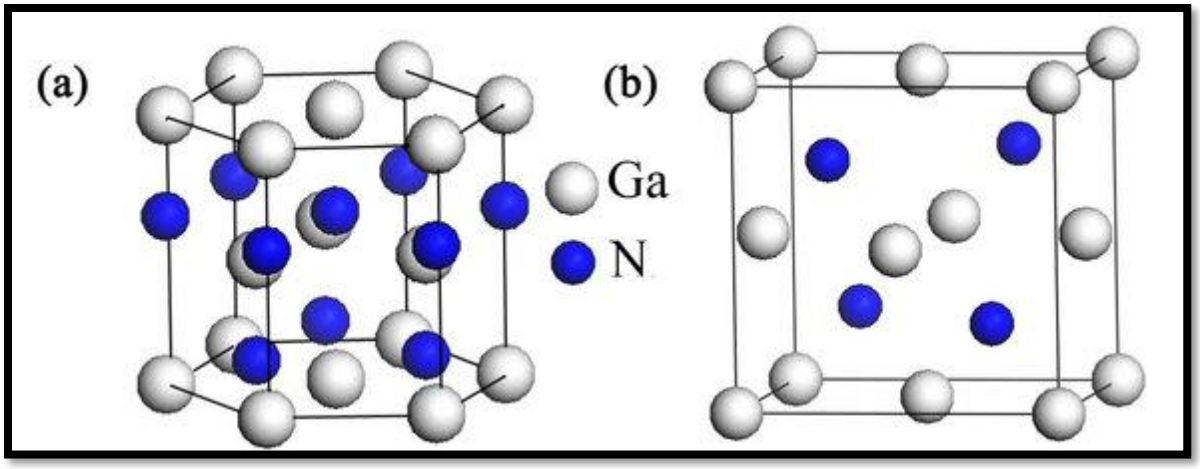

Figure 1.6 shows the wurtzite and zinc blend crystal structures of GaN as reported by Hangbo Qin *et at.* (63)

1.6.3 Electronic structure

It is observed that the valence band and conduction band of wurtzite GaN meet at the Γ point indicating direct transition bandgap. Further, the bandgap of the GaN is reported to be 3.4 eV which classifies it as wide bandgap semiconductor. Further, the GaN possess varies attractive electrical properties such as a large electrical breakdown field of 1.2–1.8 × 10^6 V cm^{-1}, high electron mobility of 1000 cm^2 V^{-1} s^{-1}.

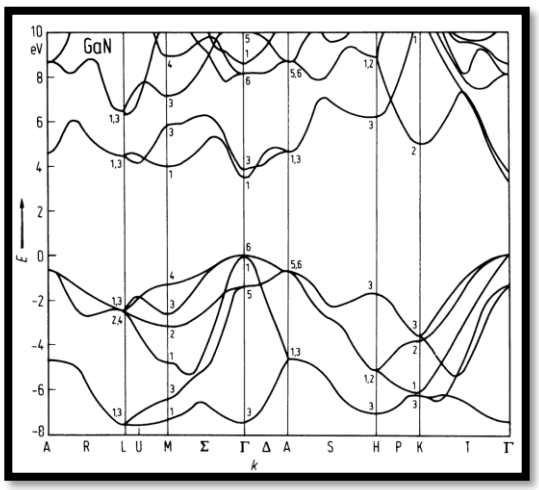

Figure 1.7 shows band structure of wurtzite GaN structure as reported by Michele Goano *et al.*(64)

Thermal conductivity of GaN is 130 $Wm^{-1}K^{-1}$ which is quite high and allows high temperature operations of GaN. [25-29] In this regard, GaN has emerged as an ideal candidate for various optoelectronic and power device applications.

1.7 Gallium oxide (Ga_2O_3)

1.7.1 Introduction

Gallium oxide (Ga_2O_3) belongs to a group of ultrawide bandgap semiconductors as it possesses bandgap of 4.5 eV to 4.9 eV.[44-47] The ultrawide bandgap of gallium oxide corresponds to deep ultraviolet region i.e UV-C region of the electromagnetic radiation. This invariantly separates Ga_2O_3 from other conventional wide bandgap semiconductors like GaN and SiC. The solar blind ultraviolet photodetectors are of great importance as they can accurately detect a weak signal of solar blind irradiation (200-280 nm) at earth's ground level. Ga_2O_3 has a detection range of 250-275 nm and is insensitivity to visible and infrared radiation makes it a perfect candidate for deep ultraviolet region photodetector. Thus, Ga_2O_3 has attracted a lot of research for its possible application in power electronics, transparent electronic devices, sensing, space application.[46-50] Gallium oxide is most valuable for its application as deep UV photodetector as it is blind to wavelengths above 280 nm thus making it a solar blind photodetector. Ga_2O_3 also possesses other properties such as chemical and thermal stability thus making it a good candidate for working in harsh conditions. In this regard, Gallium oxide photodetectors have been reported fabricated using nanostructures, thin films as well as single crystal. As early as 2008, Oshima *et al* have reported on the vertical Ga_2O_3 Schottky junction with a high photoresponsivity of 2.6-8.7 A/W.[46] Further, Ga_2O_3 has been studied using various types of device structure like metal-semiconductor-metal, Schottky barrier photodiode, p-n, n-n junction.[57-58] In this regard, fabrication of unconventional Ga_2O_3 based photodetectors is an interesting prospect.

1.7.2 Properties of β-Ga_2O_3

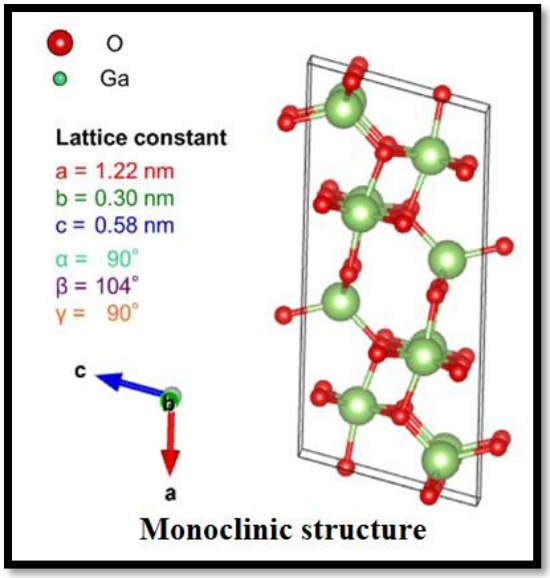

Figure 1.8 shows crystal diagram of monoclinic beta-Ga_2O_3 (β-Ga_2O_3)

Figure 1.8 shows the monoclinic structure β-Ga_2O_3 with lattice constants a= 1.22 nm, b= 0.30 nm, c= 0.58 nm. Ga_2O_3 exists in its 5 polymorphs mainly α-Ga_2O_3, β-Ga_2O_3, γ-Ga_2O_3, δ-Ga_2O_3, ε-Ga_2O_3 of which the β form is the most stable polymorph in the whole temperature range. All the polymorphs transform to β-Ga_2O_3 above the temperature range 750-900 ℃ thus β-Ga_2O_3 has attracted great attention than other polymorphs due to its stability. [3] However, among all the polymorphs the β-Ga_2O_3 has poor thermal conductivity. Thermal conductivity is dependent on the crystal direction due to crystalline anisotropy. Along the [100] plane the thermal conductivity is 13.6 W/m/k while along the [010] direction the it is 22.8 W/m/k. Typically, the thermal conductivity of gallium oxide is about one order lesser than GaN. Further, β-Ga_2O_3 shows a critical breakdown field of 8 MV/cm, good electron mobility of 300 cm^2/Vs and high chemical stability. (52-58)

1.7.3 Electronic structure of β-Ga_2O_3

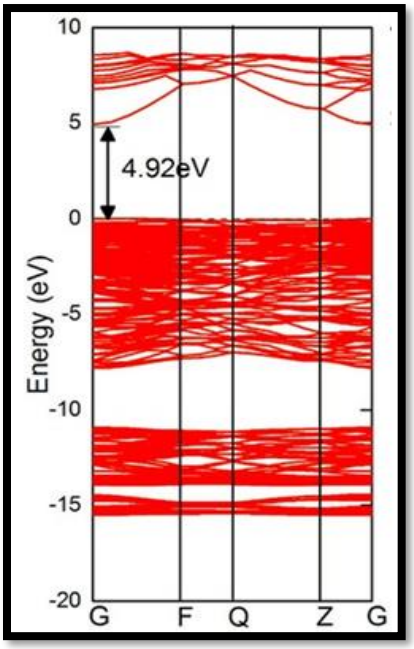

Figure 1.9 shows electronic structure (DOS) of gallium oxide as reported by Dong *et al*.[59]

Figure 1.9 shows density of states (DOS) of the β-Ga_2O_3 as reported by Dong et al.[59] The direct bandgap is observed to be 4.92 eV as both conduction band and valence band is situated at G point. Further, the delocalized Ga 4s derived states make up the conduction band giving rise to disperse band with a low electron effective mass. Concurrently formation of valence band occurs by hybridization occupied O $2p^6$ with Ga 3d, 4p, 4s orbitals. [59] It is generally accepted that β-Ga_2O_3 has a direct bandgap in the range of 4.5 eV to 4.9 eV. In this study, we have reported a band gap of 4.53 eV for β-Ga_2O_3 which was calculated by Tauc plot. Gallium oxide (β-Ga_2O_3) owing to its ultrawide bandgap is highly transparent till UV-C region. Figure 1.10 (a) shows the UV absorption spectra for β-Ga_2O_3 used in the present study. Absorption edge is observed in the wavelength range of 190-280 nm, which agrees with the theoretical values. This absorption can be attributed to

excitation of electrons from valence band to conduction band due to overlapping of incident photon energy and the bandgap of β-Ga_2O_3.

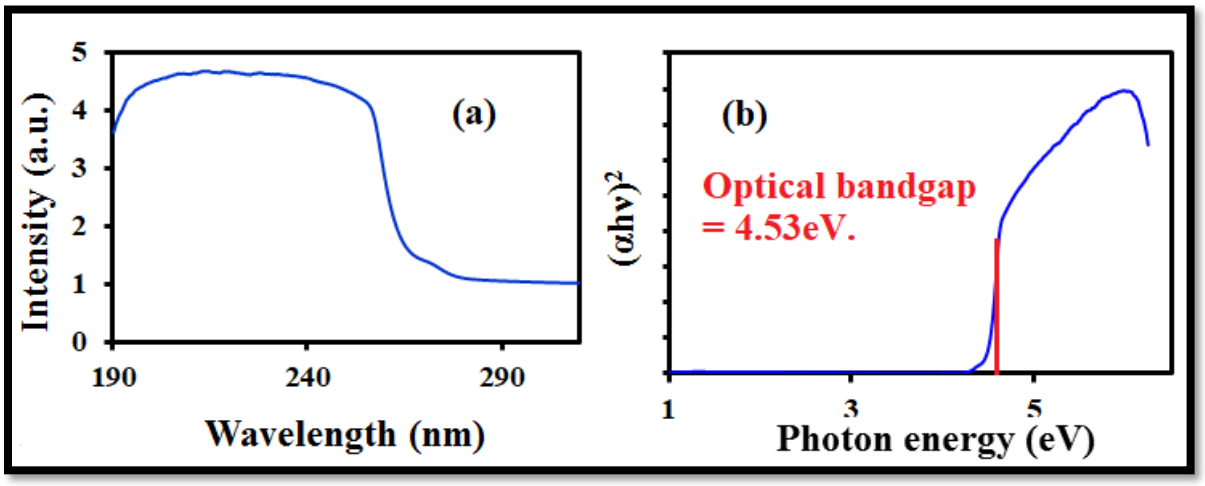

Figure 1.10 (a) shows the UV absorption spectra of β-Ga_2O_3 used in the present study. (b) shows the corresponding Tauc's plot to calculate bandgap of the 4.53eV.

Figure 1.10 (b) shows the Tauc plot for β-Ga_2O_3. The bandgap of the materials was calculated to be 4.53eV which agrees with the bandgap range 4.5eV- 4.9 eV reported in literature. Thus, β-Ga_2O_3 is completely transparent to visible and near UV irradiation making it a solar blind semiconductor.

1.8 Motivation and objective of present work

The UV photodetector is an exciting field with wide range of potential application but still it has some major challenges which have rendered fabrication of high-performance UV photodetectors. Some of the major challenges are listed below and the present thesis aims to address this issue with the hope that this research work will contribute to fabrication of good self-sustaining UV photodetectors.

1.8.1 Major challenges

1) **Choice of semiconductor:**

Since UV radiation monitoring at ground level is of utmost importance to detect leak in ozone layer as well various potential application of the UV photodetector devices, the common dilemma is choosing of ideal semiconductor. Currently UV photodetectors with detection of specific UV region i.e UV-A and UV-C with transparency to other radiation of electromagnetic spectrum are in high demand. Further, device is also expected to have good electronic properties along with good thermal, chemical and ionization stability for application in various fields like space communication environmental monitoring and should be a possible candidate to fabricate both Schottky and p-n junctions with suitable materials.

2) **Disadvantages of conventional Schottky:**

As mentioned in section 1.2, the Schottky junctions are extensively studied for various UV photodetector applications. Schottky UV photodetectors possess various advantages such as high responsivity, low response time, high quantum efficiency and ease of operation. Typically, Schottky UV photodetectors are fabricated using conventional metal contacts like Au. However, this conventional Schottky junction with metal contacts possess disadvantages like loss of incident irradiation due to high absorption coefficient of metal electrodes and the need to make them semitransparent to achieve good device performance along with surface state effect which is observed in Schottky junction due to charge carriers being majority charge carriers.

3) **Role of interface quality**

The fabrication of heterojunctions generally involves complex fabrication process with use of various chemical and destructive techniques. As mentioned in section 1.3, the Schottky junction is highly sensitive to surface states in the semiconductor and the device performance is dependent on it. Further, due to complex fabrication processes, chance of organic impurities being introduced in the heterojunction interface is quite high and this could affect device performance. Further, in various 2D/3D heterojunction the charge carrier transport mechanism and interaction of charge carriers with interface impurities is important to understand in order to achieve high performance devices.

4) **Self-powered application:**

The conventional UV photodetectors use an external battery for working which makes it very difficult to use and for maintenance. Further, this limits the use of UV photodetector for remote sensing and various other application Moreover, the batteries use harmful chemicals and are not environment friendly. Hence, the future application of UV photodetectors demands self-powered photodetectors with easy operation and low maintenance with extreme weather stability.

1.8.2 Objective of present work:

a) The present thesis has tried to address above mentioned challenges in the UV photodetector field. To overcome the 1st challenge of we have chosen two semiconductors which have different bandgaps and correspond to two different regions of UV region. GaN with a bandgap of 3.4 eV corresponds to UV-A region and possesses excellent electronic properties with potential applications. It has emerged as one of the most important semiconductors in the wide bandgap semiconductor family. Further, beta-gallium oxide

with a band gap of 4.5-4.9 eV corresponds to UV-C region and is insensitive to UV-A, UV-B and visible radiations and has found many applications for deep UV (DUV) photodetector application due to its robust and excellent electronic properties. The high chemical and thermal stability of β-Ga_2O_3 has made it a leading candidate in ultra-wide bandgap family. Both semiconductors possess high thermal, chemical and ionization stabilities. Moreover, besides favorable properties both the semiconductors have n-type conductivity which opens the possibility of fabricating both Schottky and p-n junctions with suitable materials. Hence in this present work, I have fabricated GaN based Schottky and p-n devices. Further, β-Ga_2O_3 based Schottky device is also fabricated to make a visible, UV-A and UV-B light transparent DUV photodetector.

b) To overcome 2nd challenge, i.e. drawbacks of conventional Schottky junction metal contacts, graphene which is a 2-dimensional one atom thick nanomaterial with zero bandgap has been integrated with both GaN and β-Ga_2O_3 to form unconventional Schottky junctions. Graphene with its attractive electronic properties is an ideal candidate for fabrication of transparent UV Schottky junction as graphene has exceptionally high transparency of 97.7% and hence overcomes the challenge faced by conventional metal contacts in Schottky junctions. Thus, this thesis explores the integration of graphene with GaN and β-Ga_2O_3 and studies their device properties.

c) While there have been previous reports on integration of graphene with GaN, understanding the interface quality of the heterojunction is quite important to fabricate high performance devices. As described in earlier sections, Schottky junction are especially sensitive to interface states due to being majority charge carriers and since graphene is usually transferred on GaN substrate by wet chemical transfer method, the chances of

introducing impurities in the heterojunction are high, which makes the graphene based Schottky junctions prone to be poor device performance. This motivated me to study the interface junction and effect of impurities on charge carrier transport in graphene/GaN heterojunction. While interface analysis of heterojunction has been reported using transient spectral response, I have attempted to analyze the interface using UV light illumination to check electrical hysteresis behavior. Thus, this thesis has explored the role of interfacial impurities on charge transport carriers in Schottky junctions and further in p-n junction device. Further, the charge carrier transport mechanism is explored for better understating the 2D/3D heterojunction Schottky and p-n heterojunction devices.

d) Finally, since self-powered UV photodetectors are in great demand, I have explored the possibility of self-powered operation in fabricated GaN and Ga_2O_3 based Schottky and p-n heterojunction devices. While graphene/GaN heterojunction was already reported for photovoltaic action and hence self-powered working mode by Kalita *et al.*, I have explored the possibility of the GaN based p-n heterojunction with temperature dependent characteristics as GaN possess high thermal stability. Further, fabricated graphene/Ga_2O_3 based Schottky junction are also explored for photovoltaic action and self-powered operation.

Thus, the present thesis work focuses on fabrication and studying of GaN and β-Ga_2O_3 based ultraviolet photo responsive by integrating them with novel 2D material like graphene as well wide bandgap inorganic semiconductor. It also explored the role of interfacial impurities using UV illumination on the device performance and possibility of self-powered operation. Finally, the heterojunction studied are as follows:

1) Graphene/n-type GaN Schottky junction.
2) p-type γ-CuI/n-type GaN heterojunction
3) Graphene/n-type β-Ga_2O_3 Schottky junction.

Thus, the present thesis attempts to overcome the major challenges in the UV photodetector field.

1.9 Organization of dissertation

This thesis contributes to the fabrication and characterization of GaN and Ga_2O_3 heterojunctions and studying role of quality of heterojunction interface on the device performance. Effective fabrication of unconventional Schottky UV and DUV photodetector is achieved by integration of graphene with GaN and β-Ga_2O_3 and the role of interface states and interfacial impurities has been explored with an attempt to understand the charge carrier transport mechanism in presence of interfacial impurities and its effect on the device performance. Finally, the thesis explored the fabrication of GaN based p-n heterojunction for self-powered UV photodetector applications.

Chapter 1 describes background of UV photoresponsive devices and gives a detailed account of various structures used in UV detectors. It also discusses the importance of role of interface quality in junctions and along with recent trends in UV photodetectors by introducing chosen semiconductors for the present study. Finally, it establishes the motivation and objective of present work.

Chapter 2 introduces the wonder material i.e graphene. It talks about structure, properties and band structure of graphene and why is it important for integration with various semiconductor materials.

Chapter 3 discusses the possibility of integration of graphene with GaN. The role of interfacial impurities associated along with its substantial effect on the device performance is studied in detail.

It also sheds light on charge carrier transport mechanism in the fabricated heterojunction and how this work can be utilized to study interface quality of other heterojunctions.

Chapter 4 Focuses on the fabrication of γ-CuI/GaN heterojunction by thermal evaporation technique. UV photoresponsive characteristics of the device are elucidated with temperature dependent transport behavior analysis. This work suggests that a p-type halide can be very effective on GaN for developing novel heterojunction device.

Chapter 5 discusses the possibility of fabrication of a monolayer graphene/Ga_2O_3 heterojunction for DUV photodetector application. β-Ga_2O_3 with wide bandgap of 4.5-4.9 eV belongs to solar blind UV-C region of the electromagnetic radiation spectrum. The formation of unconventional Schottky junction is extended to explore possibility of self-powered working mode of graphene/Ga_2O_3 Schottky junction.

Chapter 6 Summarizes the whole thesis and discusses future scope of research.

1.10 References

1) H. Chen, et al., Mater. Today, vol.18, no.9 , pp. 493-502, 2015.
2) B. D. Boruah, Nanoscale Adv., vol. 1, pp. 2059-2085, 2019.
3) Y. Zou et al., Sensors, vol. 18, p. 2072, 2018.
4) R. Miller et al., preprint arXiv:1809.07396, 2018.
5) L. Peng, L. Hu and X. Fang, Adv. Mater., vol. 25, no.37, p. 5321, 2013.
6) L. Su et al., Small, vol. 13, no. 45, p. 1701687, 2017.
7) F Omnès et al., Proceedings Gallium Nitride Materials and Devices II, Volume 6473, 64730E, 2007.
8) T. Zhai et al., Sensors, vol. 9, no. 8, pp. 6504-6529, 2009.
9) H. K. Biesalski et al., Arch Biochem Biophys, vol.389, no.1, pp. 1-6, 2001.
10) Z. Xu et al., IEEE Commun. Mag., vol. 46, no. 5, pp. 67-73, 2008.
11) Rogalski, Opto-Electron. Rev., vol. 4, p. 13, 2015.
12) L. Sang et al., Sensors, vol. 13, no. 8, pp. 10482- 10518, 2013.
13) W.-Y. Kong et al., Adv. Mater., vol. 28, no. 48, pp. 10725-10731, 2016.
14) T. Oshima et al., Jap. J. Appl. Phys., vol. 48, no. 1R, p. 011605, 2009.
15) J. L. Pau et al., Applied Optics, vol. 45, no. 28, pp. 7498-7503, 2006.
16) J. Golimowski et al., Analytica Chimica Acta, vol. 325, no. 3, pp. 111-133, 1996.
17) J. L. Robichaud et al., Proceedings of SPIE, vol. 4854, pp. 39-49, 2003.
18) W.C. Lien et al., IEEE Electron Device Letters, vol. 33, no. 11, pp. 1586-1588, 2012.
19) A. Vijayakumar et al., IEEE Electron Device Letters, vol. 28, no. 8, pp. 713-715, 2007.
20) C. Zhao et al., Nano Lett., vol. 16, no.2, pp. 1056-1063, 2016.
21) K. Chung et al., Science., vol. 330, no.6004, pp. 655-657, 2010.
22) J. Millan et al, IEEE Trans. Power Electron., vol. 29, no. 5, pp. 2155-2163, 2014.

23) L. Wang et al., Nano Energy, vol. 12, pp. 419-436, 2015.

24) J. C. Carrano et al., Appl. Phys. Lett., vol. 76, no.7, pp. 924-926, 2000.

25) S. P. Denbaars et al., Acta Materialia, vol. 61, no. 3 pp. 945-951, 2013.

26) O. Jani et al., Appl. Phys. Lett., vol. 91, no. 13, p. 132117, 2007.

27) T. J. Flack et al., J. Electron. Mater., vol. 45, pp. 2673-2682, 2016.

28) G. Kalita et al., Phys. Status Solidi A, vol. 215, no. 18, p. 1800089, 2018.

29) R.S. Pengelly et al., IEEE Transactions on Microwave Theory and Techniques, vol. 60, no.6, pp. 1764-1783, 2012.

30) Davide Priante., et al, Optical material express, vol. 7, no.12, pp. 4214-4224.

31) I. Akasaki et al., Jpn. J. Appl. Phys., vol. 36, p. 5393, 1997.

32) S. Nakamura, Science, vol. 281, no. 5379, pp. 956-961, 1998.

33) O. Akutas et al., Appl Phys Lett., vol. 69, pp. 3872-3874, 1996.

34) M. Meneghini et al., IEEE Transactions on Device and Materials Reliability, vol. 8, no. 2, pp. 323-331, 2008.

35) G.T. Dang et al., IEEE Transactions on Electron Devices, vol. 47, no. 4 pp. 692-696, 2000.

36) D. Donoval et al., Jour. Appl. Phys., vol. 109, no. 6, p. 063711, 2011.

37) M. R. H. Khan et al., Jour. Phys. D: Appl. Phys., vol. 28, no.6, p. 1169, 1995.

38) H. Ishikawa et al., Jpn. J. Appl. Phys., vol. 37, no. 1A, pp. 7–9, 1998.

39) Z. Zhang et al., ACS Appl. Mater. Interfaces, vol. 10, no. 20, pp. 17419-17426, 2018.

40) R. Zhuo et al., J. Mater. Chem. C, vol.6, pp. 299-303, 2018.

41) C.Y. Huang et al., Appl. Phys. Lett., vol. 112, no.23, p. 233106, 2018.

42) D. Ruzmetov et al., 2D Mater., vol. 5, no. 4, p. 045016, 2018.

43) H. Qin et al., Materials, vol. 10, no. 12, p. 1419, 2017.

44) S. Sankaranarayanan et al., Sci Rep., vol. 10, p. 14507, 2020.

45) D.Y.Guo et al., Appl. Phys. Lett., vol. 105, no.2, p. 023507, 2018.

46) T. Oshima et al., Appl. Phys. Express, vol. 1, no.1, p. 011202, 2008.

47) S. P. Denaars et al., Proc. ICDL, pp. 67-70, 2007

48) E. A. Jones et al., IEEE Trans. Emerg. Sel. Topics Power Electron, vol.4, no.3, pp. 707-719, 2016.

49) J. Millan et al., IEEE Trans. Power Electron. 29, no.5, pp. 2155-2163, 2014.

50) C.H. Kang et al., Appl. Phys. Lett., vol. 109, no.8, p. 081902, 2016.

51) M. Heilmann et al., Nano Lett., vol. 16, no.6, pp. 3524-3532, 2016.

52) C. Du et al., Small, vol. 11, no. 45, pp. 6071-6077, 2015.

53) J. K. Kim et al., Adv. Mater., vol, 20, no.4, pp. 801-804, 2008.

54) J. P. Shim et al., Appl. Phys. Express, vol. 4, no.5, p. 052302, 2011.

55) T. Egawa et al., J. Appl. Phys., vol. 82, p. 5816, 1997.

56) Q. Hua et al., Reference Module in Materials Science and Materials Engineering, Elsevier, 2020.

57) N. Prakash et al., Appl. Phys. Lett., vol. 109, no. 24, p. 242102, 2016.

58) G. Kalita et al., Appl. Phys. Lett., vol. 111, no. 1, p. 013504, 2017.

59) L. Dong et al., Sci Rep., vol. 7, p. 40160, 2017.

60) L. Sang et al., Appl. Phys. Lett., vol. 107, no.5, p. 052102, 2015.

61) S. M. Shinde et al., Jour. Appl. Phys., vol. 116, no. 21, p. 214306, 2014.

62) E Monroy et al., Semiconductor Science and Technology, vol. 18, no. 4, p. R33, 2003.

63) H. Qin et al., Materials, vol. 10, no. 12, p. 1419, 2017.

64) M. Gaono et al., J. Appl. Phys., vol. 88, no.11, pp. 6467-6475, 2000.

CHAPTER 2

2. Potential of graphene for integration with GaN and Ga_2O_3 semiconductors

2.1 Introduction and background of graphene

Single layer of graphite was theoretically studied for its electronic structure in 1947 by Philip Wallace. Further, in 1987 the term “graphene” was used by S. Mouras to define single layer of graphite, followed by many attempts to differentiate layers of graphite from its parent graphitic material. Finally, after 60 years since the first study of single layer of graphite, Andre Geim and Konstantine Novoselov were credited for the separation of single layer graphene from graphite by mechanical exfoliation method. For their discovery of graphene Andre Geim and Konstantine Novoselov were awarded the Nobel prize in Physics in 2010.

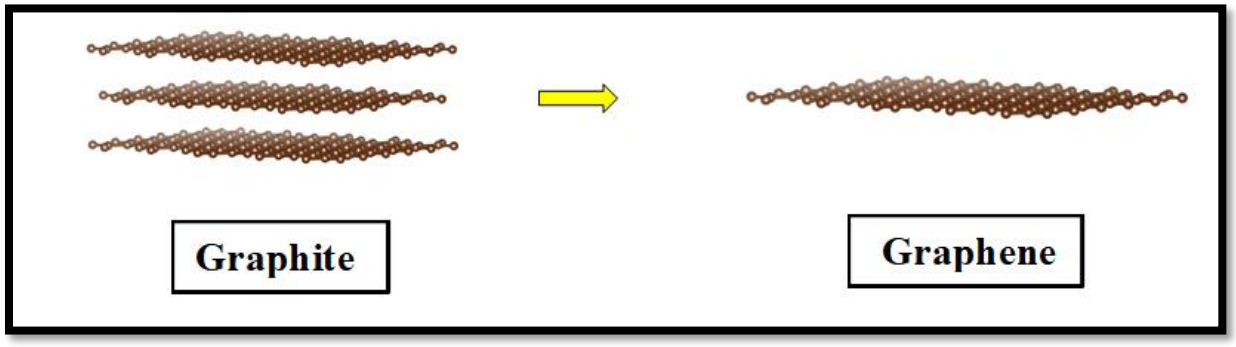

Figure 2.1 (a) shows the separation of single layer from graphite structure gives us a new material called graphene.

Graphene is a single layer of hexagonal honeycombed lattice structured carbon atoms with sp^2 hybridization bonding with each other. [(1)] This 2-Dimensional material has been researched extensively right from its synthesis to the potential application due to its various unique properties. Graphene is essentially a single layer of graphite which makes it a basic unit of various carbon nanomaterials. Figure 2.1 (a) shows the structure of single layer of graphene sheet separated from graphite sheets.

2.2 Structure of graphene

Graphene can be considered a 2-Dimentional, hexagonal lattice honeycombed and atomic scale allotrope of carbon which uses catenation property by forming sp^2 hybridization with an adjacent carbon atom. [(2)] The carbon-carbon bond is characterized by the mixing of $2s^2$ orbital with $2p_x$ and $2P_y$ orbital for forming 3 sigma bonds which gives the stability to the honeycomb structure while the remaining $2p_z$ electron forms a π- bond which hybridize with π- bond of adjacent carbon atom. The unique electronic properties of graphene can be attributed to π- bond which is characterized by half-filled bands leading to free movement of electron over the graphene sheet. Thus, in simple terms the notable electronic characteristics of graphene are due to the free movement of unpaired electrons along its plane. The length of carbon bond is 0.142 nm.

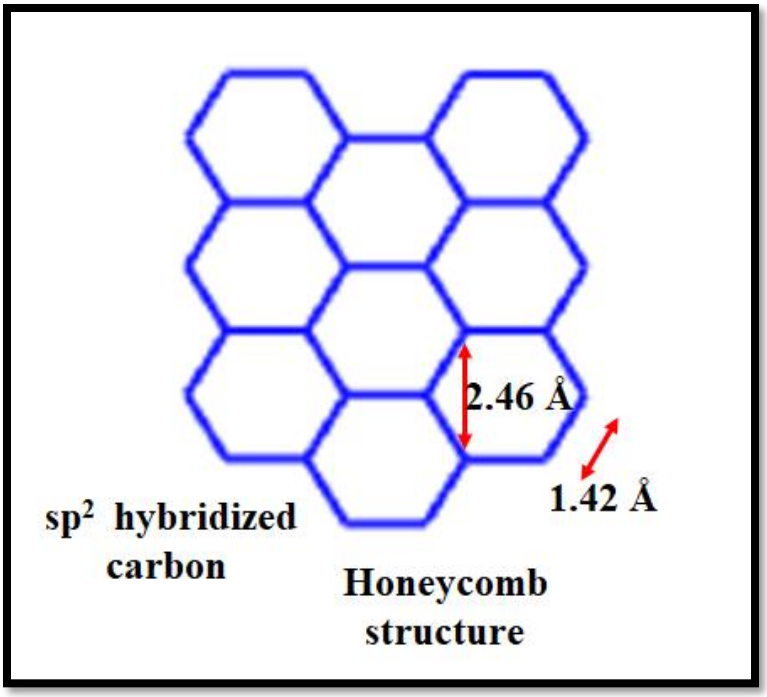

Figure 2.2 shows the honeycomb structure of graphene.

In layman's terms, graphene can be defined as the basic unit of carbon nanomaterials which when curled up gives us carbon nanotubes (CNT) and when stacked gives us fullerene. In single layer graphene, carbon atoms bond with surrounding carbon atoms with sp^2 hybridization forming a benzene ring in which each atom donates an unpaired electron. The connection between carbon atoms is tough enough and hence even with external force reconfiguration of atoms is not possible. Further, graphene can exist as monolayer, bilayer and multilayer forms depending on the method of synthesis and the properties portrayed by each can vary depending on the number of layers.

2.3 Properties of graphene

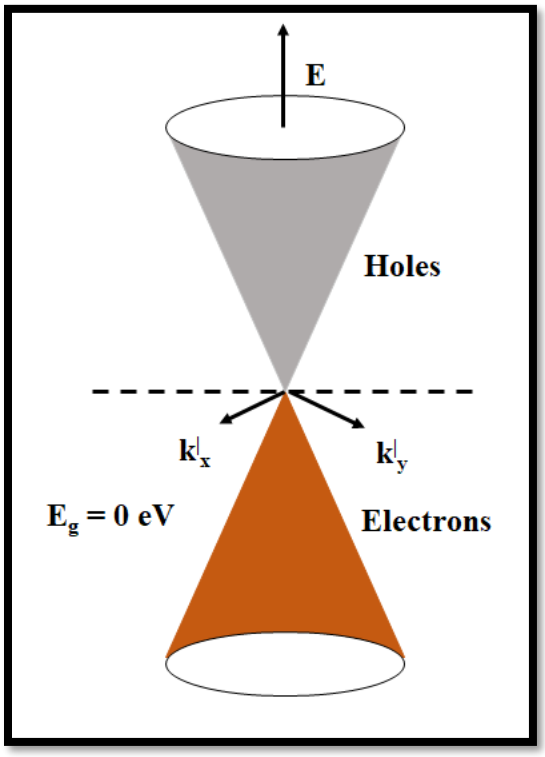

Figure 2.3 shows the band diagram of graphene, showcasing the zero-bandgap due to touching of valence and conduction band at Dirac point.

Graphene is a zero-bandgap material. Figure 2.3 shows the electronic structure of graphene, the conduction band and valence band which shows a cone like structure connected at K points called as Dirac point at the boundary of the first Brillouin zone which confirms the zero bandgap of graphene. [7-9] At the Dirac point, the energy and momentum of electrons show a linear dispersion which makes the effective mass of graphene's electrons equal to zero which in turn makes graphene's electrons as massless fermions. [7] The cone like band structure and contact between the two bands leads to the free movement of electrons i.e π electrons due to sp^2 hybridization between carbon atoms over the conduction and valence band. Due to this property, graphene is known to have an exceptionally high electron mobility of $1.5 \times 10^4\ cm^2V^{-1}s^{-1}$ which is almost 10

times greater than widely used semiconductor silicon (Si).[1,7, 10-12] Further, graphene exhibits extremely high conductivity of 10^6 S/m and a sheet resistance of 31 Ω/sq. As mentioned earlier, due to sp^2 hybridization between carbon bonds of graphene, each carbon atom donates 1 electron for π bonding which are free to move along the sheet of graphene and due to zero bandgap the electrons are free to move between the valence band and conduction band thus inculcating exceptional properties to graphene. Further, graphene exhibits a thermal conductivity of 5000 WmK^{-1} at room temperature which is about 10 times the thermal conductivity of the copper metal. Mechanical properties of graphene are interesting as well, as graphene showcases high intrinsic modulus and strength of 1.1×10^{12} Pa and 1250 Pa, respectively. At the same thickness, graphene is known to be 100 times stronger than steel. [10-16] Further, graphene also possesses extremely high specific surface area of 2600 m^2g^{-1}. Further, taking advantage of single atom thickness, monolayer graphene possesses a high optical transparency of 97.7% i.e. about 97.7% of incident light on graphene is transmitted and only 2.3% loss of incident light is incurred by graphene.[17] This particular property of graphene is well exploited for the fabrication of transparent, flexible optoelectronic devices. Thus, taking into consideration the exceptional electric, optical, mechanical properties, graphene is rightfully dubbed as the wonder material.

2.4 Characterization of graphene

Graphene can be characterized by various spectroscopic as well as microscopic techniques. Spectroscopic technique specifically Raman spectroscopy is widely used to check the quality and the number of layers in the graphene film i.e. to confirm if the synthesized graphene is a monolayer, bilayer or multilayer graphene. Raman spectroscopy is a nondestructive and inexpensive technique which is widely used to characterize not only graphene but various carbon nanomaterials. The graphene film after its synthesis using the CVD technique on a suitable substrate/catalyst like

copper is transferred on the semiconductor like Si/SiO_2 and analyzed by Raman spectroscopy to check the graphitic nature and number of layers in synthesized graphene. In the present study, the graphene is synthesized using low pressure chemical vapor deposition (LPCVD) technique and a wet chemical transfer method is employed to transfer graphene on Si/SiO_2 substrate to check the quality as well as the number of layers in the synthesized graphene. The next sections show the Raman spectroscopy of the transferred graphene on Si/SiO_2 substrate. The same method of synthesis and transfer is utilized when fabricating the graphene/GaN and graphene/Ga_2O_3 heterostructures.

2.4.1 Raman spectroscopy

Raman spectroscopy is extensively used for the characterization of 2D materials. Especially graphene, as it gives fingerprint scattering for every material. Typically, graphene samples can be distinguished between monolayer, bilayer and multilayer using Raman spectroscopy, which is relatively easy, quick, non-destructive, non-contacting measurement technique to analyze the inelastic scattering of light from a sample surface at room temperature and ambient pressure. The wavelength of the bands are affected by the energy of the laser and the following wavelengths are given for a laser excitation energy of 532.08 nm, in which an NRS-3300 laser Raman spectrometer was used to take the Raman spectra of the graphene samples both silicon and Gallium nitride substrate.

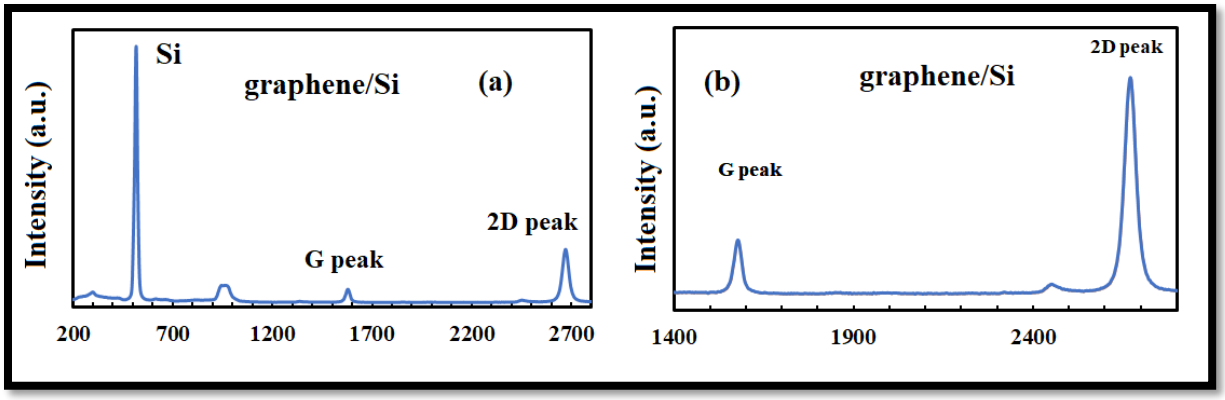

Figure 2.4 (a) shows the Raman spectra of the graphene/Si heterostructure shows the peaks for silicon as well as graphene. (b) shows the Raman spectra of graphene/Si heterostructure focusing on only graphene peaks.

The graphene/Si heterostructure was subjected to Raman spectroscopy analysis to check the crystallinity of the deposited carbon material. Figure 2.4 (a) shows the Raman spectra of the transferred graphene/Si/SiO_2 heterostructure. A high intensity peak is observed at 520 cm^{-1} which corresponds to Si/ SiO_2. [37] Since Si/ SiO_2 is a primary standard and shows the Raman spectra peak at 520 cm^{-1} our instrument is well calibrated. Further, two more high intensity peaks are observed at 1577 cm^{-1} and 2671 cm^{-1} which are labelled as G peak and 2D peak.[37,38] Usually, for carbon materials, a peak in the range of 1350 cm^{-1} corresponds to the sp^3 hybridization in the carbon material and hence is assigned to the defect present in the carbon material and is called as D peak. The absence of D peak in our sample confirms fabrication of defect free graphene sample. Further, the G peak corresponds to the crystallinity of graphitic material. The G-band is the primary mode in graphene and graphite. It represents the planar configuration sp^2 bonded carbon that constitutes graphene. [37-38] The G band is used in calculating the number of layers in graphene. The 2D peak is the secondary D peak which can be referred to as overtone of D band. It is the

result of a two-phonon lattice vibrational process, but unlike the D-band, it does not need to be activated by proximity to a defect. As a result, the 2D-band is always a strong band in graphene even when no D-band is present, and it does not represent defects. It is also used to calculate the number of layers in graphene. Mainly the ratio of intensity of 2D peak and G peak (I_{2D}/I_G) is considered and if I_{2D}/I_G is ≥ 2, it signifies that the graphene is single layer.[34,37,38] For our sample the I_{2D}/I_G is 3.3 which confirms that graphene transferred on Si/SiO_2 is a single layer graphene.

2.5 Graphene based optoelectronic devices

As discussed in earlier sections, graphene being a 2D material with exceptional electrical properties, zero bandgap, one atom thickness is an ideal candidate for integrating with various conventional semiconductors for application in high performance optoelectronics and power devices. [18-23] Graphene has been integrated with conventional semiconductors like silicon, GaAs, GaN for various device application. Graphene with its zero bandgap behaves as a semimetal and when integrated with semiconductor material forms a Schottky junction. Graphene integration with semiconductors has found many applications such as photodetector, LED's, optoelectronic modulators, solar cells. [24-32] Recently, Noorazi *et al* reported-on graphene/Si-based Schottky junction for protein detection. [33] Using the optical transparency and metal like behavior, graphene has emerged as a leading candidate for replacing the indium tin oxide (ITO) as transparent conducting electrodes. Graphene has found many applications in flexible and transparent optoelectronic devices. Further, graphene has also been integrated with various wide bandgap and ultrawide bandgap semiconductors like GaN, Ga_2O_3 for LEDs and UV and DUV photodetector application. [25-32,35] Kalita et al have reported on photovoltaic action in graphene/GaN based Schottky barrier diodes. [34] While Kong et al have reported on the good photoresponsivity in graphene/Ga_2O_3 Schottky diode. [36]

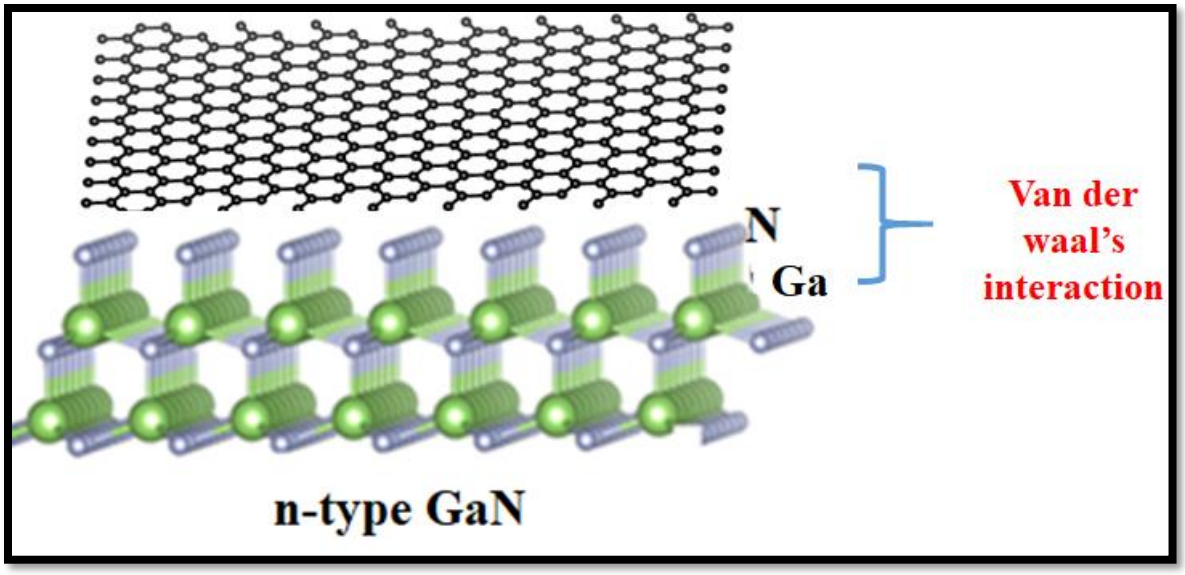

Figure 2.5 ball and stick diagram of n-type GaN and graphene to form a unconventional Van der waal's heterojunction.

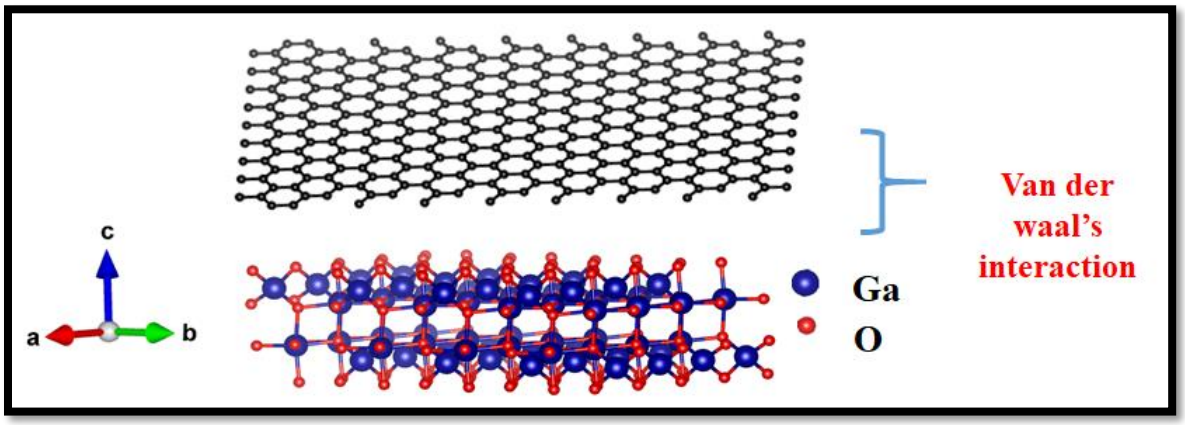

Figure 2.6 ball and stick diagram of β-Ga_2O_3 and graphene to form a unconventional Van der waal's heterojunction.

Thus, considering the excellent electronic properties of graphene, it is an interesting prospect to integrate graphene with various novel semiconductors for photodetector and optoelectronic application.

2.6 Motivation of integrating graphene with semiconductors:

As mentioned earlier the conventional metal Schottky contacts present disadvantages of blocking the incident radiation, need of semitransparent metal contacts. Further, Schottky junctions are inherently quite sensitive to the interface of the metal-semiconductor junction. Thus, a need for unconventional metal contact free Schottky junction is in high demand. In this regard, graphene which is a single atom thick 2-dimensional material which possess excellent properties like zero bandgap, exceptionally high electron mobility, extremely high transparency is an ideal candidate to replace conventional metal electrodes. Graphene with its zero bandgap behaves as semi metal and hence when integrated with semiconductors behaves as Schottky devices. Moreover, with 97.3% transparency due to its single atom thickness, graphene can transmit almost all the incident radiation to the semiconductor and overcomes the major challenge possessed by conventional metal contacts. In this regard, integration of graphene with GaN and Ga_2O_3 is an interesting prospect and should be explored to achieve high device performance.

2.7 References

1) Z. Zhen et al., Graphene, pp. 1-12, Academic Press.

2) R. B. Heimann et al., Carbon, vol. 35, no. 10-11, pp. 1654-1658, 1997.

3) A. Hirsch et al., Nat. Mater., vol. 9, no. 11, pp. 868-871, 2010.

4) K. S. Novoselov et al., Science, vol. 306, no. 5696, pp. 666-669, 2004.

5) H. W. Kroto et al., Nature, vol. 318, no. 6042, pp. 162-163, 1985.

6) S. Iijima et al., Nature, vol. 354, no. 6348, pp. 56-58, 1991.

7) J. Wang et al., Appl. Mater. Today, vol. 16, pp. 1-20, 2019.

8) H. C. Neto et al., Rev. Mod. Phys., vol. 81, no. 1, pp. 109-162, 2009.

9) A. K. Geim et al., Phys. Today, vol. 60, no. 8, pp. 35-41, 2007.

10) Z. H. Ni et al., Nano Lett., vol. 7, no. 9, pp. 2758-2763, 2007.

11) K. S. Kim et al., Nature, vol. 457, no. 7230, pp. 706-710, 2009.

12) K. I. Bolotin et al., Solid State Commun., vol. 146, no. 910, pp. 351-355, 2008.

13) C. Lee et al., Science, vol. 321, no. 5887, pp. 385-388, 2008.

14) S. Stankovich et al., Nature, vol. 442, no. 7100, pp. 282-286, 2006.

15) A. A. Balandin et al., Nano Lett., vol. 8, no. 3, pp. 902-907, 2008.

16) M. D. Stoller et al., Nano Lett., vol. 8, no. 10, pp. 3498-3502, 2008.

17) R. R. Nair et al., Science, vol. 320, no. 5881, pp. 1308-1308, 2008.

18) X. Li et al., Adv. Mater., vol. 22, no. 25, pp. 2743-2748, 2010.

19) G. Kalita et al., J. Phys. D: Appl. Phys., vol. 46, no. 45, p. 455103, 2013.

20) C. Xie et al., Nano Today, vol. 19, pp. 41-83, 2018.

21) S. Tongay et al., Appl. Phys. Lett., vol. 99, no. 10, p. 102102, 2011.

22) S. Kim et al., Nano Res., vol. 8, no. 4, pp. 1327-1338, 2015.

23) F. Giannazzo et al., Phys. Status Solidi A, vol. 214, no. 4, p. 1600460,2017.

24) M. Meneghini et al., IEEE Transactions on Device and Materials Reliability, vol. 8, no. 2, pp. 323-331, 2008.

25) E. A. Jones et al., IEEE J. Emerging Sel. Top. Power Electron., vol. 4, no. 3, pp. 707-719, 2016.

26) J. Millán et al., IEEE Trans. Power Electron., vol. 29, no. 5, pp. 2155-2163, 2014.

27) L. Wang et al., Nano Energy, vol. 12, pp. 419-436, 2015.

28) M. Heilmann et al., Nano Lett., vol. 16, no. 6, pp. 3524-3532, 2016.

29) C. Du et al., Small, vol. 11, no. 45, pp. 6071-6077, 2015.

30) J. K. Kim et al., Adv. Mater., vol. 20, no. 4, pp. 801-804, 2008.

31) J. P. Shim et al., Appl. Phys. Express, vol. 4, no. 5, p. 052302, 2011.

32) T. Egawa et al., J. Appl. Phys., vol. 82, no. 11, pp. 5816-5821, 1997.

33) A. A. Noroozi et al., RSC Adv., vol. 9, no. 34, pp. 19613-19619, 2019.

34) G. Kalita et al., Appl. Phys. Lett., vol. 111, no. 1, p. 013504, 2017.

35) A. Kumar et al., ACS Appl. Mater. Interfaces, vol. 8, no. 12, pp. 8213-8223, 2016.

36) W. Y. Kong et al., Adv. Mater., vol. 28, no. 48, pp. 10725-10731, 2016.

37) C. Liu et al., Appl. Phys. Lett., vol. 103, no. 21, p. 213103, 2013.

38) J. B. Wu et al., Chem. Soc. Rev., vol. 47, pp. 1822-1873, 2018.

CHAPTER 3

3. Ultraviolet light induced electrical hysteresis effect in graphene/GaN heterojunction

3.1 Introduction

In this chapter, the effect of interfacial impurities in generation of electrical hysteresis in graphene/GaN heterojunction is discussed. The focus is on the transport properties of charge carrier in the fabricated 2D/3D heterojunction. The 2D/3D heterojunctions have received significant attention due to potential wide range applications in light emitting diodes, solar cells photodiodes and other electronic devices.[1-6] A 2D graphene exhibits novel electronic properties such as high electron mobility, extremely high transparency (97%) and due to its zero-bandgap structure it forms a Schottky junction with various semiconductors. Thus, graphene has been integrated with various 3D semiconductors such as silicon, Ga_2O_3, GaN for various device application. Amongst compound semiconductors Gallium nitride (GaN) which exhibits a band gap of 3.4 eV has been explored for various optoelectronic and power electronics application.[7-9] GaN based devices have attracted significant attention due to its excellent properties like high thermal stability, high radiation stability [8-9], thus opening possibility for application in ultraviolet (UV) photodetector, LEDs, solar cells, high electron mobility transistors and high frequency power devices. [8-15] GaN integrated with conventional metal electrodes Schottky junctions have been developed for high responsive photodiodes and switching devices [14-15] The Schottky junction devices due to being majority charge carriers are very sensitive to the interface quality of metal and semiconductors[21]. Moreover, conventional Schottky junctions possess some disadvantages as

incident radiation loss due to high absorptivity coefficient of metals and hence extensive research for understanding physical properties of Schottky contacts to find a suitable substitute to replace conventional Schottky junction in order to achieve better device performance. In this prospect, graphene with its zero-band gap and high transparency could be an ideal material to replace conventional metal contacts and has been integrated with various semiconductors like GaN, Ga_2O_3, to form heterojunction-based devices. [3-5,22-26] It is expected that graphene with unique band structure due to linear dispersion of π-band near Dirac point (i.e also Fermi level) can be significant to develop unconventional Schottky junction devices. Thus, owing to unconventional graphene/GaN Schottky junction and the sensitive nature of interface of Schottky junction devices it is important to study the charge carrier transport properties at the interface of graphene/GaN heterojunction. Kumar et al. have reported on fabrication of graphene/GaN Schottky barrier diodes.[27] Kalita et al have demonstrated the temperature dependent diode and photovoltaic properties of graphene and GaN heterostructure which opens possibility of self-powered UV mode of operation in graphene/GaN heterojucntions.[24] Moreover, Lee et al. have reported photovoltaic action in graphene/GaN Schottky photodiodes.[28] Since graphene being a single atom thick material and GaN possess inherent surface states, the photocarrier transport characteristics in graphene/GaN heterojunction is governed by electrostatic molecular interactions and charge trapping phenomenon at heterojunction interface. Hence, understanding of carrier trapping process at the graphene/GaN interface can lead to developing high performance UV photodiodes. Previously transient spectroscopy has been used to detect charge trapping analysis of GaN based Schottky.[29] Here, I report on the UV light induced electrical hysteresis in graphene/GaN heterojunction due to interfacial impurities as well as surface states and its subsequent effect on the device performance.

3.2 Experimental section

This section will discuss about the fabrication of graphene and its further integration with Gallium Nitride to form graphene/GaN heterojunction. Graphene is synthesized on recrystallized Cu (111) foil by low pressure chemical vapor deposition (LPCVD). For this experiment, Cu (111) is placed horizontally into a ceramic cylinder which was then placed at the center of 90 cm long quartz tube. The quartz tube was then rested in the single zone split furnace with adequate heat insulation of glass wool to avoid heat loss. Polystyrene balls were used as carbon source precursor and placed atop a magnetic boat which was placed inside the tube about 20 cm away from the furnace to avoid precursor loss before deposition step. Once the tube is closed at both ends using metal fitters the reaction vessel is set to achieve a low pressure of approximately 2 Pa. Once the desired low pressure is obtained, the tube is purged with hydrogen gas (H_2) with flow rate of 100 sccm for 10 mins to achieve hydrogen atmosphere inside the reaction vessel to prevent oxidation of Cu substrate. During purging step, the pressure of reaction vessel increases to 800 Pa and after completion of purging step, heating of furnace is started to achieve a high temperature of 1080^{o} C for deposition step. During deposition step the gas flow into the chamber was changed by addition of argon gas (Ar-99.9% pure) with a flow rate of 21.0 sccm and flow rate of hydrogen gas was reduced to 2.1 sccm, which changes the reaction vessel pressure to 55 Pa. Once the mixed gas flow of 21:2.1 of Ar: H_2 is achieved the precursor is brought close to the furnace using a magnet at to place it 6 cm away from the furnace to achieve vaporization of polystyrene to free carbon radicals which are carried forward into the high temperature zone by Ar:H_2 gas mixture. The deposition step was set for 20 mins which allows for formation of single layer graphene on Cu (111) substrate. Finally, the cooling step was achieved by simultaneously switching off H_2 gas flow, partially opening the furnace and moving precursor approx. 20 cm away from the furnace to avoid

secondary deposition. During the cooling step the H_2 gas flow is stopped to avoid etching of deposited graphene. Once the furnace is cooled below 700 ^{o} C the split furnace is fully opened to accelerate cooling of reaction vessel. After the reaction vessel is cooled to room temperature the Cu/graphene stack was taken out of reaction chamber and subjected to wet transfer process to remove graphene layer from Cu substrate. The synthesized graphene on Cu foil is coated with a poly (methyl methacrylate) (PMMA) layer by spin coating method. Then, PMMA coated graphene/Cu stack was dried in an oven at 80 ^{o} C for 15 mins. The dried sample was dipped in iron (III) nitrate nonahydrate solution [$Fe_2(NO_3)_3 9H_2O$] to etch the Cu foil. The concentration of iron nitrate solution was 10 mg/ml, where the etching rate of Cu can be controlled with the concentration of solution. After the etching of Cu foil, a free-standing PMMA/graphene layer was obtained, which was transferred to a petri dish filled with deionized water. Further the PMMA/graphene was treated with dilute HNO_3 solution to remove residual iron nitrate.

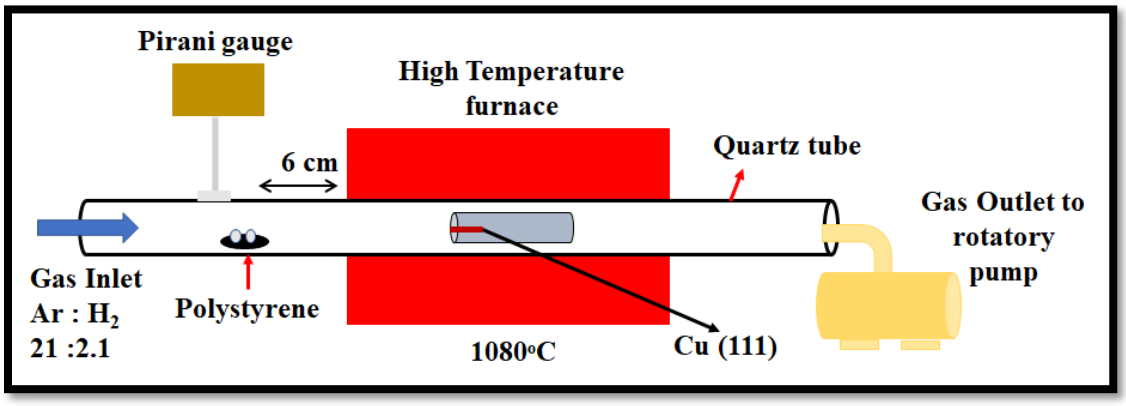

Figure 3.1 schematic diagram of low pressure chemical vapor deposition of graphene using polystyrene as carbon source.

The treated PMMA/graphene stack was again put in a petri dish filled with deionized water and finally transferred onto the GaN substrate. The water bubbles were removed by slow air blowing and drying in oven at 80 ˚C for 15 mins. The PMMA layer is removed by dipping in acetone and isopropyl alcohol at room temperature as PMMA is soluble in organic solvent and graphene is not. The graphene and GaN heterostructure was characterized by spectroscopic and microscopic analysis prior to device fabrication. Gold (Au) as contact to graphene and Indium (In) as bottom contact were deposited on GaN by thermal evaporator system using a shadow mask under a high vacuum (7×10^{-4} Pa) condition.

3.3 Results and discussion

In this study, after the synthesis of graphene by LPCVD technique, graphene is transferred on free standing GaN substrate using wet chemical transfer method and the fabricated heterostructures were then analyzed by both spectroscopic and microscopic techniques such as Raman spectroscopy, scanning electron microscopy (SEM), and X-ray photoelectron spectroscopy (XPS). An NRS 3300 laser Raman spectrometer with a laser excitation wavelength of 532.08 nm was used to study the transferred graphene on GaN substrate. SEM analysis was performed on graphene/GaN heterostructure using JEOL JSM-7001FF. XPS analysis was performed by using a versa probe with a monochromated Al Ka excitation source (1486.6 eV). Metal electrodes were deposited by thermal evaporation technique using ULVAC VPC-260F. A two-probe system and a Keithley 2401 source meter were used for current density voltage (J-V) characteristic measurements. The C-V analysis of the devices was performed by Agilent 4284A Precision LCR meter. In the present study, the first fabricated graphene/GaN heterostructure showed possible presence of impurities after analyzing by EDAX as well as XPS techniques and hence another

graphene/GaN heterostructure was fabricated by taking special care to avoid inculcating impurities at the interface. Nevertheless, both the fabricated device was analyzed for the *J-V* characteristics. Herein after, the graphene/GaN device which showed high electrical hysteresis and low photoresponsivity was named Device 1 and the second graphene/GaN device which showed low electrical hysteresis and high photoresponsivity is named Device 2.

3.3.1 Raman spectroscopy

The fabricated graphene/GaN heterostructure was subjected to Raman spectroscopy at various random points to confirm transfer of a continuous graphene on GaN substrate.

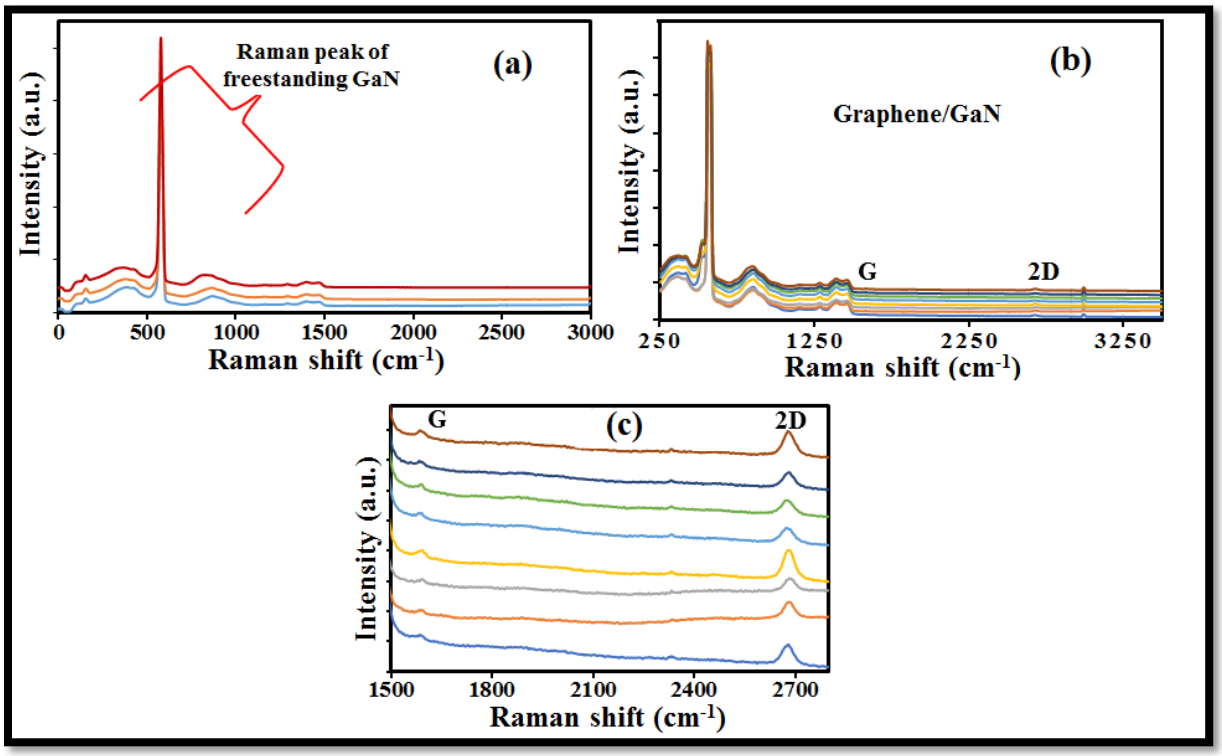

Figure 3.2 shows the Raman spectra of the free standing GaN at various points. (b) shows the Raman spectra of graphene/GaN heterostructure (device 1) at various points. (c) shows the G and 2D peaks of graphene transferred on GaN.

Figure 3.2 (a) shows the Raman spectroscopy of free standing GaN at various points, the high intensity peak at ~565 cm^{-1} and a broad peak at ~1400 cm^{-1} are attributed to GaN. The Raman spectra shows overlapping peaks at random points signifying uniformity of GaN substrate. Figure 3.2 (b) show the Raman spectroscopy of the fabricated graphene/GaN heterostructure at various points. Along with GaN peaks, G peak and 2D peak of graphene were also observed. Figure 3.2 (c) shows Raman spectra for only graphene transferred onto GaN substrate. The G peaks and 2D peaks were obtained in the range 1586 cm^{-1} to 1591cm^{-1} and 2673 cm^{-1} to 2684 cm^{-1}, respectively which indicates a blue shift (6-11 cm^{-1}) in G peak and red shift (6-17 cm^{-1}) in 2D peak in compared to pristine graphene. [28] This blue and red shift observed for the transferred graphene can be due to the unintentional doping effect and electronic interaction of graphene with the GaN substrate.[24] The ratio of intensity 2D peak to G peak (I_{2D}/I_G) was observed to be around 3 which signifies the presence of monolayer graphene film over the GaN substrate. The consistent presence of the G and 2D peaks in the spectra taken at random points on the fabricated graphene/GaN heterostructure confirms the presence of uniform monolayer graphene on GaN substrate. Further, the graphene/GaN heterostructure was subjected to structural and elemental analysis.

3.3.2 FESEM and EDX analysis

FE-SEM studies were performed with JEOL JSM-7800F using lower electron detector (LED) with an accelerating voltage of 5 kV. Electron beam interaction with the sample produce secondary electrons which are converted to signal and subsequently used to construct the image. High resolution images are possible up to few micrometers. The emitted secondary electrons are close to specimen surface which gives very sharp images. Further within the same set up EDAX analysis was carried out using instrument. The electron beam hits the inner shell of an atom, knocking off an electron from the shell, while leaving a positively charged electron hole. When the electron is

displaced, it attracts another electron from an outer shell to fill the vacancy. As the electron moves from the outer higher-energy to the inner lower-energy shell of the atom, this energy difference can be released in the form of an X-ray. The energy of this X-ray is unique to the specific element and transition. EDX can be used for both qualitative and quantitative analysis, enabling users to identify both the type of elements that are present as well as the percentage of each element's concentration within the sample. And as with traditional SEM, the technique requires little to no sample preparation and is non-destructive, meaning that it doesn't damage the sample. EDX analysis is increasingly being used to understand the elemental composition of the sample and by extension the impurities present in the sample.

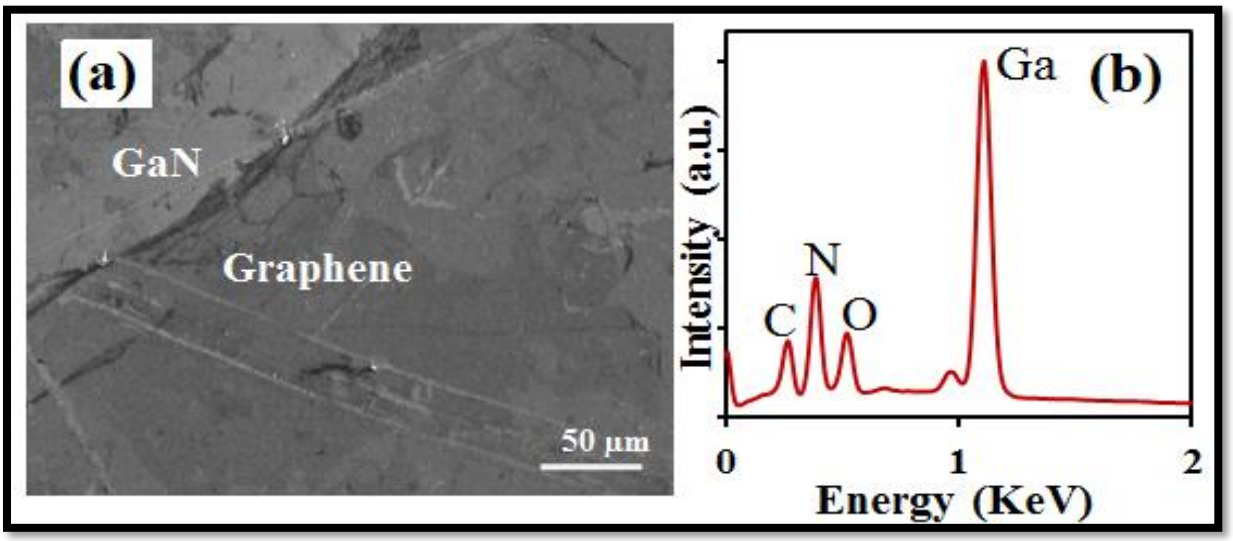

Figure 3.3 (a) shows the FESEM image of the graphene/GaN heterostructure (Device 1) (b) shows the EDAX spectra of the graphene/GaN heterostructure signifying the presence of Ga, N, C and O elements in the sample.

Figure 3.3 (a) shows the FESEM images of fabricated graphene/GaN heterostructure. A continuous graphene film can be seen well attached to the GaN substrate due to van der Waal's

force of attraction. Figure 3.3 (b) shows the EDAX spectra of the fabricated graphene/GaN heterostructure. A high intensity peaks of Gallium (Ga) and Nitrogen (N) is observed due to GaN being the substrate materials. A carbon (C) and oxygen (O) is peak is also observed. While the carbon peak corresponds to graphene transferred on GaN substrate, the presence of high intensity oxygen peak was unexpected and can be attributed to presence of impurities at the heterostructure interface as well as surface defects of GaN. Thus, after EDAX analysis there is a suspicion of the interfacial impurities at the interface of fabricated graphene/GaN heterostructure, which can be due to wet chemical transfer method being used for transfer of graphene on GaN substrate. Nevertheless, the fabricated heterostructure was subjected to thermal evaporation technique for deposition of gold (Au) and Indium (In) on graphene and GaN respectively to serve as metal contacts for J-V characterization of the graphene/GaN heterojunction. Further, the graphene/GaN heterojunction was analyzed by X-ray photoelectron spectroscopy for better understanding of the elemental composition of the sample.

3.3.3 X-ray photoelectron spectroscopy

Elemental analysis, chemical and electronic state analysis of the prepared samples can be obtained by X-ray photoelectron spectroscopy (XPS). As the name suggests, surface of the sample is irradiated by mono-energetic Al Kα X-rays. Mono-energetic photon knocks out the electron from atoms in the surface region. Electrons emitted in this manner are referred to as photoelectrons. Elements present in the sample can be identified based on kinetic energies and binding energies of their photoelectrons. Intensities of photoelectrons provide information about the concentration of elements in the sample. The surface and interface of graphene/GaN heterojunction sample was analyzed by XPS. Figure 3.3 (a) shows the XPS survey spectra with the peaks for Ga3d, C1s and O1s before and after transferring the graphene film.

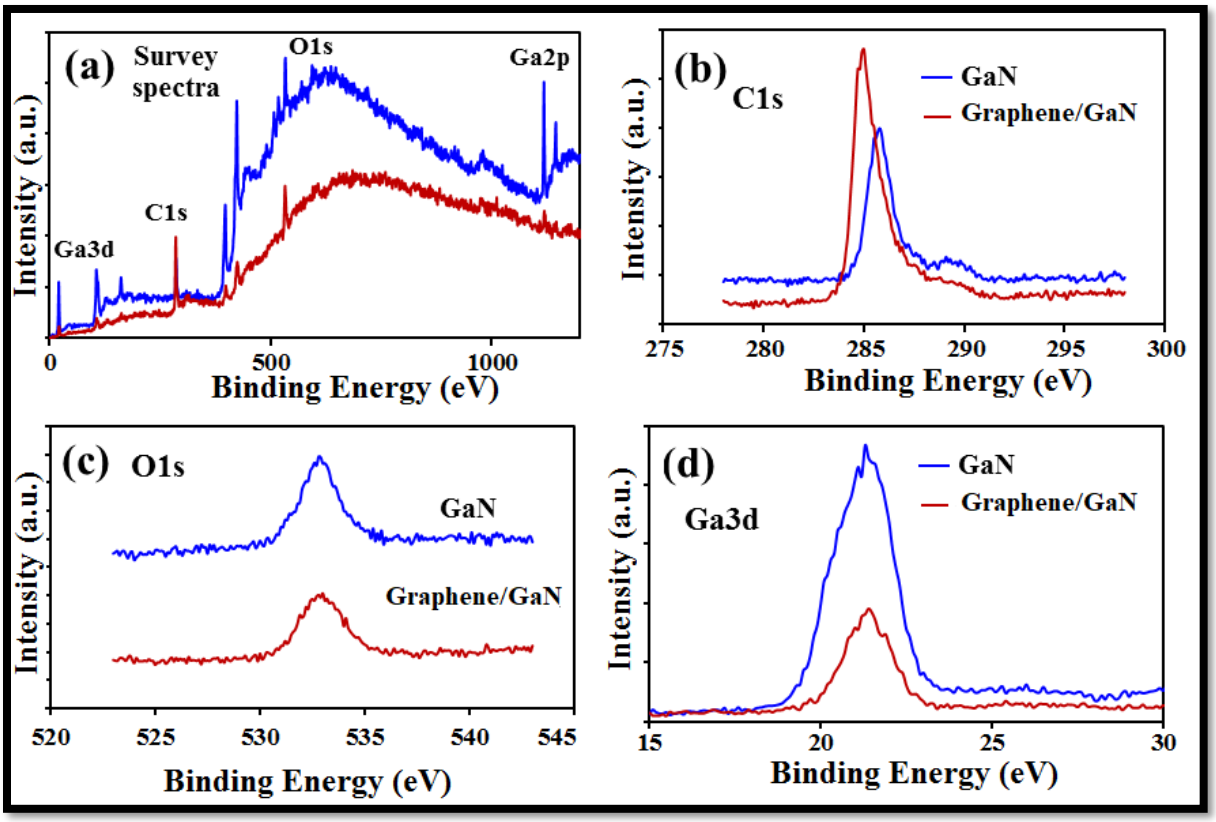

Figure 3.4 (a) shows the XPS survey spectra of bare GaN and graphene/GaN heterostructure (Device 1) (b) C1s (c) O1s (d) Ga3d shows the core level peaks for the GaN and graphene/GaN heterostructure samples.

Then, the individual XPS peaks were analyzed to investigate the state of Ga, C and O atoms. Figure 3.3 (c) shows the O1s peak with peak-centers at 532.9 eV for both the GaN and graphene/GaN samples. The inherent O impurities on the GaN surface and after the graphene transfer process were detected. Similarly, figure 3.3 (b) shows the C1s peak for the pristine GaN and graphene/GaN samples. The graphene/GaN sample shows peak position at 285 eV, while the C impurities of GaN sample shows a higher binding energy of 285.5 eV. The C atoms of graphene and impurities showed significantly different bonding properties considering the sp^2 hybridization and C-O, Ga-

O related surface defects. Figure3.3 (d) shows the Ga3d peak before and after the graphene transfer on GaN surface. The Ga3d peak core level is obtained at 21.3 eV for the pristine GaN sample which remained unchanged for after graphene transfer however reduction in Ga3d peak intensity is observed. This unexpected behavior could be attributed to little contact between graphene and GaN surface owing to interfacial impurities. Hence, an inconsistent shift of the Ga3d peak is observed for this fabricated graphene/GaN heterostructure. This result agrees with that of the EDAX study wherein an unusually high intensity Oxygen peak is observed for this graphene/GaN heterostructure (device 1). Next, the second graphene/GaN heterostructure in which graphene transfer is carefully monitored is analyzed by XPS spectra.

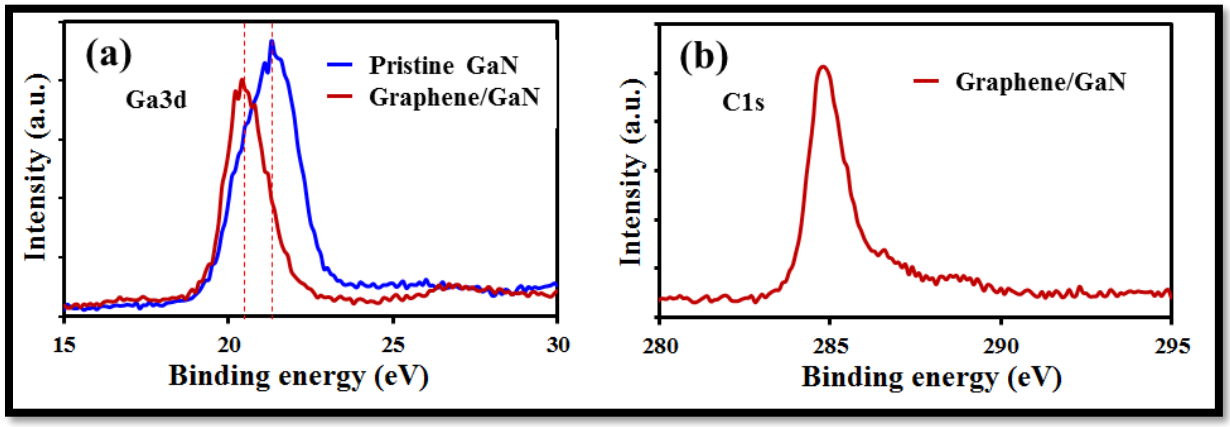

Figure 3.5 shows XPS spectra of device 2 (a) Ga3d peak of pristine GaN and graphene/GaN heterostructure with carefully transferred graphene film (b) C1s peak of the graphene for graphene/GaN heterojunction.

Figure 3.5 shows the XPS spectra of graphene/GaN (device 2) in which graphene transfer was carefully monitored. Figure 3.5 (a) shows the Ga(3d) core peak of the pristine graphene and graphene/GaN heterostructure. A shift in Ga(3d) peak is observed after the transfer of graphene.

This shift is consistent with the previously reported literature and indicates good contact of graphene film with GaN substrate. [24] This shows that the interfacial interaction strongly depends on the surface/interface impurities of the graphene and GaN heterojunction. [24,31] Figure 3.5 (b) shows the C (1s) core peak at 285 eV of the graphene/GaN heterostructure confirming the presence of graphene on GaN substrate. The barrier height ($q\phi_B$) for the graphene/n-GaN heterojunction can be calculated from the Ga3d XPS peak as given in the following equation.

$$q\emptyset_B = E_g - (E_{Core}^G - E_{VC})$$

In the equation, E_g is the band gap of GaN, E_{Core}^G is the core binding energy of the Ga3d peak following graphene coating, and E_{VC} is the energy difference between the Ga 3d core level and the valence-band maximum for n-GaN. The barrier height of the graphene/n-GaN heterojunction was obtained around 0.7 eV for the device with careful transfer of graphene film i.e. device 2. The XPS analysis of a graphene/GaN device with low hysteresis and high photoresponsivity (device 2) shows that the graphene film is in good contact with GaN surface due to which a shift in Ga3d peak can be observed.

3.3.4 Current density– voltage characteristics (J-V)

Figure 3.6 (a) shows the J-V characteristics for applied bias voltage range of -2V to + 2V under dark condition. A rectifying characteristic was obtained with low reverse saturation current (~0.0032 mA/cm^2) and high turn-on voltage (~1V) which is unusual as typically Schottky junction are characterized by low turn on voltage. Figure 3.6 (b) shows the forward and reverse sweeps in dark and UV illumination (300-400 nm) for voltage range of -2V to +2V. A photoresponsivity was obtained for UV illumination along with pronounced electrical hysteresis effect as the forward and reverse sweep do not overlap.

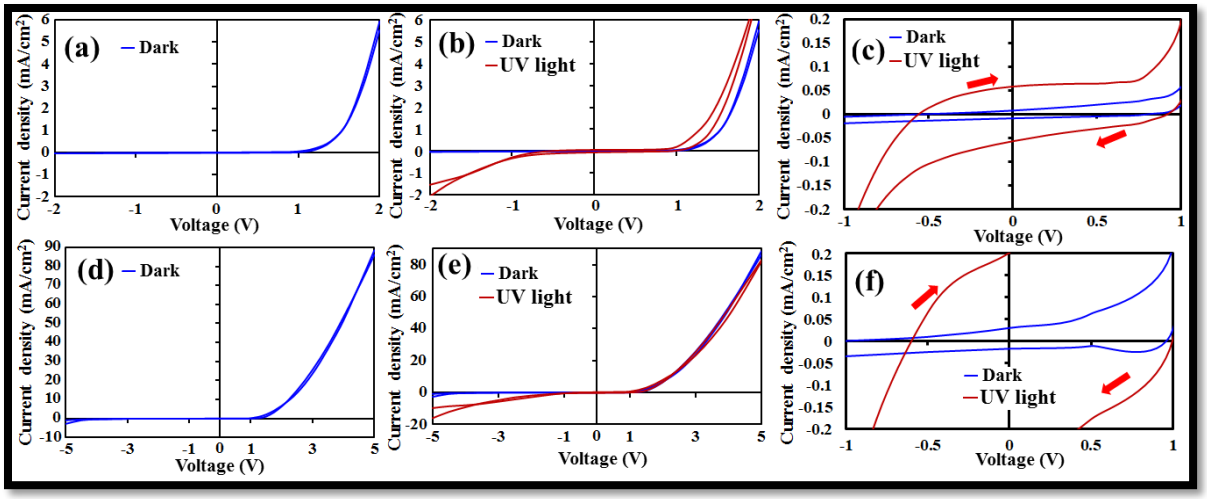

Figure 3.6 shows J-*V* characteristics of the Device 1 for (a) voltage range of -2V to 2V in dark condition, (b) J-V curve in dark and UV light illumination (-2V to 2V). (c) J-V curve (-1V to 1V) in dark and UV illumination, presenting the hysteresis behavior. (d) J-V characteristics for -5V to 5V in dark. (e) J-V curve in dark and UV illumination (-5V to 5V). (f) J-V curve (-1V to 1V) in dark and UV illumination, presenting the hysteresis behavior (forward and reverse sweeps).

It is observed in figure 3.6 (c) that electrical hysteresis is enhanced under UV illumination compared to dark condition. Subsequently, the device characteristics were analyzed under higher applied bias voltage of -5V to +5V. Figure 3.6 (d) shows the Schottky junction characteristics with excellent rectification without much change in turn-on voltage at higher applied bias voltage. Figure 3.6 (e) shows the J-V characteristics in dark and UV illumination in voltage range of -5V to +5V, a consistency in photoresponsivity is observed. Figure 3.6 (f) shows the J-V characteristics for the lower bias voltage (-1V to +1V) and significant enhancement in electrical hysteresis and larger hysteresis window under UV illumination is observed which is similar to performance under applied bias voltage of -2V to +2V. The increase in hysteresis window is due to generation of higher number of charge carrier under high applied bias voltage and generation of photocarriers

under UV illumination which results in higher charge carrier transportation and subsequent trapping and de-trapping at the graphene/GaN interface.

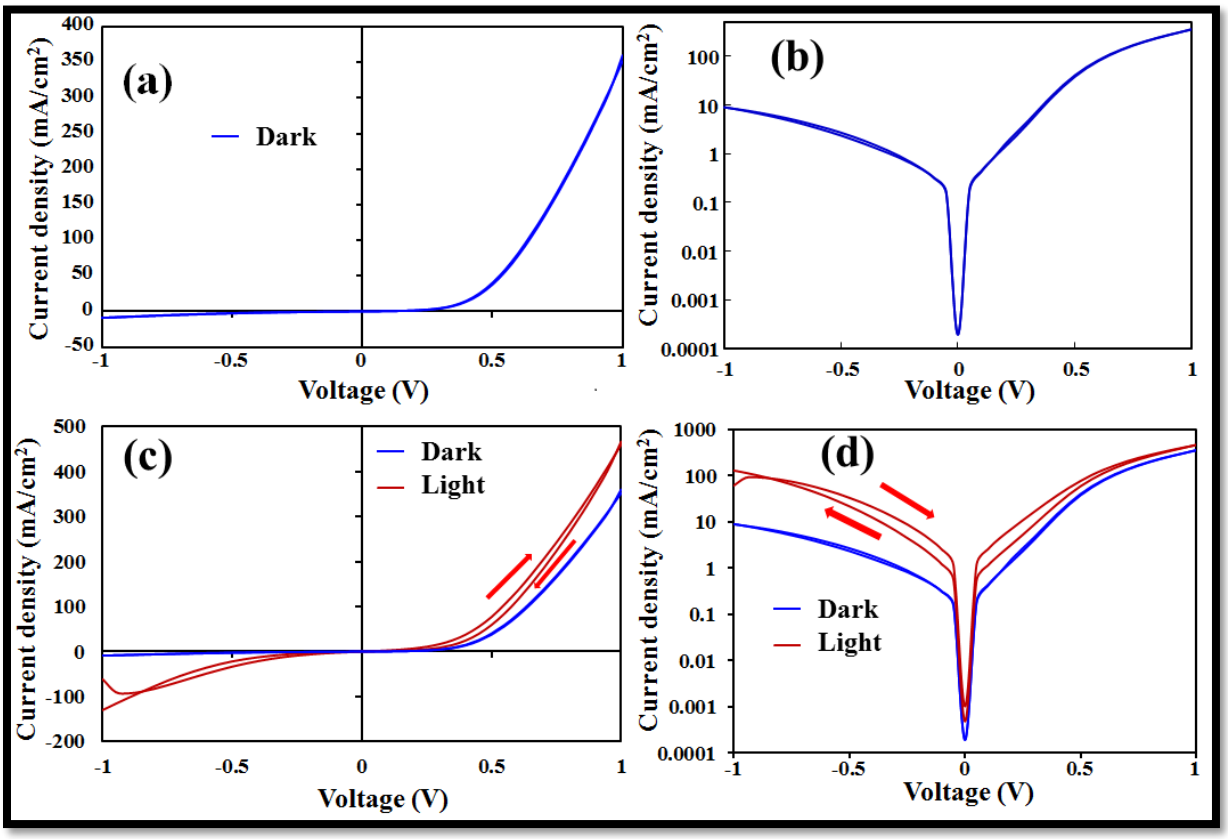

Figure 3.7 shows the J-V characteristics of device 2 i.e. graphene/GaN Schottky junction with a cleaner transferred graphene. (a) J-V characteristics in dark condition in applied voltage range of -1V to +1V, (b) log plot of J-V characteristics in dark, (c) J-V characteristics in dark and UV light in voltage range of -1 V to +1V, (d) log plot of J-V curve for dark and UV illumination conditions (forward and reverse sweeps).

Figure 3.7 shows J-V characteristics of a graphene/GaN Schottky junction with a cleaner transferred graphene i.e Device 2. Figure 3.7 (a) shows the J-V characteristics in dark condition in applied bias voltage range of -1V to +1V, presenting excellent rectification ratio and high forward

current density. The reduction in turn-on voltage is observed than that of the previous device. Good performance of device under dark condition i.e reduction in turn-on voltage as well as increase in forward current density can be explained with better electron transport at the graphene/GaN interface. However, higher saturation current (~8.91 mA/cm^2) for the device is observed which is consistent with previous study.[24] Figure 3.7 (b) shows the log plot of J-V characteristics in dark condition for reverse and forward voltage sweeps which overlapped each other and hence confirmed absence of electrical hysteresis. The absence of electrical hysteresis and good photoresponsivity can be attributed to better transfer of graphene with minimum residual impurities which subsequently results in lowering the magnitude of charge trapping phenomenon. The ideality factor for device 2 was calculated using J-V characteristics and computed to 2.84 and a barrier height (ϕ_B) of 3.323 at room temperature (298K) was obtained. Further, the device 2 was analyzed using UV illumination. Figure 3.7 (c) shows the *J-V* characteristics under dark and UV light in applied voltage range of -1V to +1V. Interestingly, presence of hysteresis was observed under UV illumination, which was absent in dark condition (no UV illumination). Further, excellent UV photoresponsivity of 1.4 A/W at a low reverse bias voltage (-1V) was obtained, irrespective of the UV light induced electrical hysteresis. Table 2 shows the comparative photoresponsivity of graphene/GaN Schottky device with reported values. However, a photovoltaic action was not observed as previously reported for the graphene/GaN (GaN film on sapphire) lateral heterojunction, attributing to recombination of generated photocarriers at zero bias voltage, which is consistent with observed electrical hysteresis behavior of the device.[24] These results clearly suggest that presence of interfacial impurities and defects of GaN significantly affect device properties and photodiode characteristics. Further, the devices were checked with C-V analysis as discussed below to clarify the observed J-V characteristics.

Table 2: Comparative photoresponsivity (A/W) of various graphene/GaN heterostructures.

Materials and device structures	Photoresponsivity (A/W)	Applied voltage (V)
graphene/hBN/GaN (Lateral) [20]	0.012	-1.5
graphene/GaN (Lateral) [28]	0.11	-1.0
graphene/GaN (Lateral) [25]	0.361	-10.0
graphene/GaN (vertical device) [This study]	1.4	-1.0

3.3.5 Capacitance-voltage characteristics (C-V)

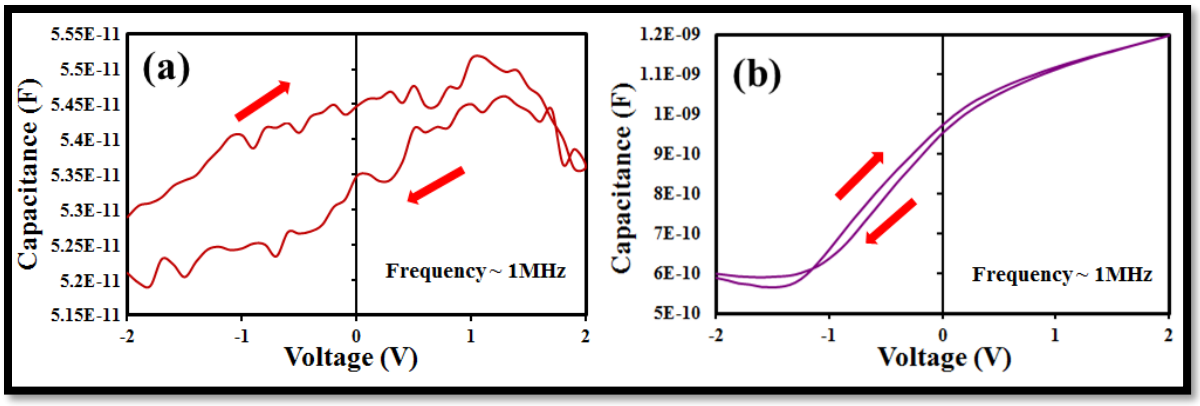

Figure 3.8 C-V curve of graphene/GaN heterojunction devices with (a) interfacial impurities (device 1) (b) Device 2 with cleaner transferred graphene.

Effect of residual impurities on the space charge dependent capacitance and interface trap dependent hysteresis for the graphene/GaN heterojunction is observed in C-V characteristics. Figure 3.8 (a) shows the C-V curve for a bias voltage range of -2 to +2 V for the device (1) with high interfacial impurities. A large C-V hysteresis window is observed which is consistent with the J-V characteristics, signifying the trapping of charge carriers by interfacial impurities. Figure 3.8 (b) shows C-V curve with the device fabricated with cleaner transferred graphene i.e. device 2, presenting a voltage dependent capacitance curve for depletion region in a Schottky junction

device. The graphene due to a proper contact with the GaN surface behaved as an ideal Schottky junction with a space charge region, whereas the device 1 due to high interfacial impurities did not show similar characteristics in the measured voltage range. Further, figure 3.8 (b) shows the presence of hysteresis due to slight mismatch of forward and reverse sweep in device 2, which can be attributed to presence of interface states. The presence of hysteresis in the device fabricated with clean graphene indicates presence of surface states in the GaN sample. Similar interface traps can be observed from the C-V analysis of previously reported AlGaN/GaN heterostructures devices. [32] The trapping/de-trapping effect in the device is further discussed in terms of band diagram as follows.

3.3.6 Band diagram:

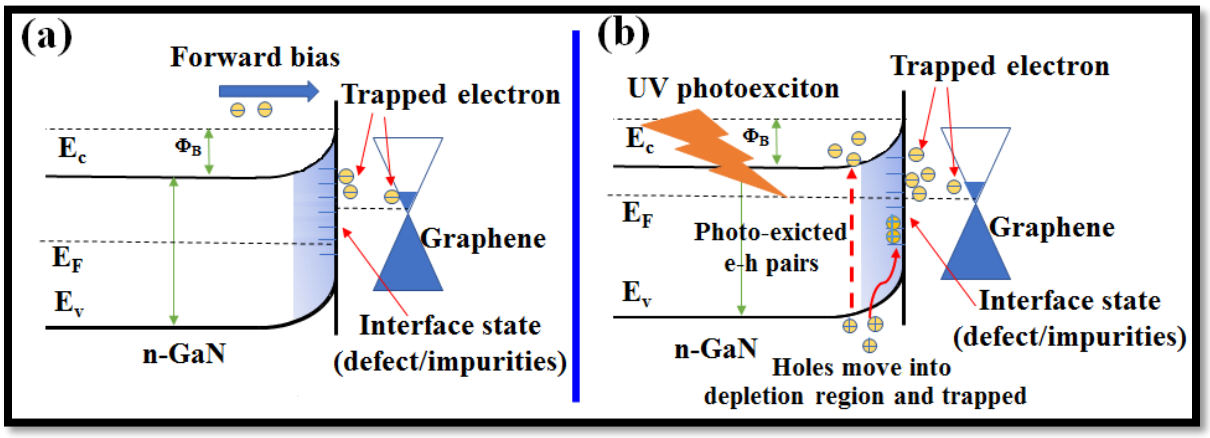

Figure 3.9 shows (a) band diagram for graphene/GaN heterojunction Schottky junction with interfacial states under applied bias voltage (b) band diagram under UV illumination, where photogenerated carriers (electrons and holes) trapping/de-trapping occurs at the interface of graphene/GaN.

Figure 3.9 (a) shows the energy band diagram for graphene/GaN heterojunction Schottky junction with interfacial state due to residual impurities and surface defects of GaN. The graphene with semi-metallic properties act as a Schottky contact, where the work function significantly changes with the doping level. Under the applied forward bias as shown in the band diagram electrons flow towards graphene in forward bias condition and due to presence of interfacial impurities trapping of electrons is observed which leads to interfacial charge accumulation. Figure 3.9 (b) shows the band diagram under UV illumination, where UV photo exciton are generated which results in higher number of charge carriers (electrons and holes) getting trapped at the graphene/GaN interface and hence enhancing the electrical hysteresis window. Previously, charge trapping process in graphene and MoS_2 based transistors and its subsequent electrical hysteresis effect has been reported.[33-35] It has been observed that the impurities in graphene as well as the formation of sp^3 and dangling bonds in presence of hydrogen and hydroxyl radicals creates the surface states for electron trapping.[36] Further, deep level traps and inherent surface defects in GaN are the main cause of carrier trapping in GaN based heterojunction devices.[29,37] Thus, the results suggest that the electrical hysteresis due to charge trapping can occur due to the both graphene impurities and trap states of GaN in the fabricated Schottky device.

3.3.7 Possible origin of impurities at the interface

As mentioned earlier the wet chemical transfer method is marred with possibility of introducing impurities in the heterojunction due to use and long exposure of water and various chemicals. Below figure shows the schematic diagram of wet chemical transfer method employed for fabrication of both graphene/GaN heterostructure.

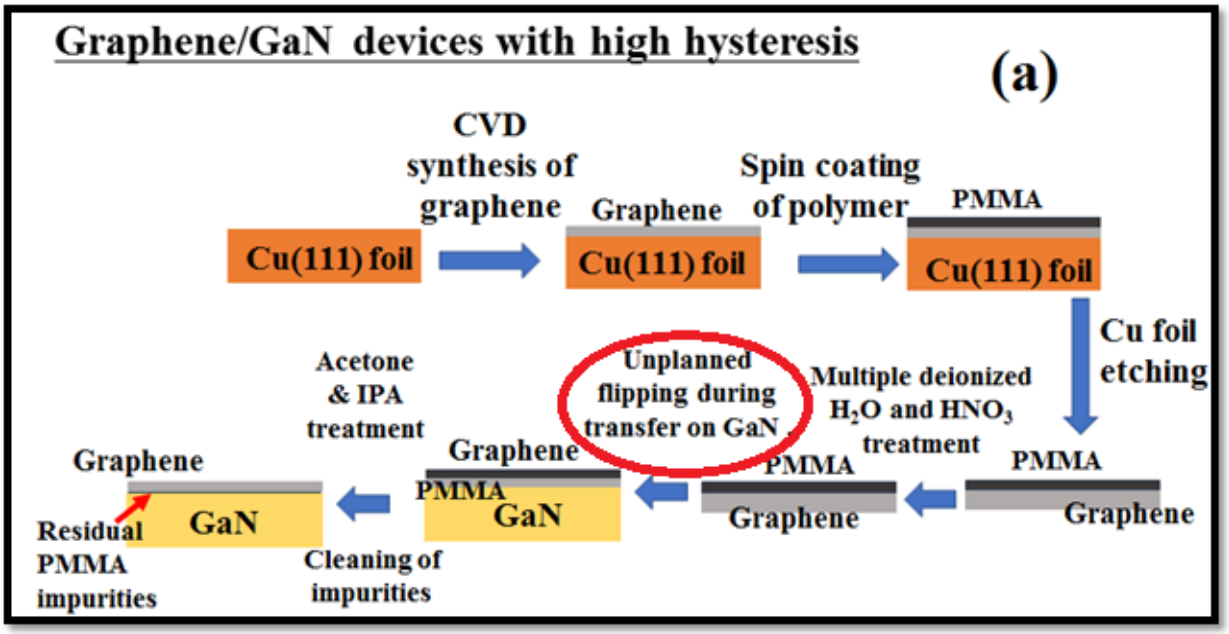

Figure 3.10 shows schematic diagram for transfer process employed for device 1 which showed high electrical hysteresis and low photoresponsivity.

Figure 3.10 shows schematic diagram for transfer process employed for device 1 which showed high electrical hysteresis and low photoresponsivity. After the CVD synthesis the graphene is coated with PMMA solution and transferred to ferric nitrate solution to etch copper. After etching is completed and subsequent washing of PMMA/graphene stack with dil. HNO_3 solution and deionized water, the PMMA graphene stack is transferred onto the GaN substrate. We estimate that during this step i.e transfer of PMMA/graphene stack on GaN substrate an unintentional flip occurred of the PMMA/graphene stack which resulted in PMMA being sandwiched between graphene and GaN substrate. Thus, during the removal of PMMA using acetone and isopropyl alcohol the sandwiched PMMA layer is not completely removed due to limited exposure to solvent as graphene which is above PMMA film will act as a cover for PMMA since graphene is non-reactive to acetone and isopropyl alcohol. Thus, the residual PMMA at the interface acts as

impurities at the interface and leads to trapping and de-trapping of charge carriers (electrons and holes) at the heterojunction interface thus inducing electrical hysteresis in the device.

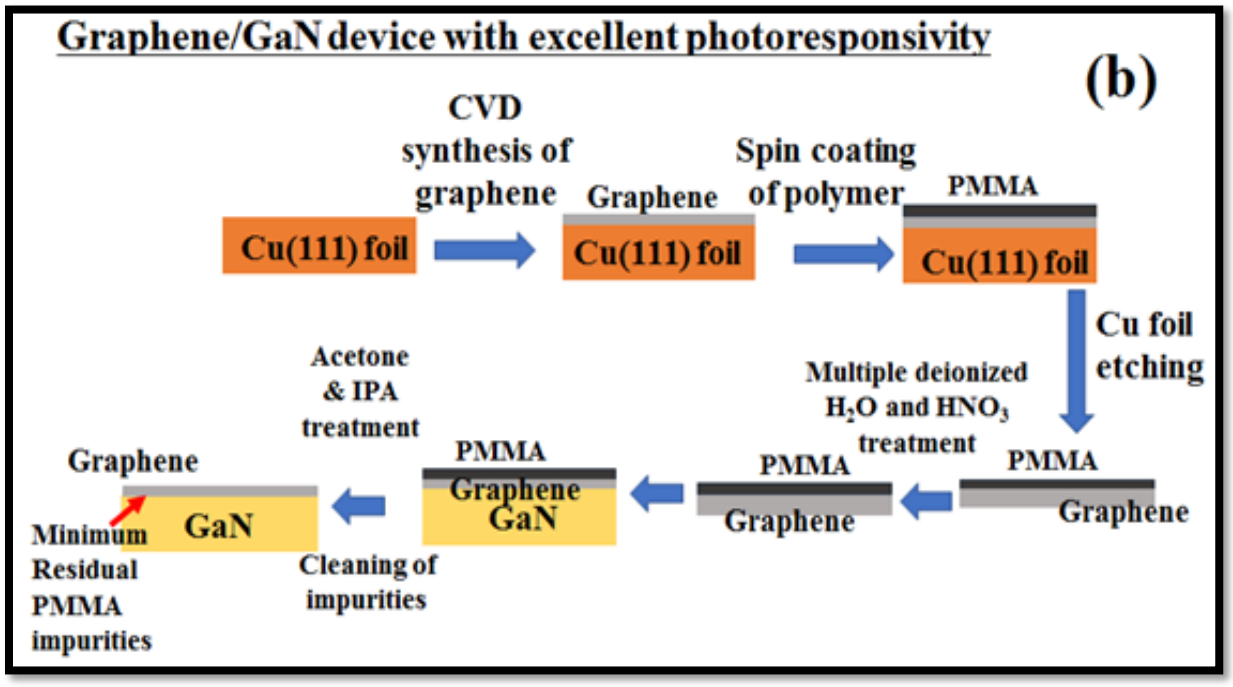

Figure 3.11 shows schematic diagram for transfer process employed for device 2 which showed high photoresponsivity and low electrical hysteresis.

Figure 3.11 shows schematic diagram for transfer process employed for device 2 which showed high photoresponsivity and low electrical hysteresis. A similar wet chemical transfer process is employed while taking special precaution to avoid flipping of PMMA/graphene stack during transferring it onto GaN substrates. Thus, in this device the graphene was sandwiched between PMMA and GaN substrate which is the way it is supposed to be and results in removal of upper PMMA layer and producing graphene/GaN heterojunction with minimum residual PMMA impurities at heterojunction interface. This results in good transport of charge carries through the

heterojunction interface without trapping and de-trapping phenomenon and hence excellent photoresponsivity with low electrical hysteresis is observed.

3.3.8 UV spectroscopy

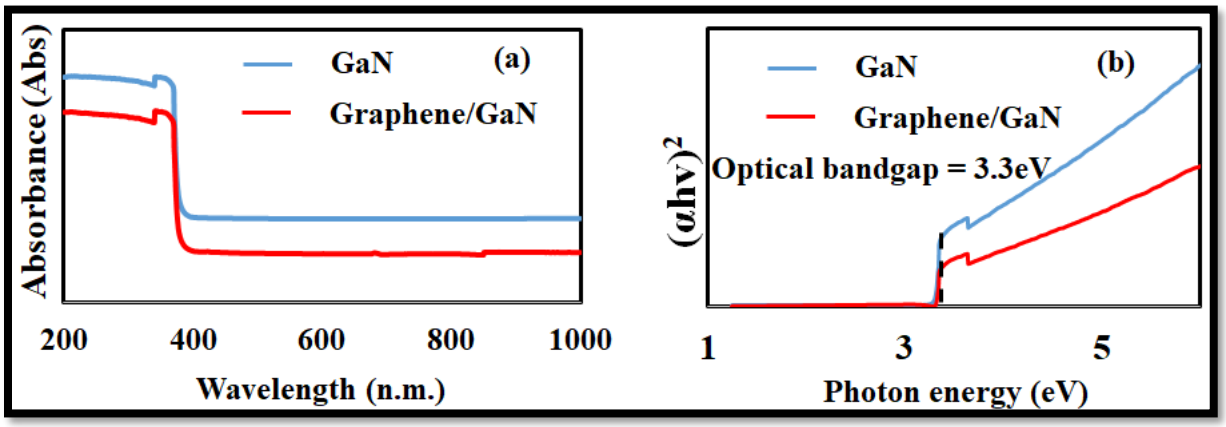

Figure 3.12 shows (a) UV absorption spectra of freestanding GaN and newly fabricated graphene/GaN heterojunction (b) Tauc plot to calculate optical bandgap of the pristine GaN.

Further, a new graphene/GaN heterostructure was fabricated using same transfer method to check the UV absorption spectroscopy of graphene/GaN device. Figure 3.12 (a) shows the UV absorption spectroscopy of pristine freestanding GaN and graphene/GaN heterostructure. An absorption in the range of 365nm is observed which corresponds to the absorption of UV light and transition of electrons to conduction band. Other than minor reduction in absorption intensity no other change was observed before and after the transfer of graphene. Figure 3.12 (b) shows the Tauc's plot for pristine GaN and graphene/GaN heterostructure. A band gap of 3.3 eV is observed for the for the pristine GaN is unchanged after the graphene transfer, which agrees with the literature study.

3.4 Conclusion

In conclusions, I have demonstrated the effect of UV light illumination induced electrical hysteresis in the graphene/GaN heterojunction. We have further explored the role of residual impurities and surface states on the device performance. A LPCVD synthesized graphene was transferred on freestanding GaN substrate using wet chemical transfer method. The transfer process directly affects the device properties and induces electrical hysteresis behavior. An electrical hysteresis behavior is observed under dark condition and increase in hysteresis window is observed under UV illumination due additional photocarriers generated by UV illumination. This hysteresis behavior is attributed to presence of residual PMMA impurities at the interface, which is act as trap sites for charge carrier at the interface. Further, a clean graphene free of PMMA impurities is transferred on GaN and analyzed for electrical hysteresis behavior. The clean graphene/GaN heterojunction did not show hysteresis under dark condition however under UV illumination hysteresis was observed which signified presence of surface states that act as trap sites. Thus, I report on simple UV illumination technique for checking the interface quality of heterojunctions and identifying on the type of impurity present at the heterojunction interface.

3.5 References

1) X. Li et al., Adv. Mater., vol. 22, no. 25, pp. 2743-2748, 2010.
2) G. Kalita et al., J. Phys. D: Appl. Phys., vol. 46, no. 45, p. 455103, 2013.
3) C. Xie et al., Nano Today, vol. 19, pp. 41-83, 2018.
4) S. Tongay et al., Appl. Phys. Lett., vol. 99, no. 10, p. 102102, 2011.
5) S. Kim et al., Nano Res., vol. 8, no. 4, pp. 1327-1338, 2015.
6) F. Giannazzo et al., Phys. Status Solidi A, vol. 214, no. 4, p. 1600460, 2017.
7) M. Meneghini et al., IEEE Transactions on Device and Materials Reliability, vol. 8, no. 2, pp. 323-331, 2008.
8) E. A. Jones et al., IEEE J. Emerging Sel. Top. Power Electron., vol. 4, no. 3, pp. 707-719, 2016.
9) J. Millán et al., IEEE Trans. Power Electron., vol. 29, no. 5, pp. 2155-2163, 2014.
10) L. Wang et al., Nano Energy, vol. 12, pp. 419-436, 2015.
11) M. Heilmann et al., Nano Lett., vol. 16, no. 6, pp. 3524-3532, 2016.
12) C. Du et al., Small, vol. 11 no. 45, pp. 6071-6077, 2015.
13) J. K. Kim et al., Adv. Mater., vol. 20, no. 4, pp. 801-804, 2008.
14) J. P. Shim et al., Appl. Phys. Express, vol. 4, no. 5, p. 052302, 2011.
15) T. Egawa, et al., J. Appl. Phys., vol. 82, no. 11, pp. 5816-5821, 1997.
16) G. T. Dang et al., IEEE Trans. Electron Devices, vol. 47, no. 4, pp. 692-696, 2000.
17) D. Donoval et al., J. Appl. Phys., vol. 109, no. 6, p. 063711, 2011.
18) M. R. H Khan et al., J. Phys. D: Appl. Phys., vol. 28, no. 6, p. 1169, 1995.
19) H. Ishikawa et al., Jpn. J. Appl. Phys., vol. 37, no. 1A, pp. 7–9, 1998.

20) G. Kalita et al., Phys. Status Solidi A, vol. 215, no. 18, p. 1800089, 2018.

21) A. B. McLean et al., Semicond. Sci. Technol., vol. 2, no. 7, p.404, 1987.

22) S. Chandramohan et al., " Appl. Phys. Lett., vol. 100, no. 2, p. 023502, 2012.

23) N. Prakash et al., Appl. Phys. Lett., vol. 109, no. 24, p. 242102, 2016.

24) G. Kalita et al., Appl. Phys. Lett., vol. 111, no. 1, p. 013504, 2017.

25) H. Tian et al., Opt. Express, vol. 26, no. 5, pp. 5408-5415, 2018.

26) H. Tian et al., Appl. Phys. Lett., vol. 113, no. 12, p. 121109, 2018.

27) A. Kumar et al., ACS Appl. Mater. Interfaces, vol. 8, no. 12, pp. 8213-8223, 2016.

28) J. H. Lee et al., ACS Appl. Mater. Interfaces, vol. 10, no. 16, pp. 14170-14174, 2018.

29) L. Sang et al., Appl. Phys. Lett., vol. 107, no. 5, p. 052102, 2015.

30) B. P. Jaisi et al., Cryst. Eng. Comm., vol. 20, no. 36, pp. 5356-5363, 2018.

31) X. Lu et al., IEEE Trans. Electron Devices, vol. 64, no. 3, pp. 824-831, 2017.

32) Y. J. Lin et al., Appl. Surf. Sci., vol. 322, pp. 225-229, 2014.

33) C. H. Lin et al., J. Appl. Phys., vol. 105, no. 5, p. 054502, 2009.

34) H. Wang et al., ACS Nano, vol. 4, no. 12, pp. 7221-7228, 2010.

35) C. Lee et al., " Nanotechnology, vol. 29, no. 33, p. 335202, 2018.

36) M. Z. Iqbal et al., Carbon, vol. 123, pp. 168-173, 2017.

37) Z. Q. Fang et al., Appl. Phys. Lett., vol. 87, no. 18, p. 182115, 2005.

CHAPTER 4

4. Formation of effective CuI-GaN heterojunction with excellent ultraviolet photoresponsive photovoltage

4.1 Introduction

Among group III-nitride compound semiconductors, gallium nitride which is a wideband gap semiconductor (3.4 eV) has attracted wide device application-based research due to its excellent electronic properties. [1-6] GaN possesses various outstanding optical and electronic properties like direct band gap, high critical breakdown field, stability at high temperature operation and high electron saturation velocity and hence it has found application in solar cells, photodiodes, light emitting diodes (LED's) and high electron mobility transistors. [7-16] GaN based devices provide a unique advantage over other traditional semiconductors such as its operating capability at high output power, high frequency and high temperature conditions. [15-21] As aforementioned, GaN has been widely researched and combined with various other semiconductors and 2D materials like graphene and transition metal chalcogenides (TMDC's) to fabricate van der waal's heterostructure devices. [6,14.24-27]. Graphene with its zero bandgap forms a Schottky junction with GaN. Further, growth of 2-dimentional GaN layer using epitaxial graphene and liquid metal has also been reported which has been an important step in development of GaN based van der waal's heterostructures.[22,23] The earlier chapter of this thesis discussed the transport properties in graphene/GaN heterojunction in presence of interfacial impurities. Kalita et al have reported on a photovoltaic action in graphene/GaN heterojunction. [55] Further, transition metal dichalcogenides with their direct band gap form a p-n and n-n^+ heterojunctions and are an interesting prospect for

fabrication of p-n heterojunction. [6,25-28] In this prospect, integration of a highly p-type wide band gap semiconductor with n-type GaN can be significant to develop GaN based UV photodetectors.

In the search for a p-type semiconductor, zinc-blend γ-copper iodide (γ-CuI) which possess a wide bandgap of (3.1 eV) and excellent p-type conductivity (>40 $cm^2 V^{-1} s^{-1}$ in bulk) could be a good candidate to integrate with n-type GaN to form a p-n heterojunction .[37,38] Copper iodide (γ-CuI) has been integrated with other organic/inorganic semiconductors for stable device performance.[29,30] The copper iodide (CuI) exists in three different crystalline phases i.e. α, β, and γ which are dependent on temperature.[31] The cubic γ-phase is found stable till 369°C above which it undergoes phase transition to hexagonal β-phase which in turn undergoes phase transition to the cubic α-phase above 407°C.[39,40] Due to its stability in the normal temperature range for electronic application, γ-CuI has been explored for fabrication of heterojunction photovoltaic devices, organic electronics, bipolar diodes for transparent electronics.[41-43] A p-n heterojunction of γ-CuI/ZnO showed excellent rectifying diode characteristics while ultrathin 2D nanosheets of γ-phase CuI for fabrication of van der Waal's heterostructures has been reported. [44-46]. In this prospect, it is indeed interesting to explore the possibility of integrating a p-type γ-phase CuI with n-type GaN for developing an effective heterojunction device. After studying the Schottky junction properties of graphene/GaN heterojunction, this thesis proceeds to explore the formation a p-n heterojunction between p-type γ-CuI and n-type GaN. As aforementioned GaN based device possess an advantage of operating capability at higher temperature, this study evaluates the J-V characteristics of the fabricated γ-CuI/GaN heterojunction up to a high temperature of 373K. In contrast to previous reports, this chapter discusses for the first time to my knowledge the fabrication of γ-CuI/GaN heterojunction device with excellent ultraviolet photoresponse and high photovoltage. In what follows, the fabrication of γ-CuI/GaN

heterojunction and diode characteristics with excellent UV photoresponsive photovoltage were elucidated with temperature dependent transport behavior analysis.

4.2 Experimental section

For this study, a Si-doped (doping level~ 2×10^{18} cm^{-3}) GaN film with a thickness of ~2 µm deposited on sapphire substrate by metalorganic chemical vapor deposition (MOCVD) technique was used. The deposition of CuI layer on GaN was achieved by high vacuum thermal evaporation process. Copper iodide powder was procured from Wako pure chemical industries ltd (95% purity) and directly deposited on GaN substrate by the thermal evaporation process at room temperature and pressure of $6x10^{-4}$ Pa.

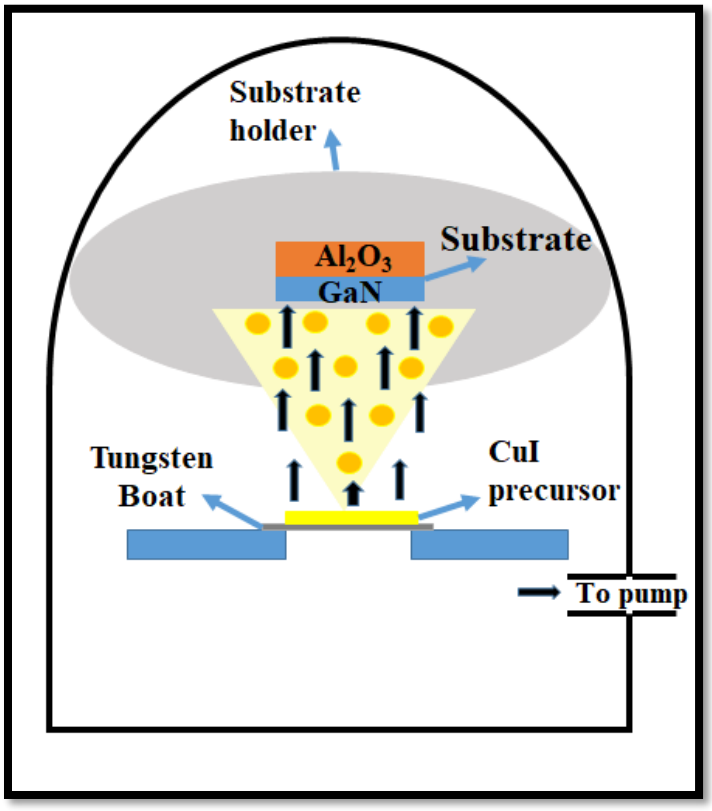

Figure 4.1 shows the experimental setup of the thermal evaporation chamber for deposition of CuI on GaN film.

The thickness of deposited γ-CuI layer can be controlled with evaporation rate, amount of precursor and deposition time. The fabricated heterostructure was analyzed by spectroscopic as well as microscopic techniques to confirm the deposition of uniform γ-CuI layer on GaN substrate before fabricating the heterojunction. The fabricated heterojunction was once again subjected to thermal evaporation technique under high vacuum for metal electrode deposition to complete the device configuration. Considering the work function of γ-CuI and GaN, gold (Au) and Indium (In) was deposited on γ-CuI and respectively to fabricate a horizontal device. Figure 4.1 shows the schematic of thermal evaporation reaction vessel showcasing the deposition of CuI powder on GaN substrate.

4.3 Results and discussion:

The synthesized materials were analyzed by microscopic as well as spectroscopic methods. Scanning electron microscope (SEM) analysis was carried out by using JEOL JSM 5600 instrument with an accelerating voltage of 20 kV. Raman analysis was performed by the NRS 3300 laser Raman spectrometer with a laser excitation wavelength of 532.08 nm. X-ray diffraction analysis was performed with Rigaku RINT-2100. X-ray photoelectron spectroscopy (XPS) analysis was done by versa probe using monochromated Al Kα excitation source (1486.6 eV). Current density-voltage (J-V) characteristics of the CuI-GaN heterojunction device were carried out at various temperature using a two-probe system and Keithley 2401 source meter. The temperature-dependent J-V characteristics was measured by placing the device on a hot plate integrated with digital temperature controller. Quantum efficiency (QE) measurement was performed by using the SM-250 hyper monochromatic light system in the wavelength range of 300-1100 nm.

4.3.1 Ball and stick crystal diagram:

Figure 4.2 shows the cross-section stick-and-ball crystal structures of the cubic γ-CuI on n-type GaN. The n-type GaN with its electron affinity of 4.1 eV and the p-type γ-CuI of 2.5 eV indicates suitability to create a large built-in-field at the heterojunction interface. Thus, the interface properties of the p-type γ-CuI and n-type GaN can be interesting to develop a diode for photoresponsive device and transparent electronics.

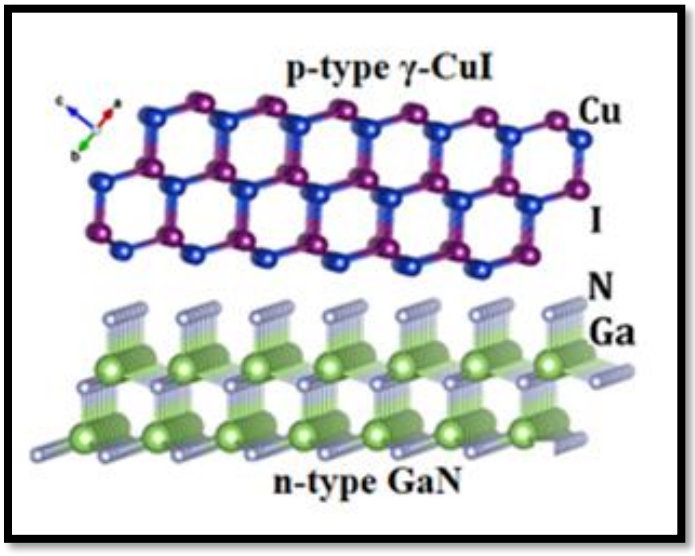

Figure 4.2 shows ball and stick model of CuI and GaN crystal structure.

The fabricated γ-CuI/GaN heterostructure was then initially analyzed by Raman spectroscopy as shown below.

4.3.2 Raman spectroscopy

The fabricated heterostructure was anazlyzed by Raman spectroscopy by taking Raman spectra at two random points. Figure 4.3 shows Raman spectra of fabricated heterostructure. A high intensity peak is observed at 120 cm^{-1} which corresponds to optical transverse mode of Cu-I bonding

vibration in the deposited CuI films.[53] Further, two peaks at higher wavenumber were observed around 578 cm^{-1} and 747 cm^{-1} which correspond to GaN film.[6] The presence of high intensity peaks at 120 cm^{-1} cm as well as at 578 cm^{-1} and 747 cm^{-1} at two random points on the fabricated heterostructure confirmed the presence of continuous γ-CuI layer on GaN film.

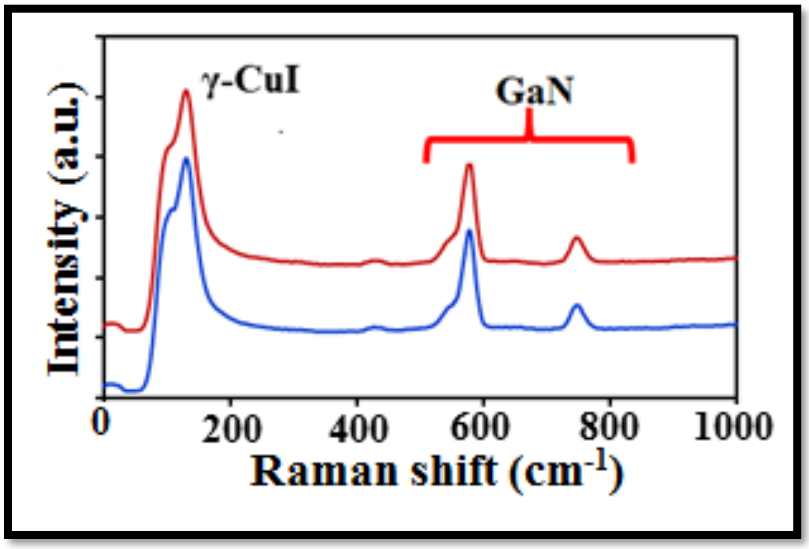

Figure 4.3 shows Raman spectra of the γ-CuI/GaN heterostructure at various points.

Thus, by Raman spectroscopy we obtain preliminary confirmation of fabrication of γ-CuI/GaN heterostructure. The heterostructure was further analyzed by XRD spectroscopy to confirm the crystallinity of CuI film on GaN film.

4.3.3 X-ray diffraction analysis

Prior to XRD analysis of the fabricated γ-CuI/GaN heterostructure, a γ-CuI film was deposited on glass substrate under similar condition used for the fabrication γ-CuI/GaN heterostructure and was subjected to XRD analysis to check the crystallinity of the of the γ-CuI film by comparing it with the JCPDS database. Figure 4.4 shows the X-ray diffraction spectra of γ-CuI film on glass and GaN along with standard diffraction spectra for GaN (JCPDS card number. 50-0792) and γ-CuI

(JCPDS card number. 06-0246). A strong diffraction peak corresponding to (111) plane is observed in comparison to (220), (331) and (422) planes indicating preferable orientation growth of CuI crystal along (111) plane.

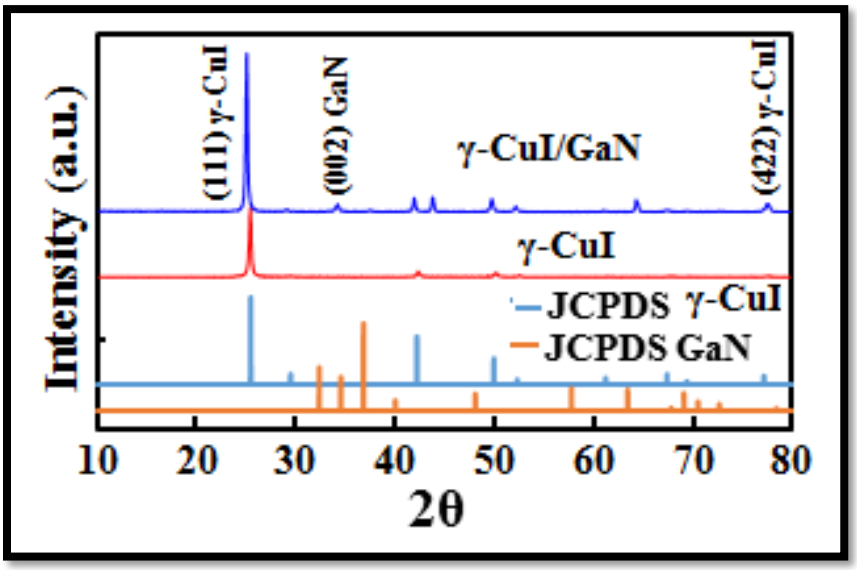

Figure 4.4 shows the XRD spectra of the thermally evaporated γ-CuI film on glass and γ-CuI/GaN heterostructure comparing with the JCPDS values, dominant (111) orientation of γ-CuI cubic crystal was obtained on GaN.

The lattice mismatch between γ-CuI and GaN is significantly higher and hence the growth along (111) plane can be attributed to the lowest surface energy for growth along CuI (111) plane.[47,48] Considering the layered structure of GaN, the integration of γ-CuI can lead to formation of van der Waals heterostructures. In this study, the thickness of γ-CuI film is much higher, hence a continuous and uniform γ-CuI film is achievable on GaN substrate for heterojunction device fabrication. Thus, after confirming good crystallinity of the γ-CuI film on GaN, the heterostructure was analyzed by FE-SEM to get a visual image of heterostructure interface.

4.3.4 Field emission scanning electron microscopy:

Figure 4.5 shows the FESEM cross sectional view of the fabricated γ-CuI/GaN heterostructure. A continuous γ-CuI film on GaN can be observed with a clear boundary.

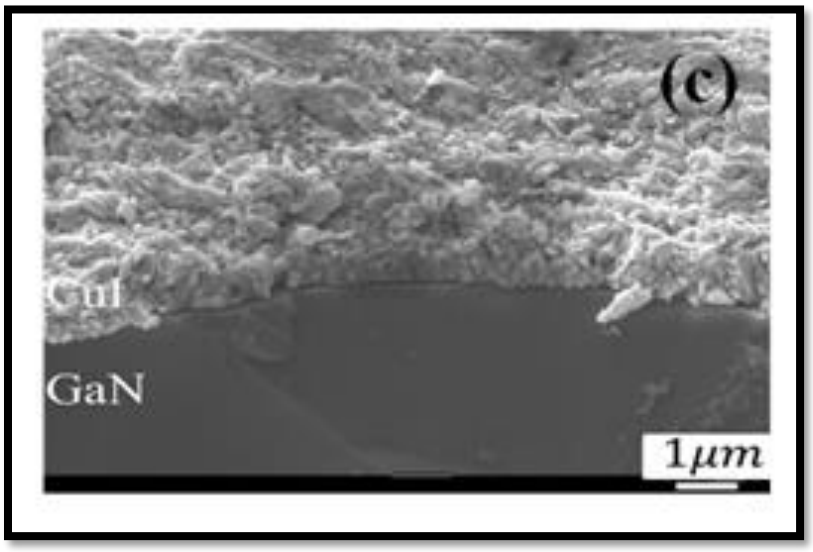

Figure 4.5 shows the FESEM cross sectional view of γ-CuI/GaN heterostructure.

The thickness of γ-CuI film is much higher (approx. 1 μm) and hence a uniform film is obtained on GaN substrate. Further, the heterostructure was subjected to X-ray photoelectron spectroscopy to confirm its elemental composition.

4.3.5 X- ray photoelectron spectroscopy

To investigate the chemical composition, the fabricated γ-CuI/GaN heterostructure was investigated by XPS analysis. Figure 4.6 (a) shows the XPS survey spectra for the pristine GaN and γ-CuI/GaN heterostructure, showing the expected Ga3d peak of GaN, Cu2p and I3d peaks for γ-CuI respectively. Along with the expected peaks, some unexpected peaks of carbon and oxygen

impurity can be observed which can be attributed to surface chemisorption, while no other impurity peaks were observed for the fabricated γ-CuI/GaN heterostructure. Figure 4.6 (b) shows the Ga3d peaks for the pristine GaN and after deposition of γ-CuI on GaN. Due to high thickness of CuI film, Ga3d peak for the heterostructure was not observed as the incident X-rays cannot penetrate CuI film to detect below GaN surface.

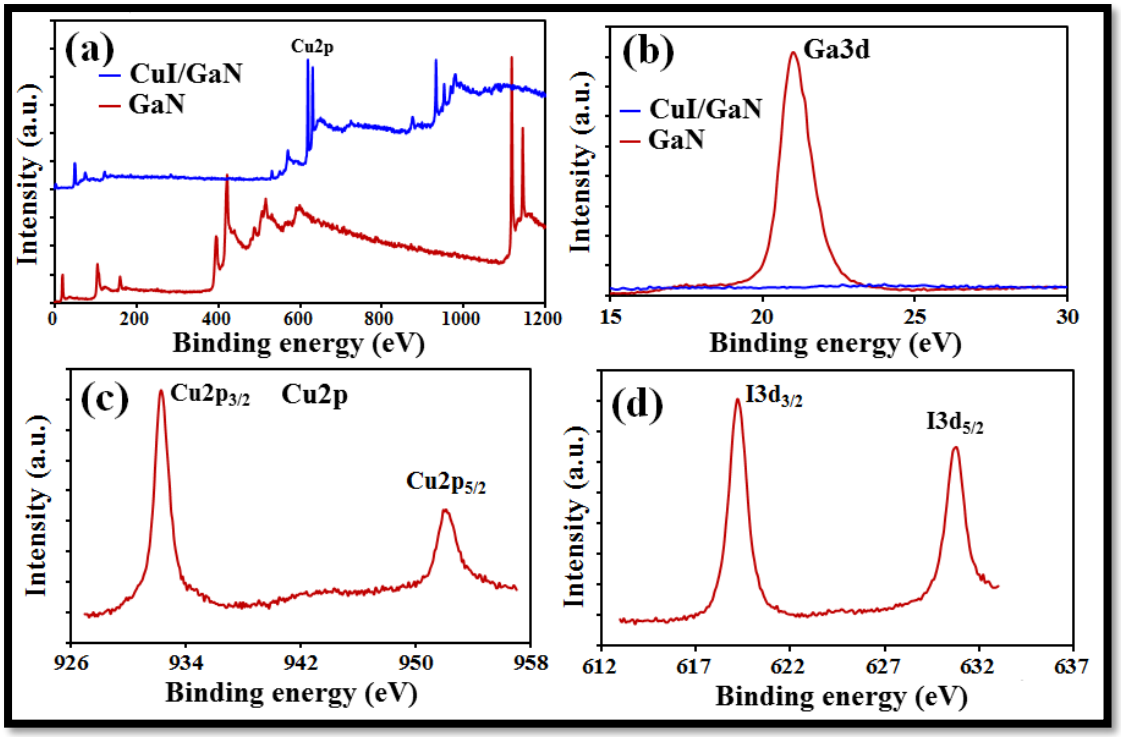

Figure 4.6 shows XPS (a) survey spectra indicating the Ga3d peak of GaN, Cu2p and I3d peaks for CuI, (b) Ga3d peaks for the GaN and CuI/GaN heterostructure. (c) Cu ($2p^{3/2}$~932.2 eV and $2p^{1/2}$~952 eV) (d) I ($3d^{5/2}$~619.5 eV and 631 eV for $3d^{3/2}$) peaks of the CuI film on GaN.

Figure 4.6 (c) shows the Cu2p peak, presenting the $2p^{3/2}$ and $2p^{1/2}$ binding states at the binding energy of ~932.2 and 952 eV. Similarly, Figure 4.6 (d) shows the I3d peak, presenting the binding states for $3d^{5/2}$ and $3d^{3/2}$ at 619.5 and 631 eV for the γ-CuI film on GaN. A stable thermally evaporated γ-CuI film on GaN is observed for the fabricated heterojunction. Thus, after confirming

the presence of continuous and uniform γ-CuI film on GaN, the fabricated heterostructure was again subjected to thermal evaporation technique to deposit metal contact of gold (Au) and Indium (In) on γ-CuI and GaN respectively to fabricate a horizontal Au/γ-CuI/GaN/In heterojunction, which was then further explored to check its electronic properties by J-V characteristics.

4.3.6 Current density–voltage characteristics (J-V)

The fabricated device was analyzed by J-V characteristics to check the suitability of forming an effective heterojunction device. Initially, the device was checked under applied bias voltage of -2V to +2V in dark condition to check its diode characteristics, following which the device was checked under high applied bias voltage of -20V to +20V. Further, since GaN based devices have advantage of operating at higher temperature, the fabricated device was analyzed for temperature dependent J-V characteristics in the temperature range of 298K to 373K. Subsequently, considering the large binding energy of 62 meV and 28 meV for the direct band gap γ-CuI and GaN respectively, the device was then investigated for its UV photoresponsive characteristics. Further, the effect of temperature on photovoltaic effect for the fabricated device was evaluated in the temperature range of 298K to 373K. Finally, to check the interface quality of the fabricated heterojunction the device was checked for presence of electrical hysteresis under dark as well as UV illumination.

Figure 4.7 (a) shows the schematic diagram of Au/γ-CuI/GaN/In horizontal heterojunction device on Al_2O_3 substrate. Metal contact of gold (Au) which has work function of ~5.1 eV was deposited on γ-CuI layer considering its p-type conductivity and high work function while Indium (In) with work function of ~4.12 eV was deposited on n-type GaN. Figure 4.7 (b) shows the J-V characteristics under dark condition for applied bias voltage of -2V to +2V. Inset shows its corresponding log plot. A rectifying diode behavior with rectification ratio of 10^2 is observed. The

log plot and its slope were used to evaluate the ideality factor (n) at room temperature using the following equation (1), which presents the deviation of diode characteristics from ideal case.

$$J = J_0 . (e^{\frac{qV}{nkT}} - 1) \quad \text{……..} \quad (1)$$

where, J is the current density flowing through the diode, V is the voltage across the diode, J_0 is the saturation current density, n is the ideality factor and T is the temperature in kelvin. The q and k are constants i.e. charge on electron and Boltzmann's constant.

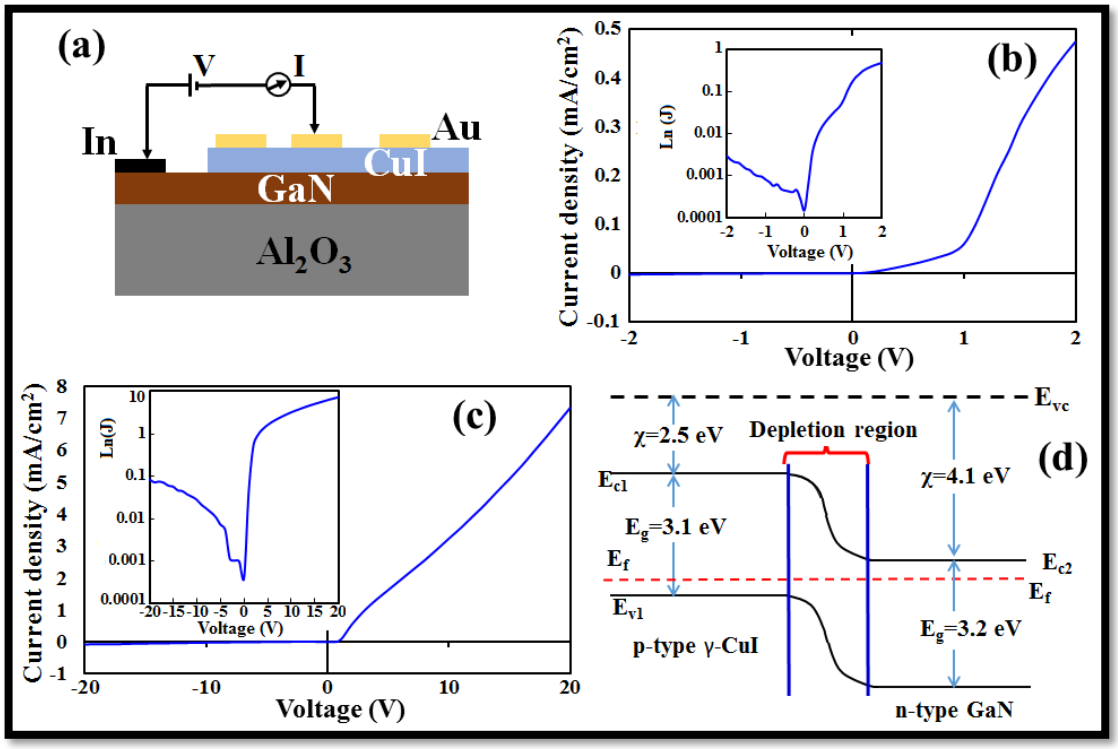

Figure 4.7 (a) schematic diagram of the γ-CuI/GaN heterojunction device on Al_2O_3 substrate. (b) J-V characteristics under dark condition (inset shows the log plot). (c) J-V characteristics for higher applied bias voltage (-20V to +20V), presenting low reverse saturation current (inset shows the log plot), (d) probable energy band diagram for the γ-CuI/GaN heterojunction device.

The logarithmic form of the equation (1) is shown in equation (2) which is used for calculating the ideality factor. [6]

$$L_n(J) = L_n(J_0) + \left(\frac{q}{nkT}\right)V \quad \ldots\ldots \quad (2)$$

The ideality factor for the fabricated device at room temperature i.e. 298 K computed to 8.5, which is quite high and can be due to unoptimized interface and metal contacts on γ-CuI and GaN. Further, as GaN based devices have been shown to operate at high operating voltage, the J-V characteristics of the fabricated γ-CuI/GaN heterojunction was checked at applied bias voltage of -20V to +20V. Figure 4.7 (c) shows the J-V characteristic at higher bias voltage range of -20.0 to +20.0 V, in which rectification behavior and ratio was consistent with lower applied voltage and indicates stability of γ-CuI/GaN heterojunction at higher operating voltage. Inset of figure (c) shows the log plot for the higher applied voltage condition. The J-V characteristics confirmed that the γ-CuI/GaN heterojunction can be suitable as p-n junction diode for high bias voltage operations. Figure 4.7 (d) shows the probable energy band diagram for the γ-CuI/GaN heterojunction device. The band gap γ-CuI and GaN are 3.1 and 3.2 eV respectively which is in similar range and leads to formation of effective heterojunction without much pining of valence and conduction band. The difference in electron affinity and work functions of the two materials ensured formation of a significant build in field ($\phi_{GaN} - \phi_{\gamma\text{-CuI}} = V_{bi}$) in the range of 0.95 eV at the heterojunction interface of γ-CuI/GaN. Subsequently, as GaN based devices are known to operate at high temperature, the fabricated device was subjected to temperature dependent J-V analysis.

Figure 4.8 (a) shows the J-V characteristics for -2V to +2V applied bias voltage in the temperature range of 298~373 K where increase in forward current and effect on reverse saturation current is observed. Figure 4.8 (b) shows the J-V curve in the voltage range of -2Vto 0V, showcases the

reverse saturation current (J_0) under dark condition for temperature range of 298 K to 373 K. A fluctuation in reverse saturation current was observed which can be attributed to the fact that reverse saturation current was is in the order of µA and as a result, a small change in temperature significantly affected the reverse saturation current. Figure 4.8 (c) shows the log plot of the J-V curve with change in temperature (298~373 K). The log plot clearly indicates high sensitivity of saturation current to increasing temperature for the fabricated heterojunction device. The effect of temperature on enhancing saturation current is consistent with figure 4.8 (b)

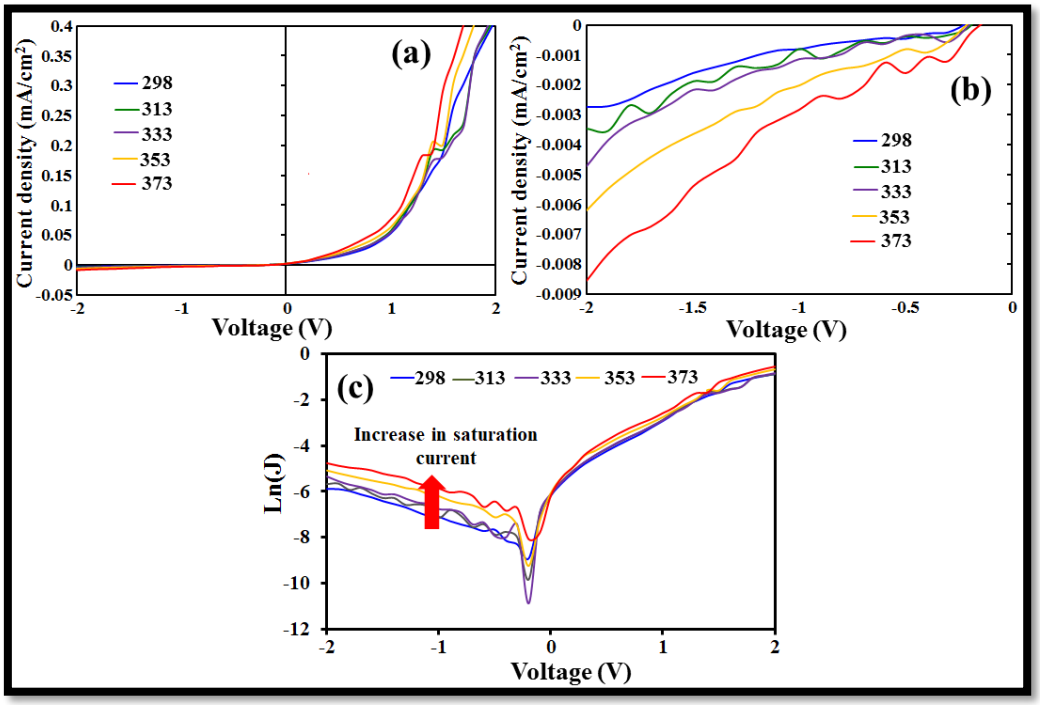

Figure 4.8 J-V characteristics under dark conditions in the temperature range of 298 K to 373 K (a) for applied bias voltage of -2V to +2V and (b) -2V to 0V (c) Log plot in voltage range of -2V to +2V.

Ideality factor was calculated at 373 K and was computed to 6.1 which is still high and again can be attributed to unoptimized interface and respective metal contacts on γ-CuI and GaN. Subsequently, the heterojunction was investigated for its UV photoresponsive properties. Figure 4.9 (a) shows the J-V characteristic under dark and UV illumination (100 mW/cm^2) for the γ-CuI/GaN heterojunction device. A photovoltaic action with an open circuit voltage (V_{oc}) of 0.93 V and short circuit current density (J_{sc}) of 0.49 mA/cm^2 is observed. The high photovoltage could be attributed to large internal build-in-field at the interface of p-type γ-CuI and n-type GaN heterojunction due to large difference in electron affinity and work function between two materials.

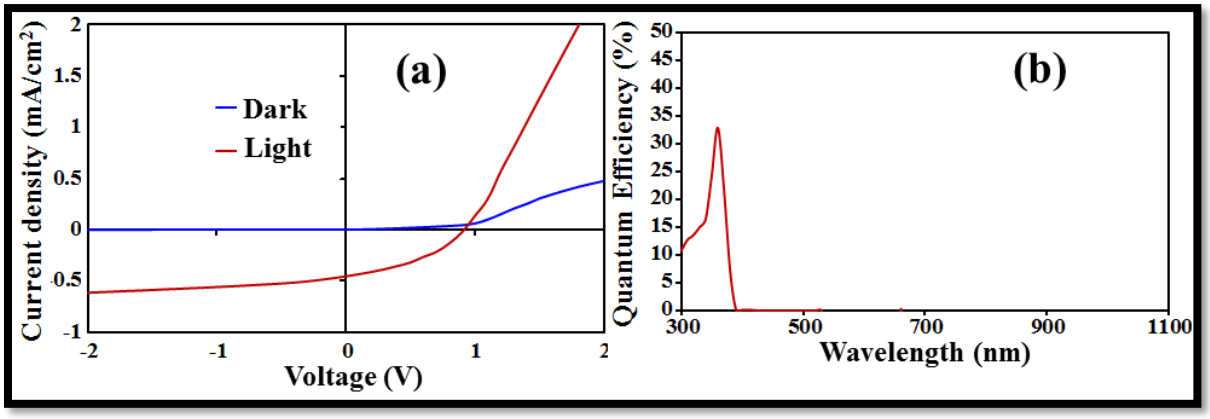

Figure 4.9 (a) J-V characteristic under dark and UV light illumination (100 mW/cm^2) conditions for the γ-CuI/GaN heterojunction device. (b) corresponding quantum efficiency (QE) curve.

The photovoltage is consistent with build-in-potential as estimated from the work function difference of the two materials. The high photovoltage also signifies that the recombination loss of the UV excited photocarriers is less compared to many other GaN heterojunction devices. The obtained photovoltage in the fabricated γ-CuI/GaN is quite higher than that of reported graphene/n-GaN Schottky heterojunctions.[6] However, the observed photovoltage for the single junction γ-

CuI/GaN device is comparatively lower than that of InGaN/GaN based multiple quantum well photovoltaic devices while the QE is comparable to the quantum well device.[49] Irrespective of the previous reports, the γ-CuI/GaN heterojunction showed a good UV photodiode characteristic with high photovoltage and can be unique for developing self-powered UV photoresponsive devices. The, device was then checked for its quantum efficiency, which is basically a measure of how effectively a device can convert incident photons into electrons (i.e. IPCE ratio) which is dependent on wavelength of the incident light. Figure 4.9 (b) shows the corresponding QE curve for the heterojunction device and a peak value of 33% at 360 nm wavelength (UV region) was obtained, which is in good agreement of the theoretical bandgap of GaN. The good QE value is consistent with effective photovoltaic action in the fabricated γ-CuI/GaN heterojunction device. These results signify that a transparent diode and high photovoltage UV photodetectors with self-powered mode of operation can be developed using γ-CuI/GaN heterostructure. Subsequently, the fabricated device was evaluated for its temperature dependent UV photovoltaic properties in the temperature range of 278 K to 283 K. Figure 4.10 (a) J-V characteristics under UV illumination in the temperature range of (298 K -373 K) for the fabricated γ-CuI/GaN heterojunction under applied bias voltage of -2V to +2V. The variation in photovoltaic action is evident with change in applied temperature. Figure 4.10 (b) shows the effect of change in temperature on J_{sc} and V_{oc} values for the heterojunction. With an increase in temperature, increase in J_{sc} while decrease in V_{oc} is observed. Figure (c) shows the variation of J_{sc} and V_{oc} in the temperature range of 298 K to 373 K for the fabricated γ-CuI/GaN heterojunction. The decrease in V_{oc} with increase in temperature can be attributed decrease in the band gap of the photoresponsive materials as well as the diode saturation current (J_0).[51,52]

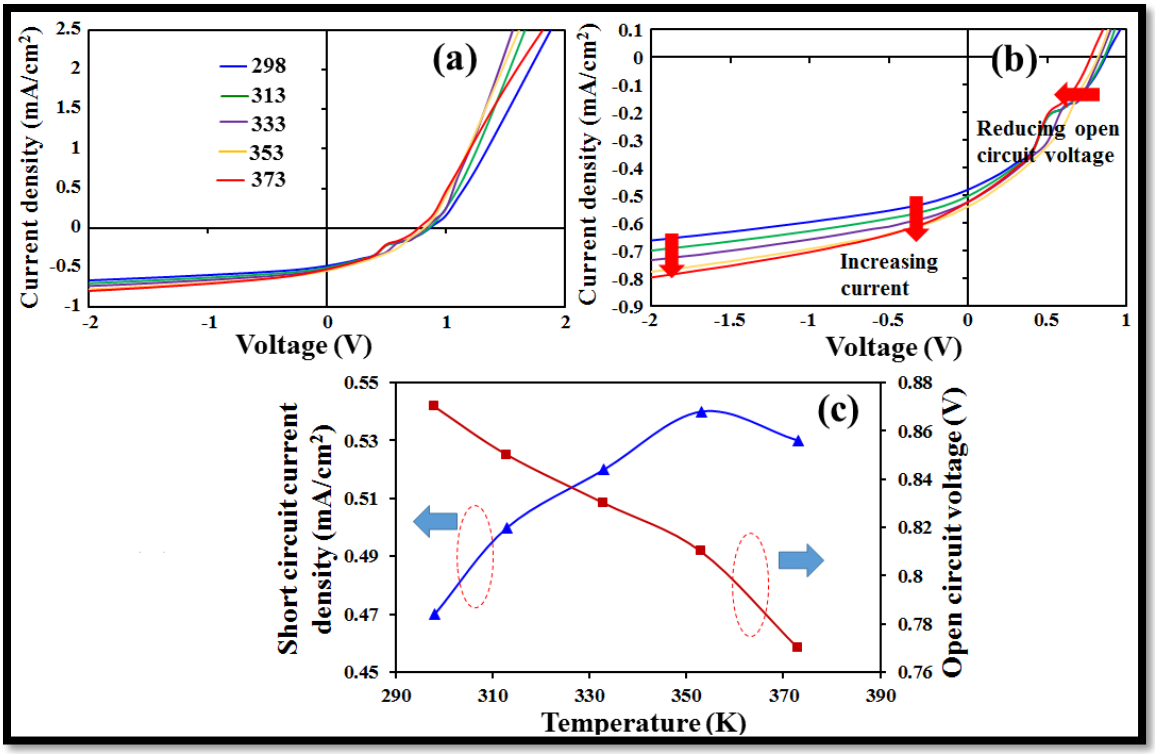

Figure 4.10 J-V characteristics under UV illumination in the temperature range of (298 K -373 K) (a) -2V to +2V and (b) +1V to -2V (c) variation in open circuit voltage (V_{oc}) and short circuit current density (J_{sc}) with change in temperature (298~373 K) for the fabricated heterojunction.

The band gap of a semiconductor reduces with increase in temperature as expressed in the following equation (3).

$$E_g(T) = E_0 - \left(\frac{\alpha T^2}{T+\beta}\right) \quad \ldots\ldots\ldots \quad (3)$$

where, $E_g(T)$ is the band gap of the semiconductor at a temperature T, E_0 is the band gap value at T=0 K, α and β are fitting parameters characteristic of a given material. [51]

Further, the V_{oc} can be related to the saturation current (J_0) of the device as shown in equation (4).[52] In the equation, q is the elementary charge and K is the Boltzmann constant. J_L is the light generated current density and J_0 is the saturation current density. J_0 depends on the recombination, where V_{oc} is then a measure of the amount of recombination in the device. Thus, increase in J_0 leads to increase in recombination i.e. with increase in temperature as observed in figure 4c there was a decrease in V_{oc} of the device.

$$V_{oc} = \frac{nkT}{q} ln\left(\frac{J_L}{J_0} + 1\right) \quad \ldots\ldots\ldots \quad (4)$$

Thus, variation of photovoltage with respect to temperature can be directly related to the band gap and saturation current of the device.[52,53] While, slight reduction in J_{sc} at a higher temperature (373K) is observed, however the photovoltaic action as well as diode behavior was consistent. The stable photovoltaic action is obtained at a high temperature of 373 K, which is quite higher than the normal operating temperature of photovoltaic devices. This indicates that the γ-CuI/GaN photoresponsive device is quite stable around 373K with outstanding photovoltage. Finally, the fabricated heterojunction was evaluated for to check the heterojunction interface quality i.e presence of interfacial impurities by UV light illumination.

Figure 4.11 (a) shows the *J-V* curve in forward and reverse sweep for the γ-CuI/GaN heterojunction at applied bias voltage of -2V to 2V in dark condition where the forward and reverse sweep overlap each other indicating absence of electrical hysteresis and thus absence of residual impurities at the heterojunction interface. Figure 4.11(b) shows the J-V characteristics for dark and UV illumination. The forward and reverse sweeps under UV illumination also overlap each other. Thus, absence of electrical hysteresis even under UV illumination is observed indicating no role of surface states of GaN substrate in charge transport properties.

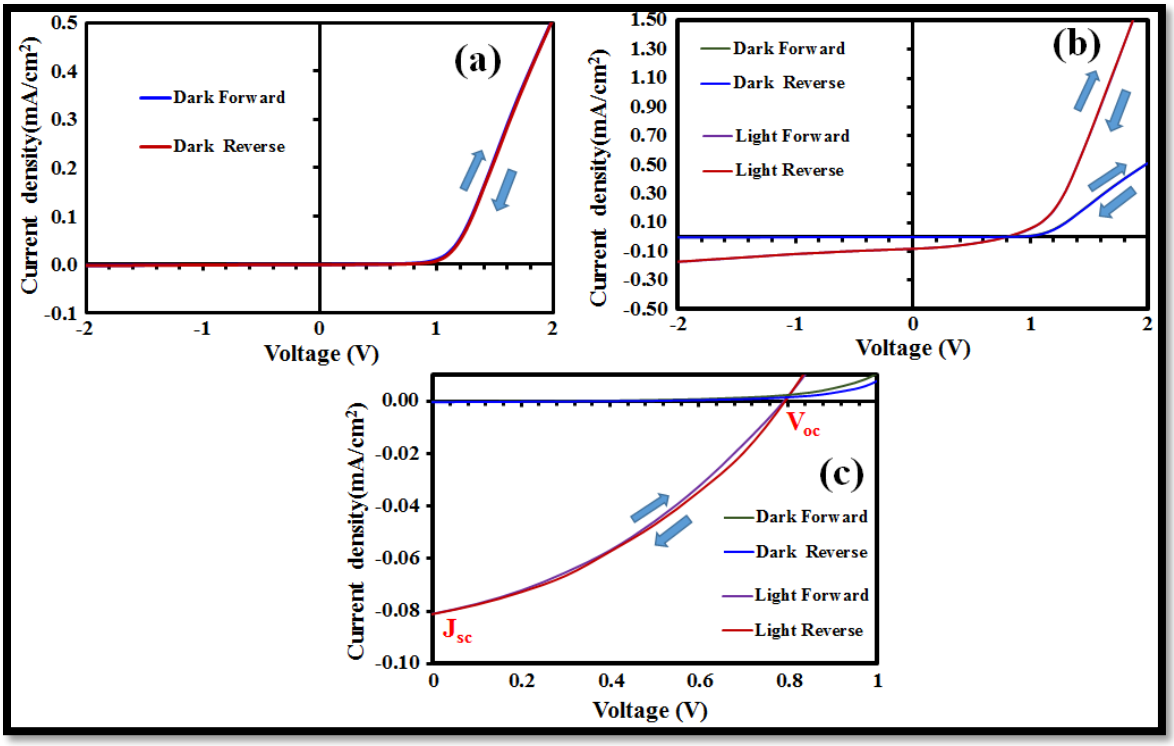

Figure 4.11 J-V characteristics of the fabricated γ-CuI/GaN heterojunction under dark and UV illumination (a) forward and reverse sweep in voltage range of -2V to +2V in dark (b) forward and reverse sweep for bias voltage of -2V to 2V in dark and under UV light illumination (c) *J-V* curve showing no change in J_{sc} and V_{oc} in forward and reverse sweep measurements under UV illumination.

As discussed in the previous chapter, the heterojunction interface can be evaluated by simply checking for presence of electrical hysteresis under UV light illumination. Thus, if the impurities/surface defects are present at the interface, they act as trap for charge carriers and induce electrical hysteresis in the heterojunction.[50,51] The absence of an electrical hysteresis in both dark and UV light conditions signify low interface defects for the p-type γ-CuI and n-type GaN film heterojunction device. Further, figure 4.11 (c) shows the V_{oc} and J_{sc} of the photovoltaic device under the UV illumination for forward and reverse sweeps measurements. The overlapping V_{oc}

and J_{sc} values for the forward and reverse sweeps measurements signify an impurity free interface of the fabricated γ-CuI/GaN heterojunction. This can be an important aspect for the γ-CuI/GaN heterojunction device to achieve high UV photoconversion efficiency without interface recombination of photocarriers. Thus, this finding showed that a visible light transparent diode and UV photoresponsive device with self-powered mode of operation at high temperature can be achieved integration of γ-CuI with GaN to form p-n heterojunction.

4.4. Conclusion

This study confirms the formation of an effective heterojunction with the p-type γ-CuI and n-type GaN with excellent UV photoresponsive photovoltage. The fabricated γ-CuI/GaN heterojunction displayed good rectification characteristics at a high applied bias voltage upto ±20 V with a low saturation current, which confirmed the suitability of integrating γ-CuI film with GaN. A photovoltaic characteristic with a photovoltage as high as 0.93 V and quantum efficiency of ~30 % for UV illumination was also displayed. Further investigation of temperature dependent diode and photovoltaic characteristics to understand the carrier transport behavior and UV responsivity showed enhancement in reverse saturation current with increase in temperature, while diode ideality factor reduced with increase in temperature. The temperature dependent photovoltaic action showed decrease in V_{oc} with increase in temperature which can be attributed to the effect of band gap and saturation current. Absence of electrical hysteresis under dark and UV illumination indicates suitability of fabricating impurity free interface for γ-CuI/GaN heterojunction. Finally, a consistent photovoltaic action at a temperature as high as 373 K, which is quite higher than normal operating temperature of photovoltaic device was observed for the fabricated heterojunction. Hence, the present study opens the possibility of using the fabricated heterojunction for high temperature self-powered UV photodetectors application.

4.5 References

1) Akasaki et al., Jpn. J. Appl. Phys., vol. 36, p. 5393, 1997.
2) S. Nakamura, Science, vol. 281, no. 5379, pp. 956-961, 1998.
3) Akutas, Z. et al., Appl Phys Lett., vol. 69, no. 25, pp. 3872-3874, 1996.
4) M. Meneghini et al., IEEE Transactions on Device and Materials Reliability, vol. 8, no. 2, pp. 323-331, 2008.
5) E. A. Jones et al., IEEE J. Emerging Sel. Top. Power Electron., vol. 4, no. 3, pp. 707-719, 2016.
6) G. Kalita et al., Appl. Phys. Lett., vol. 111, no. 1, p. 013504., 2017.
7) C. Zhao et al., Nano Lett., vol. 16, no. 2, pp. 1056-1063, 2016.
8) K. Chung et al., Science, vol. 330, no. 6004, pp. 655-657, 2010.
9) J. Millán et al, IEEE Trans. Power Electron., vol. 29, no. 5, pp. 2155-2163, 2014.
10) L. Wang et al., Nano Energy, vol. 12, pp. 419-436, 2015.
11) J. C. Carrano et al., Appl. Phys. Lett., vol. 76, no. 7, pp. 924-926, 2000.
12) S.P. Denbaars et al., Acta Materialia, vol. 61, no. 3, pp. 945-951, 2013.
13) O. Jania et al., Appl. Phys. Lett., vol. 91, no. 13, p. 132117, 2007.
14) T. J. Flack et al., J. Electron. Mater., vol. 45, no. 6, pp. 2673-2682, 2016.
15) G. Kalita et al., Phys. Status Solidi A, vol. 215, no. 18, p. 1800089, 2018.
16) R. S. Pengelly, IEEE Transactions on Microwave Theory and Techniques, vol. 60, no. 6, pp. 1764-1783, 2012.
17) H. Amano et al., Journal of Physics D: Appl. Phys., vol. 51, no. 16, p. 3001, 2018.
18) M. A. Khan et al., Appl. Phys. Lett., vol. 76, no. 9, pp. 1161-1163, 2000.
19) T. Egawa et al., J. Appl. Phys., vol. 82, no. 11, pp. 5816-5821, 1997.
20) J. B. Limb et al., Appl. Phys. Lett., vol. 76, no. 17, pp. 2457-2459, 2000.

21) I.C. Kizilyalli et al., Semicond. Sci. Technol., vol. 30, no. 12, p. 124001, 2015.

22) Z. Y. A. Balushi et al., Nat. Mater., vol. 15, no. 11, pp. 1166-1171, 2016.

23) Y. Chen et al., J. Am. Chem. Soc., vol. 140, no. 48, pp. 16392-16395, 2018.

24) H. Borate et al., ES Mater. Manuf., vol. 3, no. 2, pp. 22-28, 2018.

25) K. Srinivasarao, et al., Adv. Comps. Hybrid Mater., vol. 1, no. 2, pp. 364-373, 2018.

26) H. Suna et al., J. Colloid Interface Sci., vol. 547, pp. 40-49, 2019.

27) L. Zhang, J. Electrochem. Soc., vol. 164, no. 9, p. H651, 2017.

28) L. Zhang et al., J. Electrochem. Soc., vol. 164, no. 14, p. H1086, 2017.

29) Y. Sheng, Appl. Surf. Sci., vol. 465, pp. 154-163, 2019.

30) H. Sun et al., J. Colloid Interface Sci., vol. 547, pp. 40-49, 2019.

31) W. Zhao et al., Nanoscale, vol. 11, no. 1, pp. 50-59, 2019.

32) M. Moun et al., Sci. Rep., vol. 8, no. 1, pp. 1-10, 2018.

33) Z. Zhang et al., ACS Appl. Mater. Interfaces, vol. 10, no. 20, pp. 17419-17426, 2018.

34) R. Zhuo et al., J. Mater. Chem. C, vol. 6, no. 2, pp. 299-303, 2017.

35) C. Y. Huang et al., Appl. Phys. Lett., vol. 112, no. 23, p. 233106, 2018.

36) D. Ruzmetov et al., 2D Mater., vol. 5, no. 4, p. 045016, 2018.

37) J. Wang et al., J. Appl. Phys., vol. 110, no. 5, p. 054907, 2011.

38) Liu, H. et al., Adv. Mater., vol. 30, no. 34, p. 1802379, 2018

39) D. Chen et al., Cryst. Growth Des., vol. 10, no. 5, pp. 2057-2060, 2010.

40) S. Miyake et al., J. Phys. Soc. Japan, vol. 7, no. 1, pp. 19-24, 1952.

41) N. Yamada et al., Adv. Electron. Mater., vol. 3, no. 12, p. 1700298, 2017.

42) J. A. Christians et al., J. Am. Chem. Soc., vol. 136, no. 2, pp. 758-764, 2014,

43) P. Li et al., Nano Res., vol. 4, no. 10, pp. 979-986, 2011.

44) M. Grundmann et al., Phys. status solidi, vol. 210, no. 9, pp. 1671-1703, 2013.

45) Z. Yang et al., ACS Appl. Mater. Interfaces, vol. 7, no. 38, pp. 21235-21244, 2015.

46) K. Yao et al.,npj 2D Mater. Appl., vol. 2, no. 1, p. 16, 2018.

47) C. Yang et al., Sci. Rep., vol. 6, no. 1, p. 21937, 2016.

48) L. K. Dintle et al., MRS Adv., vol. 3, no. 42-43, pp. 2627-2642, 2018.

49) S. Valdueza-Felip et al., Jpn. J. Appl. Phys., vol. 52, no. 8S, p. 08JH05, 2013.

50) A.K. Ranade et al, Appl. Phys. Lett., vol. 114, no. 15, p. 151102, 2019.

51) K. P. O'Donnell et al., Appl. Phys. Lett., vol. 58, no. 25, pp. 2924-2926, 1991.

52) A. Augusto et al., J. Appl. Phys., vol. 121, no. 20, p. 205704, 2017.

53) P. Löper et al., Energy Procedia, vol. 27, pp. 135-142, 2012.

54) B. M. Morais Faustino et al., Sci. Rep., vol. 8, no. 1, p. 6867, 2018.

55) G. Kalita et al., Appl. Phys. Lett., vol. 111, no. 1, p. 013504, 2017.

CHAPTER 5

5. Photovoltaic action in graphene-Ga_2O_3 heterojunction with deep-ultraviolet irradiation

5.1 Introduction

In the last decade, gallium oxide (Ga_2O_3), a wide band gap semiconductor (4.5-4.9 eV) has attracted enormous attention for various power electronics, solar blind photodetectors, optoelectronics, light-emitting diode [1-10] Gallium oxide possesses excellent properties like good electron mobility of about 300 $cm^2V^{-1}\cdot s^{-1}$ at room temperature, high chemical and mechanical stability (Young's modulus of β-Ga_2O_3 = 232 GPa), high thermal stability (melting point ~1820 °C) which has facilitated its application in high power electronic devices.[3-4] Gallium oxide with its exceptionally high breakdown field of 8MV/cm coupled with its ultra-wide bandgap (4.5-4.9eV) has emerged as a great competitor to traditional used wide bandgap semiconductors like GaN and SiC for solar blind UV photodetector applications.[5-7] UV photodetectors are key component for various applications in the field of environmental monitoring, biological and chemical analysis, flame detection, astronomical studies, digital imaging, communication and other emerging technologies such as internet-of-things (IoT) sensors.[1-4]. Various device structures have been investigated to achieve lower power consumption and high photoresponsitivty. [13,14] Thus, the self-powered photodetectors owing to its low power consumption and easy to use advantage has emerged as the ideal candidates to replace the conventional photodetectors. [15,16] Among the wide bandgap semiconductors, GaN based conventional p-n and Schottky junction devices have been explored for self-powered photodetectors application. [17,18] In this regard, gallium oxide has emerged as possible candidate for developing solar blind DUV photodetectors.

The β-Ga_2O_3 has already been integrated with conventional metal electrodes to form Schottky junction for various device applications. [23-25] Thus, this has opened the possibility of integrating graphene with β-Ga_2O_3 to form unconventional Schottky junction. The high carrier mobility2×10^5 $cm^2\ V^{-1}\ s^{-1}$) and excellent thermal conductivity (~5×10^3 W/mK) of graphene are interesting prospects to integrate with β-Ga_2O_3.[26] Gao et al. has fabricated a graphene/β-Ga_2O_3 heterojunction Schottky diode obtaining significant DUV responsivity.[4] Again, Ai et al. has demonstrated the fast-response graphene/β-Ga_2O_3/graphene heterojunction and self-powered operation. In the present study, I have demonstrated fabrication of the monolayer graphene and β-Ga_2O_3 heterojunction Schottky diode obtaining a photovoltaic action and excellent photoresponsivity in solar-blind DUV wavelength.

5.2 Experimental

Sn-doped single crystal β-Ga_2O_3 (thickness 650 μm, donor concentration 3.0×10^{18} cm^{-3}) purchased from Tamura Corporation, Japan was used for the device fabrication. A monolayer graphene film was synthesized on recrystallized copper (Cu) foil by a low-pressure chemical vapor deposition (LPCVD) technique using similar procedure mentioned in chapter 2. Further, the synthesized graphene film on Cu foil was coated with a poly (methyl methacrylate) (PMMA) layer and dried in oven (80°C). Subsequently, the Cu foil was etched with a solution of iron (III) nitrate nonahydrate [$Fe_2(NO_3)_3.9H_2O$]. The free standing PMMA/graphene layer was treated with diluted nitric acid solution (1M) to remove the residual iron nitrate and other metal impurities. Then, the PMMA/graphene film was moved to fresh de-ionized water and transferred to the β-Ga_2O_3 substrate. The water bubbles on the graphene/β-Ga_2O_3 sample were removed by slow air blowing and dried in an oven at 80 °C for 15 min. After cooling the dried sample, PMMA coating was removed by dipping in acetone solvent. After the transfer of graphene on β-Ga_2O_3 was

accomplished, the heterostructure was analyzed by both spectroscopic and microscopic technique. Further, a vertical device structure was fabricated by depositing gold (Au) and indium (In) as metal contacts on the top of graphene and back side of β-Ga_2O_3 substrate, respectively. The metal contacts were deposited by thermal evaporation using a shadow mask at high vacuum (~10^{-4} Pa) condition. Figure 5.1 shows the schematic representation of fabrication of graphene/ β-Ga2O3 heterojunction.

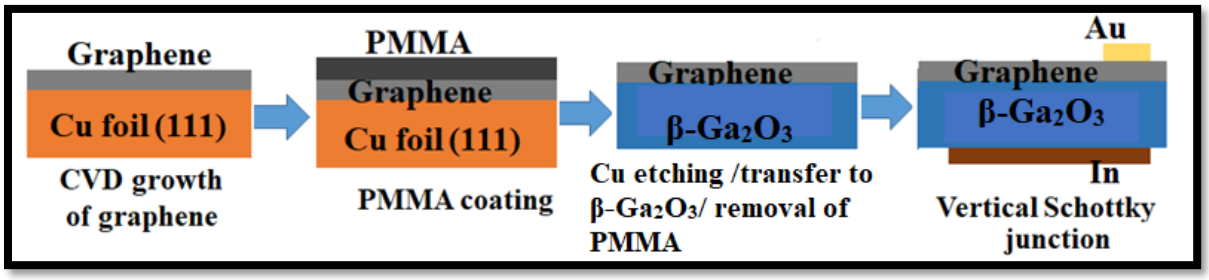

Figure 5.1 shows the schematic representation of fabrication of graphene/ β-Ga_2O_3 heterojunction.

5.3 Results and discussion

The graphene and β-Ga_2O_3 samples were characterized by scanning electron microscope (SEM), X-ray photoelectron spectroscopy (XPS) and Raman spectroscopy. Raman studies of the β-Ga_2O_3 and transferred graphene film were performed using NRS 3300 laser Raman spectrometer with a laser excitation wavelength of 532.08 nm. SEM analysis was performed by the JEOL JSM-7001FF. XPS analysis was carried out by versa probe using monochromated Al Kα excitation source (1486.6 eV). Au and In metal electrodes were deposited by ULVAC VPC-260F thermal evaporator. Current density-voltage (J-V) measurements were carried out using a two-probe system and Keithley 2401 source meter (basic accuracy of ±0.012%) at room temperature. The light

illumination J-V characteristics were carried out using SLUV-4 UV lamp (wavelength ~254 nm; power~614 μW/cm^2)

5.3.1 Raman spectroscopy

The gallium oxide (β-Ga_2O_3) sample was analyzed by Raman spectroscopy before and after the transfer of graphene. Figure 5.2 shows the Raman spectra of single crystal β-Ga_2O_3 and graphene/ β-Ga_2O_3 heterostructure.

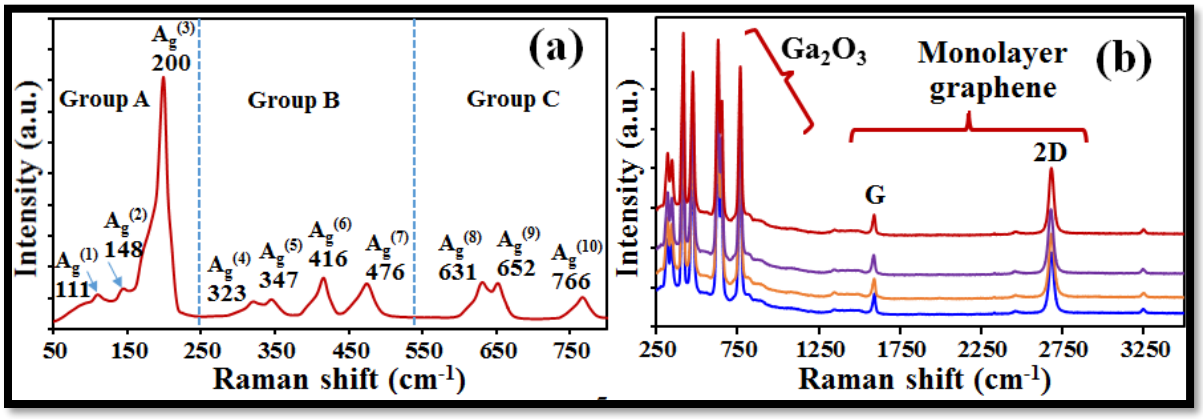

Figure 5.2 Raman spectra of (a) single crystal β-Ga_2O_3 (b) monolayer graphene/β-Ga_2O_3 heterojunction.

Figure 5.2 (a) shows Raman spectra of the single crystal β-Ga_2O_3 substrate. The Raman peaks of β-Ga_2O_3 can be categorized into three active modes, as shown in figure 5.2 (a). The low-frequency Raman peaks (Group A) bellow 200 cm^{-1} corresponds to the libration and translation of tetrahedral /octahedral chains. The mid-frequency Raman peaks (Group B) between 310 and 480 cm-1 is related to the deformation of Ga_2O_6 octahedra. The high-frequency Raman peaks (Group C) in the range 500-780 cm^{-1} signifies the stretching and bending of GaO_4 tetrahedra. Highly crystalline nature of β-Ga_2O_3 sample is observed due to high intensity peak at 200 cm^{-1}. The sample is again analyzed by Raman spectra after the transfer of graphene as shown in figure 5.2 (b). Along with

expected β-Ga_2O_3 peaks, additional peaks at higher frequencies were observed corresponding to the graphitic G and second-order two-phonon Raman mode 2D peaks. The Raman spectra is taken at various random points on the sample to confirm the presence of uniform graphene layer on β-Ga_2O_3 It is observed that the 2D peak intensity is higher than the G peak in every scan and ratio of I_{2D}/I_G~ 3 indicates presence of monolayer graphene. The peak positions of G and 2D bands were found in the ranges of (1590-1594 cm^{-1}) and (2677-2681 cm^{-1}). The G and 2D peak frequency difference were around 1088 cm^{-1}, is much less than that of pristine graphene (1120 cm^{-1}) which can be attributed to unintentional doping effect in the CVD synthesized graphene and charge transfer interaction between the n-type β-Ga_2O_3 and graphene. Further, the device was analyzed by UV absorption spectroscopy before and after the graphene.

5.3.2 UV-visible absorption spectroscopy

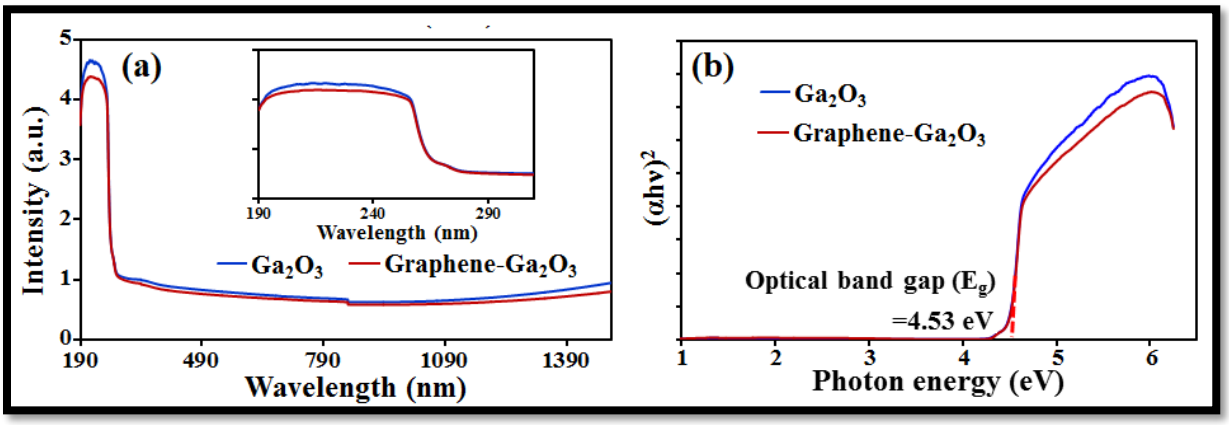

Figure 5.3 (a) shows the UV-visible absorption spectra of single crystal β-Ga_2O_3 and graphene/β-Ga_2O_3 heterostructure. (b) Tauc plot of β-Ga_2O_3 and graphene/β-Ga_2O_3 to calculate optical bandgap of the heterostructure.

Figure 5.3 (a) shows UV-visible absorption spectra of β-Ga_2O_3 before and after transferring the graphene film. Inset shows absorption spectra for 190-310 nm wavelength to focus on the

absorption peak obtained near ~ 260 nm which corresponds with theoretical value of operation in DUV region of the spectrum. It is observed that no difference in the absorption band edge of β-Ga_2O_3 before and after transferring of graphene. Figure 5.3 (b) shows Tauc plot for the pristine and graphene/β-Ga_2O_3 heterostructure samples. An optical band gap of 4.53 eV was estimated from the Tauc plot for the β-Ga_2O_3 before and after the graphene coating. Other than small reduction in DUV absorption after the graphene coating, there no further visible affect in the absorption spectra which signifies the suitability for graphene integration. Following the UV-visible spectroscopy measurement the fabricated heterostructure was subjected to FE-SEM characterization.

5.3.3 Field emission scanning electron microscopy (FE-SEM):

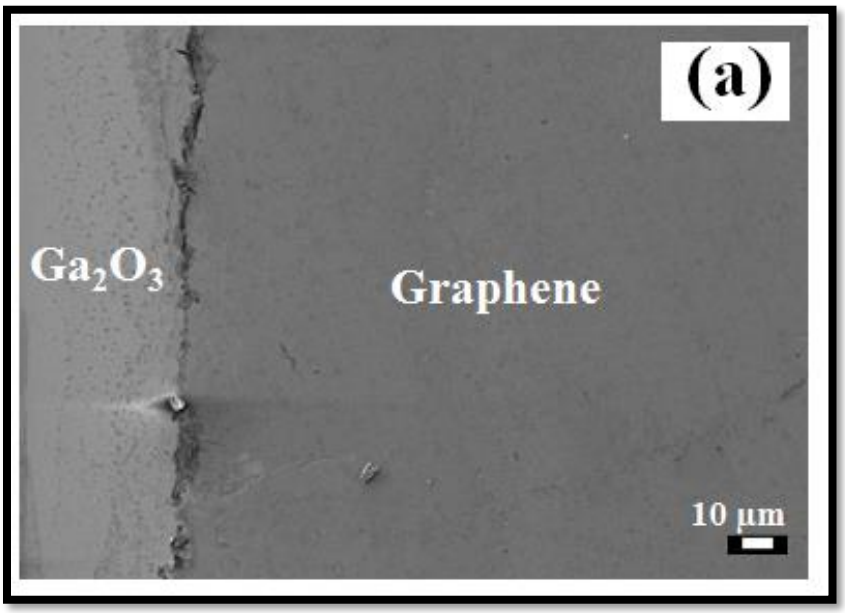

Figure 5.4 shows the FESEM image of the graphene/ β-Ga_2O_3 heterostructure.

Figure 5.4 shows an SEM image of the graphene/β-Ga_2O_3 heterostructure. A smooth surface with the transferred graphene film on β-Ga_2O_3 was obtained. The graphene film is well attached to the

β-Ga_2O_3 substrate due to van der Waal's force of attraction. Further, the heterostructure was analyzed by XPS for confirm the elemental composition of the heterostructure.

5.3.4 X-ray photoelectron spectroscopy

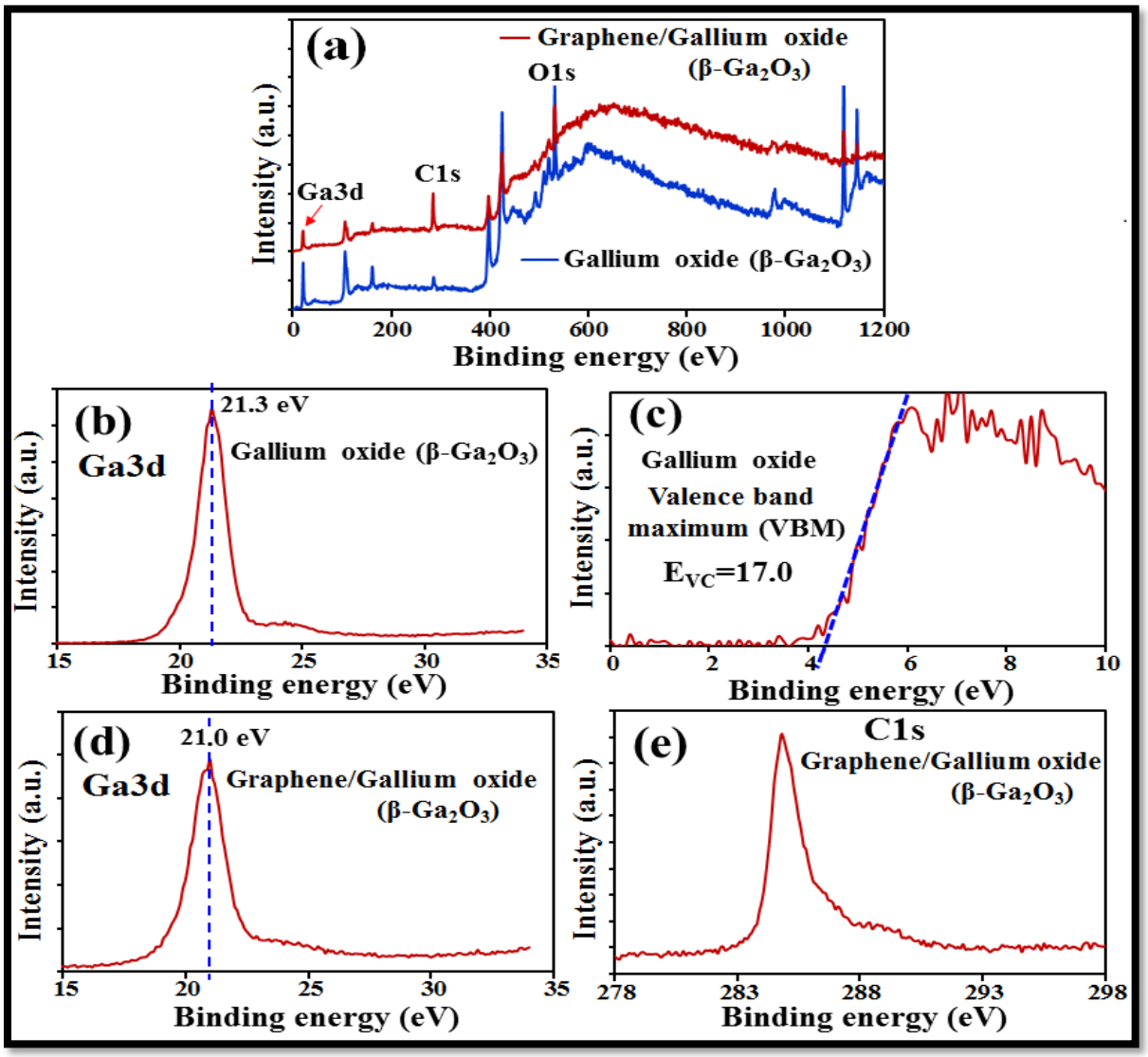

Figure 5.5 shows the (a) XPS survey spectra (b) Ga 3d peak and (c) valence band maximum (VBM) for pristine β-Ga_2O_3. (d) Ga3d peak and (e) C1s peak for graphene/β-Ga_2O_3 heterostructure.

Figure 5.5 (a) shows the XPS survey spectra of the fabricated monolayer graphene/β-Ga_2O_3 heterostructure. The expected characteristic peaks for Ga3d, Ga2p and O1s are confirmed for the pristine and graphene coated β-Ga_2O_3. A strong C1s peak is observed only for the graphene coated β-Ga_2O_3 sample which confirms good contact between graphene and β-Ga_2O_3 and absence of impurities in pristine β-Ga_2O_3 substrate. Further to confirm good contact between graphene and β-Ga_2O_3, Ga3d peak was further analyzed for the β-Ga_2O_3 sample before and after graphene transfer. In Figure 5.5 (b), a peak obtained at 21.3 eV corresponds to core level peak for pristine β-Ga_2O_3. Figure 5.5 (c) shows valence band maxima (VBM) for the pristine β-Ga_2O_3 which was calculated by extrapolating the onset of leading edge to the baseline and obtained to be 4.3eV which was used to calculate the E_{vc}. The E_{vc} which is the energy difference between the Ga3d core level and VBM β-Ga_2O_3 calculated by eq (1)

$$[E_{VC} = (E_{Ga3d}^{Ga2O3} - E_{VBM}^{Ga2O3}) \qquad \text{----------(1)}$$

The Evc of β-Ga_2O_3 sample is obtained to be 17.0 eV, which agrees with previous studies. [28]

Further, we analyzed the Ga3d peak of the graphene/ β-Ga_2O_3 heterostructure which is observed in figure 5.5 (d) shows core level binding energy of 21.0 eV [$E_{Ga3d}^{Graphene/Ga2O3}$]. Figure5.5 (e) shows the C1s spectra for the graphene/β-Ga_2O_3 heterostructure where the core peak is obtained at binding energy of 285 eV as observed for previously reported monolayer graphene. Now, the barrier height (q/φB) of graphene/β-Ga_2O_3 heterojunction is calculated using the equation.

$$[q\phi_B = E_g - \left(E_{Ga3d}^{Graphene/Ga2O3} - E_{VC}\right) \text{----------} \quad (2)$$

The barrier height (BH) of the graphene/β-Ga_2O_3 heterojunction computed to 0.53 eV. The calculated BH value can differ depending on the band gap of β-Ga_2O_3 (in the range of 4.5 to 4.9

eV) and shift in position of Fermi energy with doping level from charge neutrality of graphene. Nevertheless, XPS study confirmed a BH of more than 0.5 eV for the fabricated monolayer graphene/β-Ga_2O_3 heterojunction, which is acceptable for forming a Schottky junction. Following the characterization of the graphene/ β-Ga_2O_3 heterostructure, gold (Au) and Indium (In) electrodes were deposited on graphene and β-Ga_2O_3 respectively as metal contacts to fabricate a vertical heterojunction and analyzed it by J-V characterization.

5.3.5 Current density -voltage (J-V) characteristics

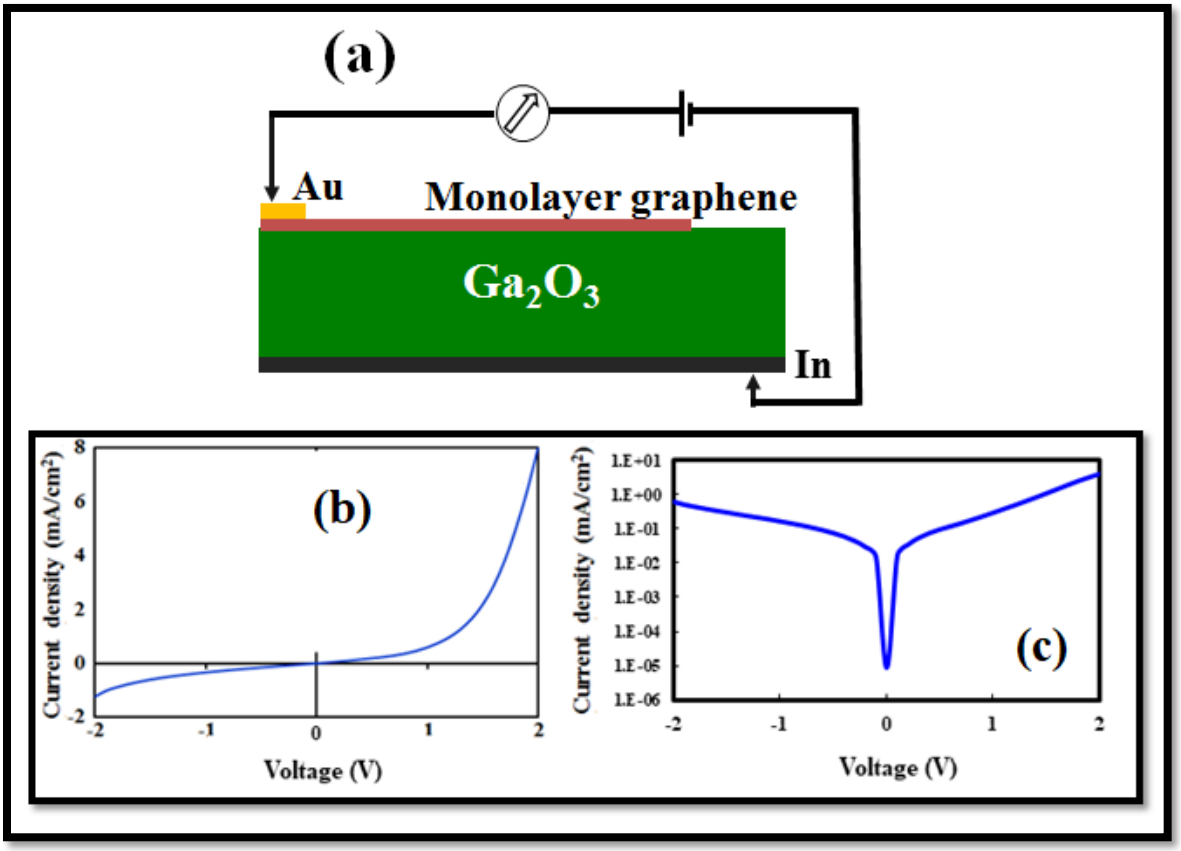

Figure 5.6 (a) shows the J-V characteristics of the graphene/β-Ga_2O_3 heterojunction under dark condition in applied voltage range of -2V to +2V. (b) shows the corresponding log plot.

Figure 5.6 (a) shows schematic diagram of a fabricated Au/graphene/β-Ga_2O_3/In vertical heterojunction Schottky junction. The vertical Schottky junction is quite interesting considering its lower sensitivity to passivation and surface states, hence can achieve better device performance. Figure 5.6 (b) shows the J-V characteristics of the graphene/β-Ga_2O_3 heterojunction under dark condition in applied voltage range of -2V to +2V at room temperature where a rectifying diode characteristic with a rectification ratio of 10 is observed. Further, due to formation of Schottky junction, an exponential increase in current with increasing voltage is observed. Figure 5.6 (c) shows the log plot for J-V characteristics under dark condition in applied bias voltage of -2V to +2V. The reverse saturation current was much higher which can be attributed to non-ideal ohmic contact as well as high carrier concentration. The J-V characteristic under dark condition was used to calculate the barrier height of the fabricated heterojunction using the thermionic model (TE) using the following equation

$$\emptyset_B = \frac{kT}{q}\left(\frac{AA^*T^2}{I_0}\right) \quad \text{.....(4.1)}$$

Where the q is the electronic charge, k is the Boltzmann's constant and T is the absolute temperature in Kelvin and I_0 is the saturation current ensuing from the straight-line intercept of the ln I-V plot, A is the area of the electrode and A* is the Richardson constant and for β-Ga_2O_3, A* used for calculation is 2.96 $Acm^{-2}K^{-2}$.

The barrier height computed to ~0.49eV which is lower than the value calculated by XPS studies and could be due to presence of tunneling components as previously reported in graphene/GaN Schottky heterojunction.[18] The device was further investigated under DUV illumination light of wavelength 254 nm with power intensity of 614 μW/cm^2. Figure 5.7 (a) shows the J-V characterization under dark and UV light illumination. The J-V curve showed an excellent

photoresponsivity of 6.1 A/W at a low reverse bias voltage (-1.5 V). The external quantum efficiency (EQE) was found to be 2980%, signifying the high photoresponsivity at a bias voltage. Figure 5.7 (b) shows the photovoltaic action obtained for the device under DUV illumination with a V_{oc} of 10 mV and J_{sc} of 4.4 μA/cm^2. Further the device was analyzed by transient spectral response.

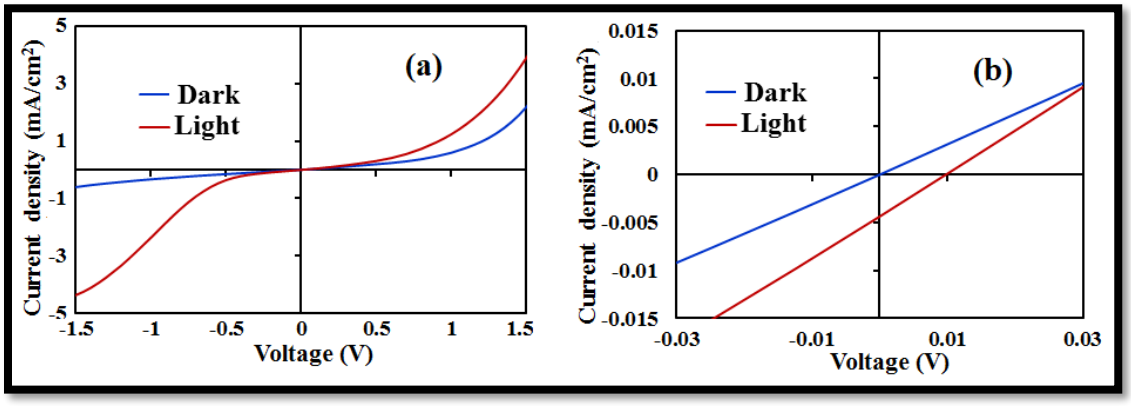

Figure 5.7 shows the J-V characterization (a) under UV light illumination in comparison under dark condition. (b) focusing in the applied voltage range of -0.03V to +0.03V displaying the photovoltaic action.

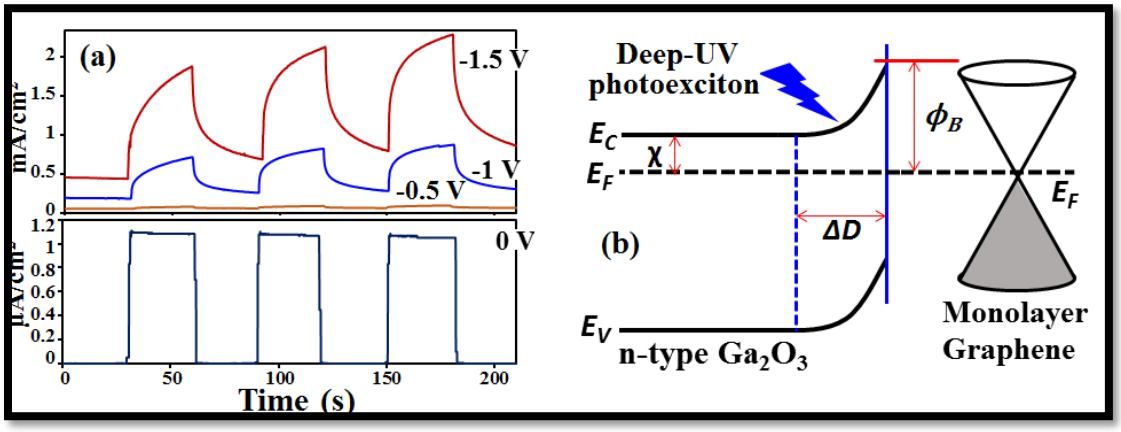

Figure 5.8 (a) shows the transient response of the device under 0V, -0.5V, -1V and -1.5V bias voltage. (b) probable energy band diagram of the graphene/β-Ga_2O_3 heterojunction device.

Figure 5.8 shows the transient response of the photovoltaic device at varies applied bias voltage which displayed high responsivity under bias conditions with slow response speed. The rise and decay curves are made up of a faster and slower response component. The fast response can be attributed to the rapid change in carrier density while the slow response component could be attributed to the carrier trapping/release process at the interface. The rise time and decay time at the bias voltage of -1.5 V were estimated to be 3.21s/26.68s and 4.41s/28.74s, respectively. Thus, the photodiode gain with high EQE at a bias voltage can be attributed to charge carrier multiplication due to charge trapping and de-trapping phenomenon [20,22,31]. Further, under zero bias voltage mode, a fast response with rise and decay time of 0.62s and 0.67s was observed with less responsivity. The fast response and low responsivity could be due to generation of photocurrent under the internal build-in-field in the graphene/Ga_2O_3 interface with no contribution from the trapped charge carriers. Figure 5.8 (b) shows the probable energy band diagram of graphene/β-Ga_2O_3 heterojunction with presence of Schottky junction potential barrier at the heterojunction interface. The presence of a suitable potential barrier at the interface of graphene and β-Ga_2O_3 enables the generated photoexciton to dissociate and separate under build-in electric field for the photons with a high energy of 4.88 eV. Further, as reported in chapter 3, Schottky device are highly sensitive towards the interface quality and surface states in the semiconductors. Presence of interface states and interfacial impurities lead to occurrence of electrical hysteresis and eventually affects the device performance. Hence, the graphene/β-Ga_2O_3 Schottky heterojunction was analyzed to check the quality of interface at the graphene/β-Ga_2O_3 Schottky heterojunction. A new graphene/β-Ga_2O_3 was fabricated using a newly synthesized graphene sample. Same method was employed for the fabrication of heterojunction as used for previous device. The next section explores the quality of interface for graphene/β-Ga_2O_3 Schottky junction.

Figure 5.9 (a) shows the J-V characteristics for a newly fabricated graphene/β-Ga_2O_3 heterojunction with forward and reverse sweep under dark condition for applied bias voltage of -2V to +2V. The fabricated device showed the rectifying diode characteristics which is similar to the previous heterojunction.

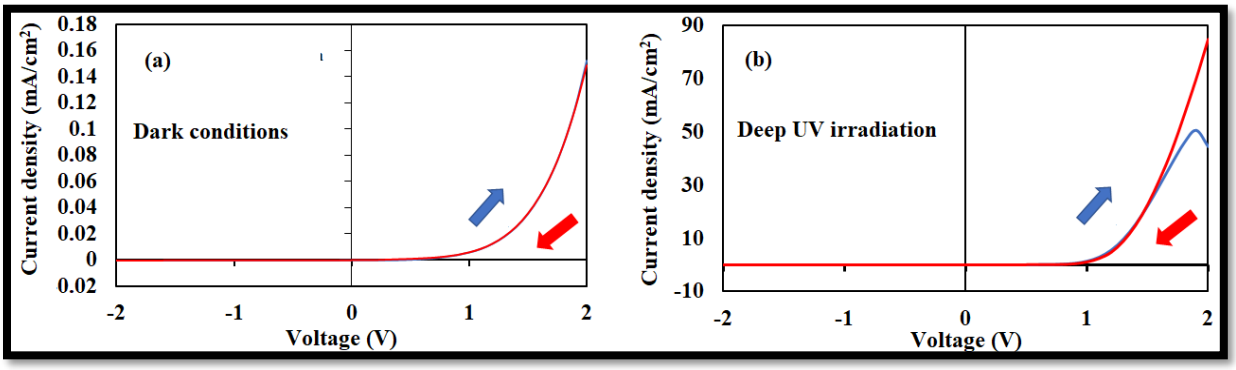

Figure 5.9 (a) shows the forward and reverse sweep under no DUV irradiation condition for applied bias voltage of -2V to +2V (b) forward and reverse sweep under DUV irradiation (254 nm) for applied bias voltage of -2V to + 2V.

Further, the forward and reverse sweep under applied bias voltage of -2V to +2V overlapped, which confirms absence of electrical hysteresis under no light condition. Since there is no electrical hysteresis under dark condition the interface of the fabricated graphene/β-Ga_2O_3 heterojunction is free of impurities, signifying good transfer of fabricated monolayer graphene on β-Ga_2O_3 substrate. Subsequently, the device was analyzed under DUV illumination (254 nm) to check for presence of electrical hysteresis in the fabricated heterojunction. Figure 5.9 (b) shows the J-V characteristics for the newly fabricated graphene/β-Ga_2O_3 heterojunction with forward and reverse sweep under DUV illumination condition for applied bias voltage of -2V to +2V. The device showed good photoresponsive characteristic as that of previously fabricated heterojunction. In this fabricated

device, hysteresis is observed for J-V characteristics at higher bias voltage range of -1.5V to -2V. The presence of electrical hysteresis at higher bias voltage can be explained by charge trapping and de-trapping phenomenon due to inherent surface states of β-Ga_2O_3 substrate, which is also observed from the transient response characteristics. Thus, the fabricated monolayer graphene/β-Ga_2O_3 heterojunction showed a rectifying diode characteristic with a photovoltaic action under DUV illumination of wavelength 254 nm. Again, charge trapping and de-trapping process is observed at a bias voltage, showing high photoresponsivity at the bias voltage with slower response time.

5.4 Conclusions

In conclusions, I have explored fabricating an unconventional monolayer graphene/β-Ga_2O_3 vertical heterojunction Schottky diode which exhibits a photovoltaic action under DUV illumination. The Raman spectroscopy confirmed the transfer of a continuous monolayer graphene on β-Ga_2O_3. Further, XPS analysis confirmed good contact between graphene and β-Ga_2O_3 due to shift in Ga3d peak while the XPS signal was also used to calculate a potential barrier of ~0.53 eV for the monolayer graphene and β-Ga_2O_3 heterojunction. The fabricated vertical Schottky diode showed a photovoltaic action with a V_{oc} of 10 mV and Jsc of 4.4 μA/cm^2 for irradiation wavelength of 254 nm. The transient response behavior showed a faster response time (rise time~0.62s, decay time~0.67s) for self-powered operation of the photodiode. Under an applied bias voltage of -1.5 V, excellent photoresponsivity (6.1 A/W) is observed with a slower response time. The higher photoresponsivity at a bias voltage can be related to carrier multiplication process due to carriers trapping/release. Finally, a newly fabricated graphene/β-Ga_2O_3 heterojunction with same methodology was studied for its electrical hysteresis behavior. Interestingly no electrical hysteresis was observed under dark condition but was induced under DUV illumination (254nm) which

implies the interface is free of residual impurities however confirms the presence of surface states in β-Ga_2O_3 which act as trap sites for charge carrier. Finally, a photovoltaic action with excellent photoresponsivity is observed for the fabricated monolayer graphene/ β-Ga_2O_3 vertical heterojunction with highly sensitive interface.

5.5 References

1) L. Sang, et al., Sensors, vol. 13, no. 8, pp. 10482-10518, 2013.

2) H. Chen, et al., Mater. Today, vol. 18, no.9, pp.493-502, 2015.

3) W.-Y. Kong et al., Adv. Mater., vol. 28, no. 48, pp. 10725-10731, 2016.

4) L. Peng et al., Adv. Mater., vol. 25, no. 37, pp. 5321-5328, 2013.

5) G. Konstantatos et al., Nat. Nanotechnol., vol. 5, no. 6, pp. 391-400, 2010.

6) H. Zhu et al., J. Phys. Chem. C, vol. 112, no. 51, pp. 20546-20548, 2008.

7) M. Liao et al., Appl. Phys. Lett., vol. 90, no. 12, p. 123507, 2007.

8) R. McClintock et al., Appl. Phys. Lett., vol. 87, no. 24, p. 241123, 2005.

9) L. Hu, et al., Small, vol. 7, no. 8, pp. 1012-1017, 2011.

10) L. Sang et al., Appl. Phys. Lett., vol. 99, no. 3, p. 31115, 2011.

11) K. Liu, et al., Sensors, vol. 10, no. 9, pp. 8604-8634, 2010.

12) J. A. Schuller, et al., Nat. Mater., vol. 9, no. 3, pp. 193-204, 2010.

13) Z. Zhou et al., Photon. Res., vol. 3, no. 5, pp. B28-B46, 2015.

14) M. Kielar et al., Sci. Rep., vol. 6, no. 1, p. 39201, 2016,

15)P.N. Ni et al., J. Mater. Chem. C, vol. 1, no. 29, pp. 4445-4449, 2013.

16) N. Prakash et al., Appl. Phys. Lett., vol. 109, no. 24, p. 242102, 2016.

17) G. Kalita et al., Appl. Phys. Lett., vol. 111, no. 1, p. 13504, 2017.

18) R. Zou et al., Small, vol. 10, no. 9, pp. 1848-1856, 2014.

19) R. Suzuki et al., Appl. Phys. Lett., vol. 94, no. 22, p. 222102, 2009.

20) S. Oh et al., ACS Photonics, vol. 5, no. 3, pp. 1123-128, 2018.

21) M. Ai et al., J. Alloys Compd., vol. 692, pp. 634-638, 2017.

22) K. Sasaki et al., IEEE Electron Device Letters, vol. 34, no. 4, pp. 493-495, 2013.

23) X. Chen et al., ACS Appl. Mater. Interfaces, vol. 8, no. 6, pp. 4185-4191, 2016.

24) S. Fujita et al., Jpn. J. Appl. Phys., vol. 55, no. 12, p. 1202A3, 2016.

25) M. Higashiwaki et al., Appl. Phys. Lett., vol. 112, no. 6, p. 60401, 2018.

26) S. J. Pearton et al., Appl. Phys. Rev., vol. 5, no. 1, p. 11301, 2018.

27) S. V Morozov et al., Phys. Rev. Lett., vol. 100, no. 1, p. 16602, 2008.

28) C. Kranert et al., Sci. Rep., vol. 6, no. 1, p. 35964, 2016.

29) H. Sun et al., Appl. Phys. Lett., vol. 111, no. 16, p. 162105, 2017.

30) X. Luo et al., Phys. status solidi-RRL, vol. 10, no. 6, pp. 485-492, 2016.

CHAPTER 6

6. Conclusion and future scope of research

6.1 Overall conclusion

In this research work, the fabrication of heterojunction UV photoresponsive devices of GaN and Ga_2O_3 with graphene and p-type γ-copper iodide (γ-CuI) were investigated considering the importance of 2D/3D heterojunction devices. The interface quality of respective fabricated devices is analyzed with and without UV illumination and device properties were clarified to achieve better UV photoresponsivity.

In this prospect, graphene/GaN Schottky heterojunction devices were fabricated and their photoresponse properties were investigated. Electrical hysteresis was observed in the graphene/GaN vertical heterojunction Schottky device and its influence on UV photoresponse characteristics was evidently found. It was confirmed that the interfacial impurities act as trap sites for charge carriers, thus inducing electrical hysteresis in the heterojunction. Excellent UV photoresponse can be achieved in the graphene/GaN heterojunction by eliminating the interfacial impurities.

The obtained electrical hysteresis effect in the graphene/GaN device was compared and examined by fabricating the γ-CuI/GaN p-n heterojunction device. The fabricated device showed excellent rectifying diode characteristics with the high applied bias voltage (-20V to +20V). The device showed excellent photovoltage of 0.93 V at room temperature under UV illumination with consistent UV photoresponsivity above room temperature (373K). The electrical hysteresis for γ-

CuI/GaN heterojunction device was not prominent, indicating interface of graphene/GaN Schottky heterojunction device are more sensitive for UV photoresponse.

Similarly, the interface properties of graphene/β-Ga_2O_3 heterojunction Schottky diode was investigated for DUV photoresponsive device applications. The device showed a small photovoltaic action with low photocurrent and photovoltage, while a large photoresponsivity of 6.1 A/W at a bias voltage of -1.5 V. The transient photoresponse showed faster photoresponse in photovoltaic mode, while significantly slower response at the bias voltage considering the charge trapping/de-trapping phenomena. The graphene/β-Ga_2O_3 Schottky heterojunction device also showed electrical hysteresis at a higher bias voltage under DUV illumination, which can be corelated with the significantly sensitive graphene/GaN based heterojunctions. Hence, it is observed that, the interface quality plays a crucial role in device performance. The interface quality can be monitored by simple UV light illumination to check for presence of electrical hysteresis as its presence indicates impurities or surface states at the heterojunction interface. Hence it can be concluded that GaN and β-Ga_2O_3 based Schottky heterojunction are highly sensitive to interface quality compared to their p-n heterojunction counterpart.

6.2 Future scope of work

From this research work, it has been understood that graphene and γ-CuI can be used to fabricate UV photoresponsive heterojunction devices with GaN and Ga_2O_3. This has opened new opportunities as well as challenges to fabricate high performances UV photoresponsive devices. The main challenge in graphene-based heterojunction with GaN and Ga_2O_3 is controlling the interface quality to achieve better device performance than the commercial devices. To address this the following research prospects can be considered:

6.2.1. Modification of transfer process or direct growth of graphene

The studied transfer process of graphene in this work can be replaced with other techniques such as, electrochemical etching of graphene from Cu foil and transfer of graphene by electrostatic charging to maintain the contact between the graphene and substrate. Another prospect is direct growth of graphene on the wide band gap semiconductor; however, quality of direct growth graphene can be a factor in device performance. This can lead to minimizing interfacial impurities as well as surface defect and enhance the UV photoresponse than that of commercial devices. At the same time, the inherent defect in GaN and Ga_2O_3 can be bottle neck in such 2D/3D heterojunction devices, hence enhancing properties of the respective materials and new/modified device fabrication techniques are way forward for this thesis work.

6.2.2 Investigation of suitable p-type semiconductor for GaN and Ga_2O_3 for photoresponse device applications

As obtained in this work, the integration of γ-CuI with GaN has resulted in excellent UV photoresponsive photovoltage with stable operation at a high temperature. This study can be expanded by integrating GaN and Ga_2O_3 with various other suitable p-type inorganic semiconductors. At present it is a fact that a suitable p-type semiconductor as a counter part of Ga_2O_3 is not yet developed. It is a challenge to fabricate effective p-type semiconductor for GaN and Ga_2O_3 devices and thereby achieving high photoresponsivity for next generation device application.

6.3 List of research achievements

Paper published related to present work

1. **Ajinkya K. Ranade**, Rakesh Mahyavanshi, Pradeep Desai, Masashi Kato Masaki Tanemura, Golap Kalita, "Ultraviolet light induced electrical hysteresis effect in graphene-GaN heterojunction", Applied Physics Letters, 114, 151102, 2019.
2. **Ajinkya K. Ranade**, Rakesh Mahyavanshi, Pradeep Desai, Masaki Tanemura, Golap Kalita, "Formation of effective CuI-GaN heterojunction with excellent ultraviolet photoresponsive photovoltage**",** Phys. Status Solidi A, 216, 1900200, 2019.
3. Golap Kalita, Rakesh D. Mahyavanshi, Pradeep Desai, **Ajinkya K. Ranade**, Masaharu Kondo, Takehisa Dewa, and Masaki Tanemura, "Photovoltaic action in graphene–Ga_2O_3 heterojunction with deep-ultraviolet irradiation", Phys. Status Solidi RRL, 12, 1800198, 2018

Other publications

4. Muhammed Emre Ayhan, Pradeep Desai, **Ajinkya K. Ranade**, Mandar Shinde, Bhagyashri Todankar, Masaki Tanemura, Golap Kalita, "Ultraviolet radiation-induced photovoltaic action in γ-CuI/β-Ga_2O_3 heterojunction", Materials Letters, 262, 127074, 2019.
5. Pradeep Desai, **Ajinkya K. Ranade**, Rakesh Mahyavanshi, Masaki Tanemura, Golap Kalita, "Influence of MoS_2-silicon interface states on spectral photoresponse characteristics**",** Phys. Status Solidi A, Phys. Status Solidi A, 216, 1900349, 2019.
6. Pradeep Desai, **Ajinkya K. Ranade**, Mandar Shinde, Bhagyashri Todankar, Masaki Tanemura, Golap Kalita, "Growth of uniform MoS_2 layers on free-standing GaN semiconductor for vertical heterojunction device application", Journal of Materials Science: Materials in Electronics, 31, 2040, 2020.

7. Rakesh D. Mahyavanshi, Golap Kalita, **Ajinkya K. Ranade**, Pradeep Desai, Masaharu Kondo, Takehisa Dewa, and Masaki Tanemura. "Photovoltaic action with broadband photoresponsivity in germanium-MoS_2 ultrathin heterojunction" IEEE Transaction on electron devices,65, 4434, 2018.
8. Rakesh D. Mahyavanshi, Golap Kalita, **Ajinkya K. Ranade**, Pradeep Desai, Masaki Tanemura, "Observing charge transfer interaction in CuI and MoS_2 heterojunction for photoresponsive device application" ACS Appl. Electron. Mater. 1, 302, 2019.

Conference attended:

1. **Ajinkya K. Ranade**, Rakesh Mahyavanshi, Pradeep Desai, Masaki Tanemura, Golap Kalita, "Schottky junction properties of graphene with nitrogen and gallium polar freestanding GaN", The 19th IEEE International Conference on Nanotechnology, Macau SAR, China, (Oral), July 2019.
2. **Ajinkya Ranade,** Pradeep Desai, Rakesh Mahyavanshi, Masaki Tanemura, Golap Kalita, "Temperature dependent ultraviolet photoresponsive behaviour in γ-CuI/GaN heterojunction**.**" The 80th JSAP Autumn Meeting, Hokkaido University, Sapporo, Japan (Poster), Sept. 2019.
3. **Ajinkya Ranade,** Pradeep Desai, Rakesh Mahyavanshi, Masaki Tanemura, Golap Kalita, "Interface dependent photoresponsivity in Graphene-GaN heterojunction" The 57th Fullerenes-Nanotubes-Graphene General Symposium, Nagoya University, Nagoya, Japan (Oral), Sept. 2019.
4. **Ajinkya Ranade, Rakesh** Mahyavanshi, Pradeep Desai, Masaki Tanemura, Golap Kalita et al., "Ultraviolet light induced electrical hysteresis effect in graphene-GaN heterojunction" The 66th JSAP Spring Meeting, Tokyo Institute of Technology, Tokyo, Japan (Oral), March 2019.